The Effects of DNA Repair Pathway Engineering on CRISPR-Mediated Genome Editing in Neuronal Cells

Inaugural Dissertation

submitted to the

Faculty of Faculty of Medicine

in partial fulfillment of the requirements

for the PhD-Degree

of the Faculties of Veterinary Medicine and Medicine

of the Justus Liebig University Giessen

by

Alabudeeb, Fatimah

of

Dhahran, Saudi Arabia

Giessen 2025

From the Department of Ophthalmology (Director: Prof. Lyubomyr Lytvynchuk)
Research Group of Experimental Ophthalmology (Head: Prof. Dr. Dr. Knut Stieger)
of the Faculty of Medicine of the Justus Liebig University Giessen

First Supervisor, First reviewer, and Committee Member: Prof. Dr. Dr. Knut Stieger
Second reviewer: Prof. Dr. Volker Busskamp, University Clinic Bonn
Committee Members: Second Supervisor, Vice-chair: Prof. Dr. Peter Friedhoff
Chair: Prof. Dr. Ralph Schermuly

Date of Doctoral Defense: 27.11.2025

I dedicate this thesis to my late father, my mother,

and my small family, my husband Akram, my son Mohammed, and my unborn baby

Table of Contents

1. Introduction

1.1 Inherited retinal dystrophies

Inherited retinal dystrophies (IRDs) are a group of genetically and clinically heterogenous disorders with a prevalence of 1 in 3-4,000 people (Hartong et al., 2006; Nash et al., 2015). There are approximately 332 genes associated with these diseases (RetNet 2025, https://RetNet.org/). Clinical presentations include difficulties with dark adaptation and night or color blindness, tunnel vision, and can eventually lead to complete blindness. These symptoms imply the gradual loss of photoreceptor cells (Figure 1) (Hartong et al., 2006).

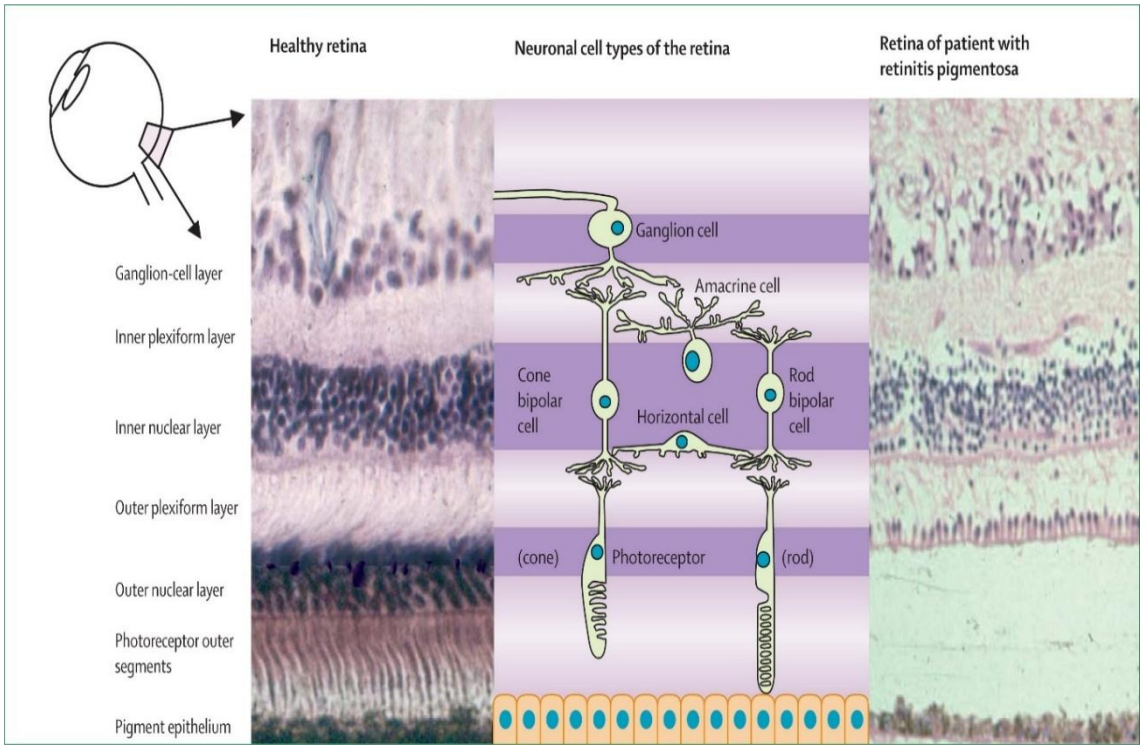

Figure 1: Comparison between a healthy retina (left) and the retina of a patient with retinitis pigmentosa (right). The outer nuclear layer, which contains the nuclei of rod and cone photoreceptors, is significantly thinned in the mid-stage diseased retina due to the degeneration of photoreceptor cells, while the inner nuclear layer remains intact, although this may change in the later stages. Reproduced from (Hartong et al., 2006). With permission from Elsevier, License Number 5907230508337

Modes of inheritance vary between autosomal recessive, autosomal dominant, and X-linked. The genetic overlap between IRDs, such as retinitis pigmentosa, cone and cone-rod dystrophies, Leber congenital amaurosis, and Stargardt disease, is complicated (RetNet, https://RetNet.org/). To diagnose IRDs, clinical evaluation, including visual acuity and field assessment, electroretinography (ERG), autofluorescence imaging (AF), optical coherence tomography (OCT), and OCT angiography are necessary (Ziccardi et al., 2019). Additionally, molecular diagnosis has evolved from simple single-gene analysis via Sanger sequencing to multi-gene panels with next-generation sequencing (NGS), whole-exome examination using whole-exome sequencing (WES), and, ultimately, comprehensive genomic analysis with whole-genome sequencing (WGS). Both genetic and clinical investigations are important to identify the exact phenotype and genotype to find the appropriate therapy (Ziccardi et al., 2019). Management of IRDs primarily involves genetic counseling, regular assessment of vision, and optometric visual rehabilitation to enhance vision. So far, there is no cure for IRDs except for Voretigene neparvovec (Luxturna), the first FDA and EMA-approved gene therapy for the treatment of RPE65-associated Leber congenital amaurosis with a sub-retinal injection of an adeno-associated viral vector carrying the coding sequence of the RPE65 gene (U.S. Food and Drug Administration, 2017; European Medicines Agency, 2018). Gene therapy research yields promising developments such as gene augmentation, which delivers the transgene using viral vectors to diseased cells with the mutated gene, and gene silencing, which downregulates the function of the mutated gene and adds a functional copy of the gene, both strategies deal with autosomal recessive and X-linked disorders. However, silencing the dominant gene or modifying the RNA to generate a functional protein is essential in autosomal dominant disorders. To overcome the limitations, such as targeting large genes or autosomal dominant diseases from gain-of-function mutations, a new approach, genome editing, has been developed. This strategy aims at correcting the sequence of the mutated gene (Gordon et al., 2019; Hu et al., 2021; Prado et al., 2020).

1.2 Genome editing

Genome engineering is a broad term for designing and manipulating genomic DNA sequences. It includes genome editing and gene editing, both are site-specific modifications of genomic DNA, whereas gene editing is only modifying one gene of the entire genome (Khalil, 2020). Therapeutic genome editing in IRDs functions either *ex-*

vivo or *in-vivo.* The *ex-vivo* genome editing process involves extracting skin biopsy, producing induced pluripotent stem cells (iPSCs), treating disease-causing mutations, re-differentiating the corrected cells into retinal pigment epithelium (RPE) or photoreceptor cells (PR), and re-implanting these cells into the eye. On the other hand, *in-vivo* genome editing directly targets the mutations in retinal cells (Yanik et al., 2017). Four major endonuclease families facilitate genome editing using DNA double-strand breaks (DSBs) and intrinsic DNA repair mechanisms. Meganucleases (MegNs), zinc finger nucleases (ZFNs), transcription activator-like effector nucleases (TALENs), and clustered regularly interspaced short palindromic repeats (CRISPR)/CRISPR-associated protein 9 (Cas9) (CRISPR/Cas9), which are classified further according to DNA recognition into two categories. MegNs, ZFNs, and TALENs bind to DNA via protein-DNA interactions. In contrast, Cas9 targets specific DNA sequences using a guide RNA by RNA-DNA and protein-DNA interactions (Cox et al., 2015). MegNs are highly specific homing endonucleases due to their ability to cleave dsDNA at the 14-40 bp recognition sites. TALEN and ZFN are artificial chimeric proteins, fusing a FokI restriction nuclease domain to a DNA-binding domain. Re-targeting of ZFN and MegNs require protein engineering, and re-targeting of TALENs requires complex molecular cloning, while in easily programmable CRISPR/Cas9, re-targeting of Cas9 does not need protein engineering, but a new guide RNA (Christian et al., 2010; Cox et al., 2015; Gaj et al., 2016; Smith et al., 2006; Khalil, 2020).

1.2.1 CRISPR/Cas technology

CRISPR was first discovered in 1987. Japanese researchers found repetitive interspaced sequences in *Escherichia coli*. Later, it was detected in archaea and other bacterial genomes. In 2005-2007, more discoveries were made, including that spacer sequences were of plasmidic and viral origins, that CRISPR-Cas was an adaptive immune system in prokaryotes, and several different Cas genes were identified (Doudna & Charpentier, 2014; Ishino et al., 2018). Research has shown that the activity of Cas enzymes is guided by short CRISPR RNAs (crRNA), the spacer sequences are similar in protospacer-adjacent motifs (PAMs) regions, and that Streptococcus thermophilus Cas9 introduces DSBs into foreign DNA. The CRISPR-Cas9 protein in Streptococcus pyogenes was described as a dual-RNA-guided DNA endonuclease that uses the tracrRNA:crRNA complex, which was then fused to a single guide RNA (sgRNA) (Adli, 2018; Doudna &

Charpentier, 2014). Due to CRISPR's flexibility, ease of use, and high editing efficiency, scientists focus their research on improving this technology. It is classified into two classes with multiple types and subtypes according to the *cas* gene, the highly investigated one is the type II CRISPR-Cas9 system from Streptococcus pyogenes (spCas9). This system needs a simple 5′-NGG PAM sequence (Adli, 2018). The CRISPR-Cas immune response process consists of three steps, adaptation, expression, and interference. First, Cas proteins recognize the PAM sequence and bind and process the foreign DNA, forming protospacers. The fragmented DNA is then incorporated into the spacer in the CRISPR array. The next two steps are Cas-dependent. During expression, a long precursor CRISPR RNA (pre-crRNA) is produced by transcription of the CRISPR, and then pre-crRNA turns into smaller crRNA by RNase III. In the last step, crRNA and Cas cleave the invading DNA to protect the cells (Deltcheva et al., 2011; Jinek et al., 2012). The molecular mechanism of CRISPR-Cas9 genome editing contains a Cas9-sgRNA complex. The sgRNA identifies the PAM sequence, and Cas9 binds and forms an R-loop with the DNA, then utilizes its catalytic function three bases upstream using two nuclease domains. The first domain is HNH (His-Asn-His), which cleaves the target strand of DNA. The second one is RuvC-like nuclease with three subdomains (RuvC-I, RuvC-II, and RuvC-III), that cleaves the non-target strand, resulting in DSBs triggering DNA repair (Gasiunas et al., 2012; Jinek et al., 2012) (Figure 2).

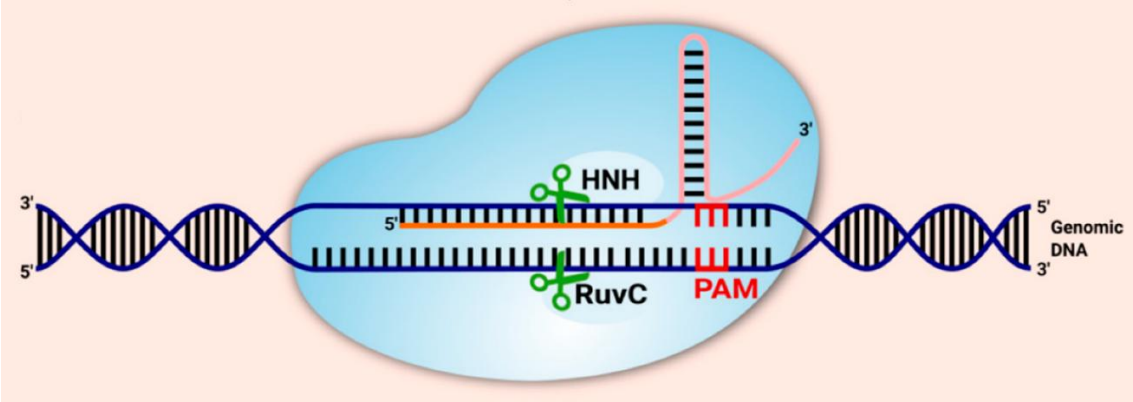

Figure 2: CRISPR Cas9 technology introducing DNA DSB. Reproduced from (Janik et al., 2020). https://creativecommons.org/licenses/by/4.0/

For the past 10 years, CRISPR technology has been improved and used by scientists for various applications like generating gene knockouts, knockout animal models, genetic

screening, and multiplexed editing (Wang & Doudna, 2023). Moreover, Casgevy (exagamglogene autotemcel) from Vertex Pharmaceuticals and CRISPR Therapeutics was recently approved as the first CRISPR-Cas9 gene editing therapy for treating severe sickle cell disease (SCD) and transfusion-dependent β-thalassemia (U.S. Food and Drug Administration, 2023; European Medicines Agency, 2024). CRISPR-Cas genome editing faces multiple obstacles. Accuracy must be achieved by minimizing off-target events via producing high-fidelity Cas variants and guide RNA modifications. Indels and bystander edits influence precision. Research has focused on enhancing the outcomes of DNA repair mechanisms through innovation and engineering, like chemically modifying enzymes in the NHEJ (non-homologous end joining) pathway or modifying the cell cycle to improve HDR (homology-directed repair). Furthermore, indels can be reduced using more advanced editing technologies that do not induce DSBs, such as base and prime editing (Anzalone et al., 2019; Wang & Doudna, 2023).

1.2.2 DNA double-strand break repair mechanisms

DNA double-strand breaks (DSBs) occur when damage affects both DNA strands (Chapman et al., 2012). DSBs are one of the most destructive forms of DNA lesions, and can be cytotoxic, triggered by endogenous and exogenous factors (Kass & Jasin, 2010; Pardo et al., 2009). Internal causes include reactive oxygen species (ROS) or exogenous ones such as ionizing radiation, ultraviolet light (UV), or chemotherapy (Pardo et al., 2009). Apoptosis and chromosomal aberrations can result from the failure to repair the DNA (Davis & Chen, 2013). The genomic integrity is restored through the DNA damage response (DDR) process, which involves DNA repair mechanisms, damage tolerance processes, and cell-cycle checkpoint pathways (Giglia-Mari et al., 2011). Sensor proteins such as the MRE11-RAD50-NBS1 (MRN) complex detect DNA lesions. Then, transducers like ATM (ataxia-telangiectasia mutated) kinase, the phosphoinositide 3-kinase (PI3K), and ATR (Ataxia telangiectasia and Rad3 related) deliver the signal to the effectors through phosphorylation of H2AX to γH2AX, which stimulates cell cycle checkpoints and repair elements (Barzilai & Yamamoto, 2004; Vítor et al., 2020). Genome editing, which includes the application of endonucleases, utilizes this DSB repair machinery. The two major repair pathways are homologous recombination (HR) or homology-directed repair (HDR), which is template-dependent, and the classic error-prone non-homologous end joining (cNHEJ) or NHEJ repair pathway. An additional

pathway, microhomology-mediated end joining (MMEJ) or alternative end joining (alt-EJ), which requires short (5-25 bp) microhomologous sequences flanking the inserted DNA repair template, is also known (Xue & Greene, 2021).

1.2.2.1 Non-homologous end joining (NHEJ)

NHEJ is fast, occurs throughout the cell cycle, and is mammalian cells' most common DNA repair pathway. It does not demand a homologous template but, on the other hand, is error-prone (Burma et al., 2006; Davis & Chen, 2013). In principle, NHEJ requires several steps, (i) detecting both DNA ends, (ii) DSB processing and forming a synaptic complex, and lastly, (iii) re-ligation (Davis & Chen, 2013; Weterings & Chen, 2008). The NHEJ process begins with binding the Ku70/80 heterodimer to the broken ends. The DNA-Ku scaffold stimulates the DNA-dependent protein kinase catalytic subunit (DNA-PKcs), creating the DNA-PKcs-Ku synaptic complex with DNA termini. After DNA-PKcs autophosphorylation, other NHEJ enzymes reach the DNA termini. DNA-PKcs phosphorylates multiple additional enzymes like Artemis, X-ray repair cross-complementing protein 4 (XRCC4), DNA ligase IV, and XRCC4-like factor (XLF). Subsequently, DNA processing of single-strand overhangs is mediated by polymerases, as well as by the Artemis nuclease. Finally, the ligation step is mediated by the XRCC4-DNA ligase IV-XLF complex (Davis & Chen, 2013; Weterings & Chen, 2008; Yang et al., 2020). Depending on the configuration of the DNA ends, polymerases and nucleases process the imperfect DNA ends, which results in the random insertion and deletion of DNA bases, forming indels (Bétermier et al., 2014; Yang et al., 2020; Zhao et al., 2020).

1.2.2.2 Homology-directed repair (HDR)

HDR is activated only in the cell cycle's S and G2 stages. HDR includes homology-directed repair triggered by a single-stranded oligodeoxyribonucleotide (ssODN) template and controlled by breast cancer susceptibility protein and Radiation sensitive 52 (BRCA1-RAD52), and also homologous recombination, triggered by a double-stranded oligodeoxyribonucleotide (dsODN) template (e.g. sister chromatid) and controlled by BRCA2-RAD51 (Smirnikhina et al., 2022). HDR is an error-free mechanism achieved using homologous sequences with several consecutive stages (Helleday et al., 2007; Li & Heyer, 2008). First, a 5′-3′ resection is performed at the DSB end with

Mre11/Rad50/Nbs1 complex assistance (Helleday et al., 2007; Shrivastav et al., 2008; Yang et al., 2020). MRN boosts the C-terminal-binding protein interacting protein (CtIP), and Nbs1 produces short single-stranded overhangs. The exonuclease 1 (Exo1) and the DNA Replication Helicase/Nuclease 2 (Dna2)/ bloom syndrome protein (BLM) complex generates long 3′ ssDNA overhangs. Secondly, replication protein A (RPA) coats the overhang. Working as mediators, the BRCA1, BRCA2, and partner and localizer of BRCA2 (PALB2) exchange RPA to DNA repair protein RAD51 homolog 1 (RAD51), forming a displacement loop (D-loop) from the homologous DNA template and ssDNA (Yang et al., 2020). Lastly, one of the HDR sub-pathways is stimulated, including the synthesis-dependent strand-annealing (SDSA) pathway, the classical double-strand break repair (DSBR), break-induced replication (BIR), and the single-strand annealing (SSA) pathway (Pardo et al., 2009; Ranjha et al., 2018). In DSBR, a double Holiday junction is formed and processed by a resolvase into a non-crossover or crossover outcome to finish the repair pathway (Kass & Jasin, 2010; Li & Heyer, 2008; Pardo et al., 2009).

1.2.2.3 Microhomology-mediated end joining (MMEJ)

MMEJ is error-prone and one of the alt-EJ, which requires microhomologous sequences (MH) (Seol et al., 2018; Sfeir & Symington, 2015; Wang & Xu, 2017). Alt-EJ can be triggered during all stages of the cell cycle. However, the activity is increased in the S phase (Bétermier et al., 2014). MMEJ is now considered a major DSB repair pathway in yeast and mammals, which repairs DSB by annealing 2-20bp microhomologous ends. MMEJ is a multistep mechanism, which includes pre-annealing, annealing, and post-annealing processes (Seol et al., 2018; Van Vu et al., 2021). Initially, 5′-3′ end resection occurs to expose microhomologous overhangs, which activate DSB sensors for MMEJ, like human poly (ADP-ribose) polymerase-1 (PARP1), and stimulate MRE11 and CtIP complex, RIF1, and BLM, which are involved in both the MMEJ and HDR pathways. HDR demands long resections. In contrast, both short and long deletions are applicable for Alt-EJ (Bétermier et al., 2014; Seol et al., 2018; Van Vu et al., 2021; Wang & Xu, 2017). The microhomology parts are annealed to each other and form 3′-flap and DNA gaps. The 3′- heterologous flaps are eliminated by XPF/ERCC1, and then DNA polymerase fills the gaps without requiring a DNA donor (Van Vu et al., 2021; Wang & Xu, 2017; Yang et al., 2020). Finally, DNA ligase III/I (Lig3/Lig1) and X-ray repair cross-

complementing protein 1 (XRCC1) initiate DNA end ligation (Patterson-Fortin & D'Andrea, 2020; Sfeir et al., 2024).

1.2.3 Mitotic cells and post-mitotic neurons

In eukaryotic cells, mitosis into two genetically equal daughter cells undergoes four cell cycle stages: G1, S, G2, and M (Figure 3). G1 is a growth stage. Followed by the replication stage S1 (Herrup, 2013; Yang & Herrup, 2007). A preparation stage, G2, is followed by the chromosome segregation stage, M (Herrup, 2013). Some dividing cells leave the cell cycle and join the reversible resting stage G0. However, post-mitotic cells, such as neurons, remain in prolonged G0 and are unable to divide (Yoshikawa, 2000).

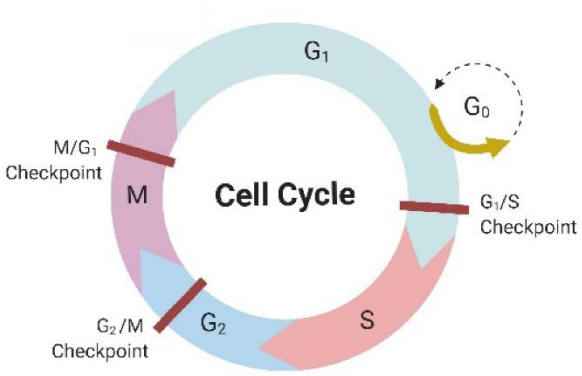

Figure 3: Stages of the cell cycle. Reproduced from (Smirnikhina et al., 2022). https://creativecommons.org/licenses/by/4.0/

Several regulatory proteins control the progression of the cell cycle. These include cyclins and cyclin-dependent kinases (CDKs) in the S to M stage transition. To restrain the cell cycle re-entry in G0/G1, mitotic growth factors control the cell cycle and increase the Cyclin D-CDK4/6 complex function. Additionally, they improve the function of the Cyclin E-CDK2 complex, which controls G1/S transition. Cyclin E-CDK2 inhibitors enhance p21, p27, and p53 function, leading to cell cycle arrest at G1 checkpoint. In addition, at G0 stage, the lack of Cyclin A controls re-differentiation (Gupta et al., 2021). As mentioned before, in genome editing, HDR is activated in the S and G2 stages of the

cell cycle in mitotic, dividing cells and rarely in post-mitotic neurons. Whereas error-prone NHEJ is accomplished in both mitotic and post-mitotic neurons. Advancements in genome editing specificity, efficiency, and delivery methods will further enhance the therapeutic development in post-mitotic neurons and the retina (Nishiyama et al., 2017).

1.3 DNA demethylation and TET3

In epigenetics, methylation at the position C-5 of cytosine (5-methylcytosine; 5mC) is an essential functional modification of genomic DNA (Guo et al., 2011; Weng et al., 2013). It was first discovered by W. G. Ruppel in 1898 in Mycobacterium tuberculosis (Ruppel, 1898). Following that, many discoveries were made concerning 5mC. CpG dinucleotide methylation is found in mammals, and minimal levels of non-CpG methylation are detected in pluripotent stem cells (Ramsahoye et al., 2000). DNA methyltransferase (DNMTs) enzymes accumulate 5mC and are responsible for the introduction and maintenance of methylation (Kohli & Zhang, 2013). The main roles of 5mC are genomic imprinting, X-chromosome inactivation, silencing of genes and genetic elements, and transcription regulation (BESTOR, 2004; Jaenisch & Bird, 2003). DNA demethylation is found in several biological processes, whether active or passive (Kohli & Zhang, 2013; Kong et al., 2019). The elimination of the methyl group from 5mC results in active DNA demethylation, whereas the loss of 5mC in DNA replication causes passive DNA methylation (Kohli & Zhang, 2013). Studies show that active DNA demethylation might occur in post-mitotic cells (Guo et al., 2011). Ten-Eleven translocation (TET) enzymes, including TET1, TET2, and TET3, oxidize 5-methylcytosine (5mC) to 5-hydroxymethylcytosine (5hmC) and then into 5-formylcytosine (5fC) and/or 5-carboxylcytosine (5caC) in a 2-oxoglutarate- and Fe (II)-dependent response (Ciccarone et al., 2014; Schuermann et al., 2016; Li et al., 2015). TETs are epigenetic regulators of gene expression, in which the 5mC conversion process initiates active DNA demethylation in DNA repair mechanisms in neurons and other cell types (Ciccarone et al., 2014; Yu et al., 2015). Moreover, TET proteins influence embryonic development, stem cell function, and differentiation (Ciccarone et al., 2014). TET Proteins contain a C-terminal catalytic domain consisting of a double-stranded β-helix (DSβH) and a cysteine-rich domain (Kohli & Zhang, 2013; Ross & Bogdanovic, 2019; Wu & Zhang, 2017). Moreover, TETs are iron (II)/α-ketoglutarate (Fe (II)/α-KG) -dependent dioxygenases (Wu & Zhang, 2017). TET1 and TET3 have a chromatin-associated CXXC domain that

binds to CpG sequences (Kohli & Zhang, 2013; Ross & Bogdanovic, 2019). Furthermore, TET3 has several isoforms: TET3o, found in oocytes, and TET3 short (TET3s), neither of which have a CXXC domain (Figure 4). TET3 full-length (TET3FL) and TET3 isoforms are increased in neuronal differentiation. In addition, TET1, TET3s, and TET3o have higher demethylation activity in comparison to TET3FL (Jin et al., 2016).

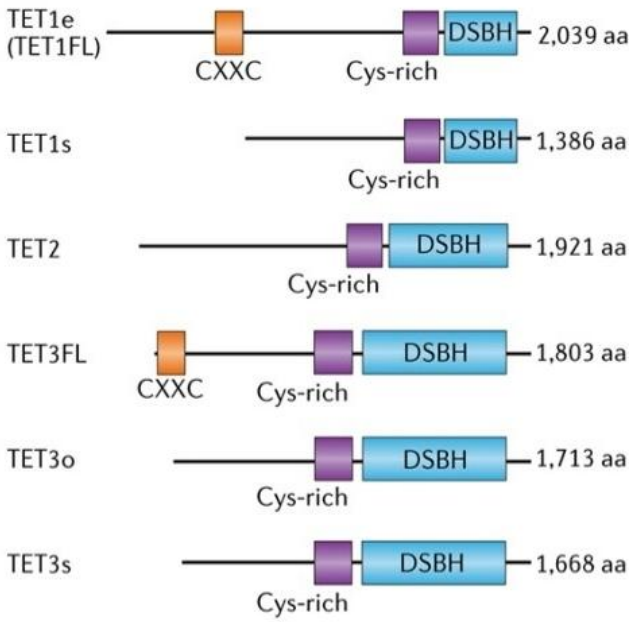

Figure 4: Structure of TET proteins. Reproduced from (Wu & Zhang, 2017). With permission from Springer Nature, License Number 5911011011468

Studies showed that TET3 is critical in early embryonic development and highly found in zygotes, cortex, and oocytes (Gavin et al., 2013; Hill et al., 2014; Santiago et al., 2014; Sun et al., 2014). During neuronal differentiation, TET2, TET3, and 5hmC levels are elevated. In Xenopus, during early eye and embryonic development, TET3 is also a transcription regulator that controls several essential developmental genes (Santiago et al., 2014a; Xu et al., 2012). Cell types and development levels influence the expression levels of TET proteins (Sun et al., 2014). TET3 activity triggers and controls ATR-dependent DDR and DNA repair (Feng et al., 2019; Jiang et al., 2017). The mechanism by which the neuronal TET3 affects the DNA is unknown. The transcriptional regulators might bind to TET3, targeting various genomic positions and regulating 5hmC levels. TET3 is an epigenetic regulator of gene expression in neurons, which functionally

associates with not yet been determined transcription factors (Perera et al., 2015). It has been shown that TET3, the main TET isoform in neurons, which is found in the mouse retina, collaborates with RE1-silencing transcription factor (REST) and histone writers to stimulate gene activation through 5hmC production and NSD3-mediated H3K36 trimethylation (Perera et al., 2015). Studies indicate that PARP1 intermingles with all the TET members, in which PARP-dependent PARylation suppresses TET-dependent hydroxymethylation and demethylation of DNA, although this interaction is not fully understood. PARP inhibition positively affects TETs' function, suggesting that using PARPi in cancer may induce TET, leading to cytotoxicity in cancer cells (Tolić et al., 2022).

1.4 PARP1

The PARP family includes 17 proteins. PARP1 is essential during DNA damage using nicotinamide adenine dinucleotide (NAD+), to catalyze mono-ADP-ribose of different acceptors (Amé et al., 1999; D'amours et al., 1999; Langelier et al., 2014). PARP1 is also involved in genomic stability, cell proliferation, differentiation, and apoptosis (D'amours et al., 1999; Gao et al., 2009; Ménissier de Murcia et al., 2003). It consists of 3 domains, the N-terminal DNA binding domain (DBD), the central auto-modification domain (AMD) that comprises 3 zinc fingers (Zn I - Zn III), and the C-terminal catalytic domain (CD) (Eustermann et al., 2010; Langelier et al., 2008). Furthermore, PARP1 is a 113 kDa protein containing 1014 amino acids (Bouchard et al., 2003). PARP1, also known as diphtheria toxin-like ADP-ribosyltransferase (ARTD1), is found in the nucleus and is responsible for 90% of the PARylation activity (D'amours et al., 1999; Huletsky et al., 1989; Ogata et al., 1981). Poly(ADP-ribosyl)ation (PARylation) is a post-translational modification catalyzed by PARP enzymes, using NAD^+ to synthesize and attach linear or branched poly(ADP-ribose) (PAR) chains onto specific amino acid residues of target proteins (Perina et al., 2014). DSBs and SSBs trigger PARP1, which acts as a sensor for DNA damage (Masutani et al., 1999; Ménissier et al., 1997; Okano et al., 2003). In HDR, PARP1 interferes with the MRN complex by activating BRCA1 through PARylation. BRCA1 is important not only for the early resection step but also in strand invasion, attaching to receptor-associated protein 80 (RAP80). In NHEJ, PARP1 connects to Ku70-Ku80, promoting the activation of DNA-PKcs. In addition, it also PARylates DNA-PKcs in order to promote its kinase activity. During chromatin remodeling, CHD2 is activated

by PARP1. In the ligation step, XRCC4 and LIG4 are both regulated by PARP1 (Ray Chaudhuri & Nussenzweig, 2017). In MMEJ, PARP1 is involved in recruiting MRN complex and CtIP, which control DSBs repair (Huang & Kraus, 2022) (Figure 5).

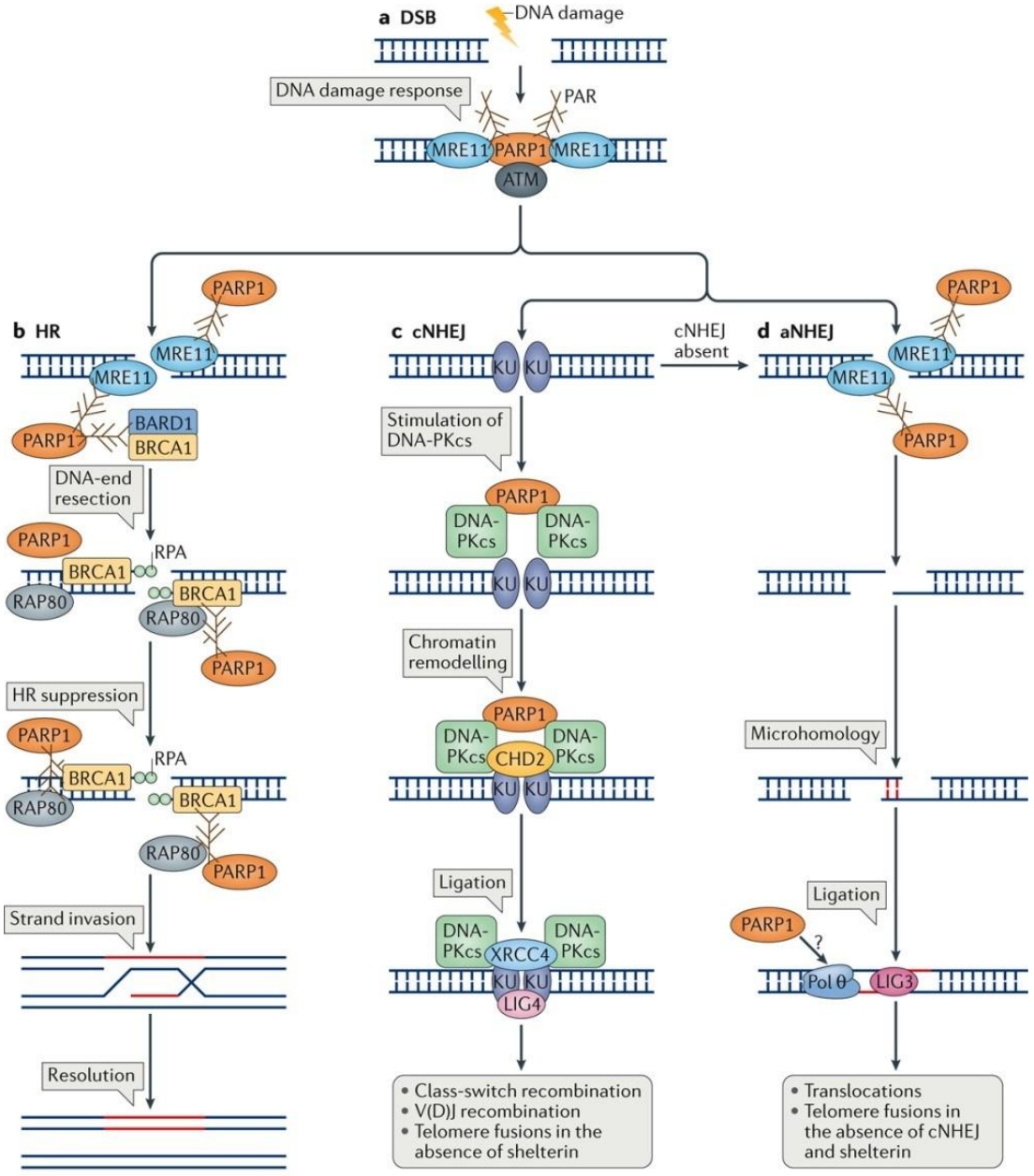

Figure 5: PARP1 and DNA DSB repair mechanisms. (A) PARP1 recognizes DSB and activates DNA damage response by interfering with MRE11 and ATM.(B) PARP1 has a function in HDR due to its interaction with MRE11, BRCA1, and BARD1. (C) In cNHEJ, PARP1 has a role through DNA-PKcs, and CHD2 association. (D) PARP1 is involved in aNHEJ. Reproduced from (Ray Chaudhuri & Nussenzweig, 2017). With permission from Springer Nature, License Number 5907231325083.

PARP inhibitors (PARPi) contend against NAD+ binding to PARP1. FDA-approved PARPi, such as Olaparib, Rucaparib, Niraparib, and Talazoparib, as anti-cancer medications, which are effective therapy options for ovarian, breast, pancreatic, and prostate cancers (Huang & Kraus, 2022).

1.5 The human inducible Neurogenin iPS (iNGN) cell line

INGNs are modified PGP1 iPS cells that are human-induced pluripotent stem cells (hiPSCs) from the personal genome project obtained from healthy adult male skin fibroblasts and then underwent reprogramming through the four Yamanaka transcription factors (Oct-4, Sox2, Klf4, and c-Myc), followed by the introduction of a bicistronic doxycycline-inducible Neurogenin expression cassette that was stably introduced using lentiviral gene delivery (Busskamp et al., 2014; Lam et al., 2017). Overexpression of Neurogenin-1 and Neurogenin-2 after adding doxycycline and activating the TET-On system triggers the differentiation of the cells into bipolar neurons within four days. This results in postmitotic homogenous bipolar neurons in a short time. Differentiated iNGNs are not viable for more than 28 days. To overcome this hurdle and ensure a successful long-term culture, astrocyte co-culture boosts neuron viability and synaptogenesis through physical and chemical factors (Busskamp et al., 2014; Lam et al., 2017). DNA repair mechanisms were studied in different model systems correlated with the cell cycle, including the iNGN cells. They found that the expression of NHEJ DNA repair pathway proteins remained constant without an abrupt decline during differentiation. In contrast, HDR and MMEJ decreased after the cells stopped cycling. These results resemble the *in-vivo* retinal activity. Moreover, regardless of the differentiation state, NHEJ was higher than HDR and MMEJ. INGNs, as an *in-vitro* model, can be a valuable candidate for studying DNA repair pathway engineering and achieving precise genome editing (Pasquini et al., 2020). The TET3KO iNGN cell line was produced using CRISPR Cas9 technology by deleting exon 7 and exon 8, resulting in the absence of functional TET3. The levels of TET3 transcripts were found to be significantly decreased in the TET3KO iNGNs, while TET1 and TET2 remained unaffected. Moreover, 5mC and 5hmC levels were quantified during the differentiation of both WT and TET3KO cells. In undifferentiated TET3KO cells, 5mC levels are higher compared to WT cells. However, on day 8 of differentiation of TET3KO neurons, 5hmC levels were decreased compared to WT neurons (Splith, 2019).

1.6 Transgene expression regulatory systems

Regulation of transgene expression is a cornerstone for various applications in the biomedical research field, such as functional genomics, gene therapy, genetically engineered transgenic animals used as human disease models, and biopharmaceutical production (Das et al., 2004; Fussenegger, 2001; Zhou et al., 2006) . To study the impact of gene activation and inactivation, transgene expression systems regulate the temporal and/or spatial control of gene expression (Bacaj & Shaham, 2007; Vilaboa et al., 2011). Temporal regulation requires gene switches containing two components: a ligand-dependent transactivator or inhibitor and a transactivator-responsive promoter. This includes tetracycline-responsive transactivators /inhibitors, mammalian steroid receptor-derived transactivators (mifepristone and tamoxifen), and rapamycin-induced transactivators. On the other hand, spatial regulation needs physical forces-activated promoters like heat shock promoters and radiation-induced promoters (Vilaboa et al., 2011).

1.6.1 Tetracycline-regulatable systems

The tetracycline regulatable systems control transgene expression in various organisms such as mammalian cell lines, plants, yeast, Drosophila, mice, and rats (Freundlieb et al., 1999; Stieger et al., 2006). There are three forms: the tetracycline-controlled transactivator system (tTA) or Tet-Off system, the reverse tetracycline-controlled transcriptional activator system (rtTA) or Tet-On system, and the tetracycline-controlled transcriptional silencer (tTS) (Zhu et al., 2002). First, the tetracycline-controlled transactivator system, which is a fusion between Tetracycline repressor (TetR) encoded in Tn10 from *Escherichia coli* and the transcription activator of the herpes simplex virus (VP16) (Forster et al., 1999; Gossen et al., 1995; Guiner et al., 2007; Shockett & Schatz, 1996; Yin et al., 1996; Zhu et al., 2002). Without tetracycline or its derivative doxycycline, tTA attaches to tet operator sequences (TetO) linked upstream of the promoter sequence of the human cytomegalovirus promoter (Pcmv), triggering gene expression (Zhu et al., 2002). However, in the presence of doxycycline (Dox), tTA disconnects from TetO, preventing gene expression (Gossen et al., 1995; Zhu et al., 2002). In contrast, the reverse tetracycline-controlled transcriptional activator system contains rtetR and VP16 and needs Dox to trigger expression (Freundlieb et al., 1999; Gossen et

al., 1995; Zhu et al., 2002). Finally, the tetracycline-controlled transcriptional silencer system comprises TetR and the KRAB domain. In the absence of Dox, the mechanism of action differs from that of tTA. tTS's connection to TetO represses expression, and with the addition of Dox, tTS disconnects from TetO, triggering gene expression (Freundlieb et al., 1999; Guiner et al., 2007; Zhu et al., 2002).

1.7 Drug-inducible CRISPR/Cas9 system (iCas)

To enhance CRISPR Cas9 precision and to overcome unwanted outcomes such as cellular toxicity and off-target cleavage, drug-inducible CRISPR/Cas9 systems were invented (Zhang et al., 2019; Zhao et al., 2018). The development of these systems marked a significant step towards timing expression and the ability to switch Cas9-mediated cleavage on and off, which is essential in various applications, like in cell signaling pathways or to study mammalian development through manipulating the regulatory networks of a certain tissue at a particular time (Liu et al., 2016). The drug-inducible CRISPR/Cas9 systems are divided into two groups according to whether the drug induction happens at the transcription or posttranslational level. The first group contains the Tet-On/Off system and Cre-dependent system. Whereas the second group contains various systems such as chemically induced proximity systems (CIP), intein splicing system, and 4-Hydroxytamoxifen-Estrogen Receptor based and nuclear localization systems, including iCas and Hybrid drug Inducible CRISPR (HIT) (Zhang et al., 2019). The iCas system offers several advantages, it is fast, versatile, reversible, simple to execute, has low background activity, and allows spatiotemporal regulation (Liu et al., 2016). This system was developed by fusing Cre recombinase with a mutated ligand-binding domain of ERT2, which is controlled by 4-OHT. Four ERT2 domains are attached to SpCas9, 2 to both C and N terminus. The ERT2 isolates Cas9 in the cytoplasm, and following the addition of 4-OHT, it translocates into the nucleus and resumes the editing task (Figure 6) (Liu et al., 2016; Zhao et al., 2018).

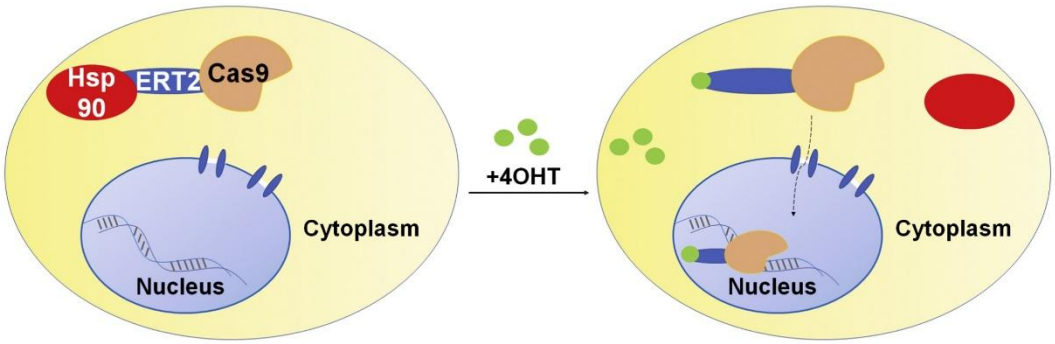

Figure 6: Schematic representation of the iCas system approach. 4-OHT activates the inducible Cas9 by binding to the ERT2 domains and transferring it from the cytoplasm to the cell nucleus, initiating DNA DSB repair. Reproduced from (Zhang et al., 2019). https://creativecommons.org/licenses/by-nc-nd/4.0/.

1.8 Methods to quantify genome editing events

Various techniques were developed to evaluate genome editing efficiency and to determine the outcomes (Germini et al., 2018; Li et al., 2023). Sequencing-based techniques include the time-consuming Sanger DNA sequencing and the more costly next-generation sequencing (NGS) followed by data analysis via software such as CRISPR Genome Analyzer CRISPR-GA (Güell et al., 2014; Sanger et al., 1977). The tracking of indels by decomposition (TIDE) method, which is based on Sanger DNA sequencing data and requires TIDE software, needs high-quality PCR products for the analysis of indel generation at the cleavage site (Brinkman et al., 2014). On the other hand, DNA denaturation-based techniques such as PCR single-stranded conformational polymorphism (SSCP) analysis or denaturing high-performance liquid chromatography (DHPLC) are only able to analyze short fragments (Germini et al., 2018; Inazuka et al., 1997; Qiu et al., 2004). Moreover, mismatch-sensitive endonucleases such as the T7 and Surveyor nucleases are time consuming and can give false positive outcomes due to poor recognition of perfectly edited DNA strands and indels (Germini et al., 2018; Hasan et al., 2023; Wang et al., 2015). As alternative approaches, indirect measurement of mutagenic DNA-DSB repair with fluorescent reporters were used, such as Traffic Light Reporter system (TLR) or a bioluminescence resonance energy transfer (BRET)-based reporter (Certo et al., 2011; Wimmer et al., 2021).

1.8.1 Bioluminescence resonance energy transfer-based reporter system (BRET)

The basic principle of resonance energy transfer techniques is described as non-radiative energy transfer between donor and acceptor species using the Förster mechanism (Förster, 1948). These techniques include Bioluminescence Resonance Energy Transfer (BRET) and Försters Resonance Energy Transfer (FRET), which study protein-protein interactions and involve dipole-dipole energy transfer from a donor to an acceptor (Luker & Piwnica-Worms, 2004; Milligan, 2004; Ozawa et al., 2013; Pfleger & Eidne, 2006). There is a spectral overlap between the donor's emission and the acceptor's excitation emission (Yamakawa et al., 2002). Both techniques are applicable to live cells in real-time, cell lysates, and with purified proteins. While FRET needs external excitation from a light source, in contrast, BRET does not require any external excitation. Instead, it uses oxidation of a substrate, such as coelenterazine, and does not lead to photobleaching and autofluorescence like FRET (Pfleger & Eidne, 2006). Moreover, it is an extremely precise, reliable, and simple-to-execute technique (Hwang et al., 2019; Sun et al., 2016). A BRET-based reporter was developed to analyze DNA repair and genome editing outcomes. After cellular transfection, BRET provides accurate measurements that can be used in a wide variety of cell lines and with different sgRNAs to assess their impact on repair activity. In addition, this system has been validated as a reliable and sensitive method for assessing the influence of CRISPR-mediated downregulation of various proteins involved in DNA repair pathways (Wimmer et al., 2021). The BRET reporter system involves a donor luciferase from *Renilla reniformis* (RLuc8) with an emission maximum of approx. 410 nm, by converting coelenterazine 400a as its substrate. The energy within the light emission is transferred to the acceptor fluorophore GFP2 (Exc. ≈ 412 nm), which results in fluorescence emission at ≈ 506 nm. The intensity of emissions (I_{em}) is measured using two different transmission filters covering blue and green wavelengths. The ratio between the emission of the fluorescent acceptor and the luminescent donor is calculated, resulting in the BRET ratio (I_{em}GFP/I_{em}Luc), then normalized with a luciferase (only) control to calculate the frameshift rate. The system was generated by designing a plasmid with RLuc8 and GFP2 to study genome editing, where the target sequence is in-frame integrated using a cloning cassette between the coding sequences of RLuc8 and GFP2. The endonuclease induces a DSB in the target site, followed by activating the repair systems NHEJ/MMEJ, resulting in a frameshift of

the GFP2 coding sequence, leading to a premature stop codon. BRET transfers energy from the donor to the acceptor unless it is repaired by introducing mutagenic indels at the target cleavage site. This will consequently decrease the BRET ratio due to a lower GFP2 expression (Figure 7). The ratio metric effect of this single molecule BRET system makes it almost independent of concentration and cell number fluctuations. Comparing it with the TLR3 system using several target sites within identical target sequences gene showed similar outcomes with less variability and greater significance (Wimmer et al., 2021).

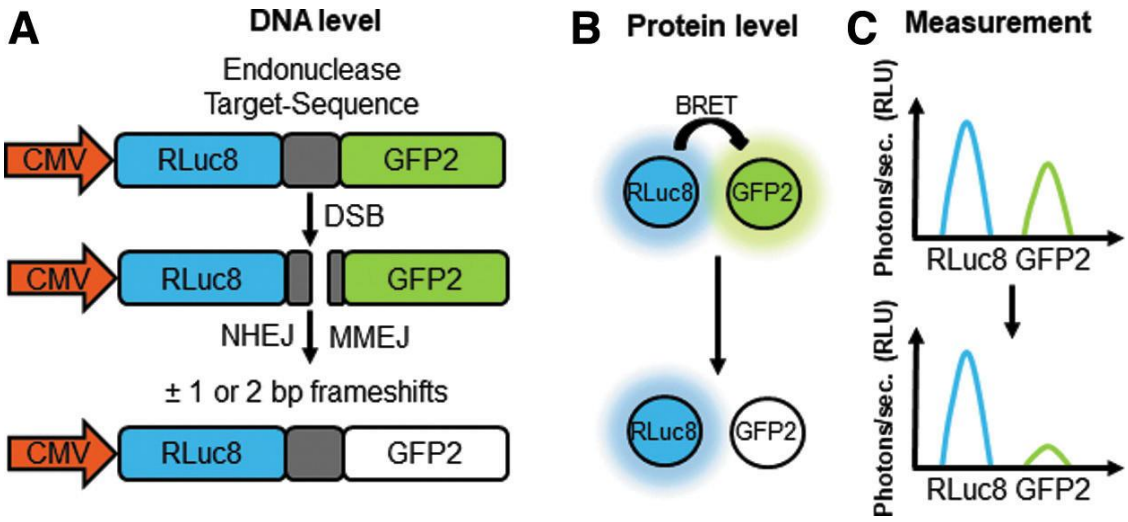

Figure 7: Schematic representation of Bioluminescence resonance energy transfer (BRET) reporter. (A) A CMV promoter followed by an in-frame endonuclease target sequence site between RLuc8 and GFP2. NHEJ or MMEJ repairs DSB, leading to ±1 or 2 bp frameshifts and causing premature stop codons in the GFP2. (B) A high energy transfer from RLuc8 to GFP2 in the unaffected BRET. A decreased energy transfer is stated for cleaved and repaired BRET. (C) Measurement of the signals. Reproduced from (Wimmer et al., 2021). With permission from Mary Ann Liebert, Inc., License Number 5907250237267.

1.9 Pathway engineering approaches

Several studies have been conducted focusing on modulating and engineering DNA repair pathways to enhance the precision of genome editing in various model systems through reversible chemical inhibitors or overexpression, such as improving HDR via inhibiting the NHEJ pathway by targeting the responsible proteins (Pawelczak et al., 2018). It has

been shown that after using ligase IV inhibitor, enhancement of HDR was noticed (Hu et al., 2018). In addition, the use of pharmacological inhibition of DNA-PKcs and Ku70/80 can increase HDR-mediated repair events as a result of NHEJ reduction (Gavande et al., 2020; Robert et al., 2015). Moreover, improving HDR by cell cycle synchronization using nocodazole (Lin et al., 2014). In cancer research, inhibiting specific DNA repair pathways can be useful when combined with chemotherapeutic drugs (Helleday et al., 2008). Furthermore, epigenetic inhibitors can be utilized to regulate DNA repair (Karakaidos et al., 2020). The majority of these studies were conducted in dividing cells *in-vitro* and there has not been much progress so far in post-mitotic neurons, even though this is necessary prior to *in-vivo* applications in the retina.

2 Aim of the study

This study aims to characterize and analyze DNA double-strand break repair mechanisms to improve CRISPR Cas-mediated genome editing efficacy in mature neurons using iNGN cell lines as a relevant *in-vitro* cell culture model system. Additionally, the iNGN TET3KO cell line is further investigated to determine the impact of the TET3 protein on DNA repair at various stages of differentiation. A comparison of the Cas9 and iCas systems, using the iNGNs as well as the HEK293T cell line as an additional control, allows a more informed choice of the system to use. Identifying the effects of engineering the DNA repair pathways by modulating PARP1 protein level is of particular interest. This study also utilizes the BRET reporter system to quantify genome editing outcomes.

3 Material and methods

3.1 Material

3.1.1 Chemicals and reagents

Table 1: Chemical and reagents

Name	Manufacturer
6x Purple DNA loading dye	New England Biolabs (NEB), Frankfurt, Germany
Accutase	Anprotec, Bruckberg, Germany
Agarose	Genaxxon Bioscience, Ulm, Germany
Boric acid	Carl Roth, Karlsruhe, Germany
Coelenterazine 400a	Nanolight Inc., Pinetop, USA
Corning Matrigel Growth Factor Reduced (GFR) Basement Membrane Matrix, LDEV-free	Corning, Wiesbaden, Germany
DPBS, no calcium, no magnesium	Thermo Fisher Scientific (Gibco), Waltham, USA
Dimethylsulfoxid (DMSO)	Merck, Darmstadt, Germany
DNA Stain Clear G	SERVA, Heidelberg, Germany
EDTA	Sigma Aldrich, Darmstadt, Germany
Ethanol	Carl Roth, Karlsruhe, Germany
Geltrex LDEV-Free, hESC-Qualified, Reduced Growth Factor Basement Membrane Matrix	Thermo Fisher Scientific (Gibco), Waltham, USA
Glycine	Carl Roth, Karlsruhe, Germany
Isopropanol	Sigma Aldrich, Darmstadt, Germany
KCl	Carl Roth, Karlsruhe, Germany
KH_2PO_4	Sigma Aldrich, Darmstadt, Germany
L-Glutamine 100X	Anprotec, Bruckberg, Germany

Lipofectamine Stem Transfection Reagent	Thermo Fisher Scientific (Invitrogen), Waltham, USA
Luria Broth (LB)	Thermo Fisher Scientific (Invitrogen), Waltham, USA
Methanol	Carl Roth, Karlsruhe, Germany
$MgCl_2$	Carl Roth, Karlsruhe, Germany
Na_2HPO_4	Carl Roth, Karlsruhe, Germany
NaCl	Sigma Aldrich, Darmstadt, Germany
Polyethylenimine	Polysciences, Warrington, USA
SDS	Carl Roth, Karlsruhe, Germany
Skim milk powder for botting	SERVA, Heidelberg, Germany
T4 DNA ligase	New England Biolabs (NEB)
TRIS	Carl Roth, Karlsruhe, Germany
Triton X-100	Carl Roth, Karlsruhe, Germany
TrypLE Express Enzyme (1X), no phenol red	Thermo Fisher Scientific (Gibco), Waltham, USA
Tween 20	Carl Roth, Karlsruhe, Germany

3.1.2 Media and Supplements

Table 2: Media and Supplements

Name	**Manufacturer**
B-27 Supplement (50x), serum-free	Thermo Fisher Scientific (Gibco), Waltham, USA
DMEM High Glucose	Anprotec, Bruckberg, Germany
DMEM/F-12 (1:1) + L-Glutamine + 15 mM HEPES	Thermo Fisher Scientific (Gibco), Waltham, USA
Fetal Bovine Serum	Anprotec, Bruckberg, Germany
GlutaMAX Supplement	Thermo Fisher Scientific (Gibco), Waltham, USA
L-glutamine	Anprotec, Bruckberg, Germany

Neurobasal-A Medium	Thermo Fisher Scientific (Gibco), Waltham, USA
RevitaCell Supplement (100X)	Thermo Fisher Scientific (Gibco), Waltham, USA
StemFlex Medium	Thermo Fisher Scientific (Gibco), Waltham, USA
Y-27632 (Dihydrochloride)	Stem Cell Technologies, Cologne, Germany

3.1.3 Buffers

Table 3: Buffers

Name	**Components**
10x PBS	1.37 M NaCl 27 mM KCl 100 mM Na_2HPO_4 18 mM KH_2PO_4 In dH_2O
10x TBE	1M Tris 0.82 M Boric acid 10 mM EDTA In dH_2O

3.1.4 Enzymes and Antibodies

Table 4: Enzymes and Antibodies

Name	**Manufacturer**
AfeI	New England Biolabs (NEB), Frankfurt, Germany
Anti-GAPDH (rabbit, monoclonal)	Cell Signaling, Danvers,USA
Anti-rabbit IgG peroxidase conjugate (goat, polyclonal)	Sigma-Aldrich, Darmstadt, Germany

AsiSI	New England Biolabs (NEB), Frankfurt, Germany
AvrII	New England Biolabs (NEB), Frankfurt, Germany
BbsI-HF	New England Biolabs (NEB), Frankfurt, Germany
BmtI-HF	New England Biolabs (NEB), Frankfurt, Germany
BplI	Thermo Fisher Scientific, Waltham, USA
BsiWI-HF	New England Biolabs (NEB), Frankfurt, Germany
EcoRI-HF	New England Biolabs (NEB), Frankfurt, Germany
HindIII-HF	New England Biolabs (NEB), Frankfurt, Germany
KpnI-HF	New England Biolabs (NEB), Frankfurt, Germany
MluI-HF	New England Biolabs (NEB), Frankfurt, Germany
NcoI-HF	New England Biolabs (NEB), Frankfurt, Germany
NdeI	New England Biolabs (NEB), Frankfurt, Germany
NheI-HF	New England Biolabs (NEB), Frankfurt, Germany
NotI-HF	New England Biolabs (NEB), Frankfurt, Germany
NspI	New England Biolabs (NEB), Frankfurt, Germany
TET3 Polyclonal Antibody	Thermo Fisher Scientific (Invitrogen), Waltham, USA
XbaI	New England Biolabs (NEB), Frankfurt, Germany

3.1.5 Bacterial strains

Table 5: Bacterial strains

Name	Manufacturer
One Shot TOP10 Electrocomp *E. coli*	Thermo Fisher Scientific (Invitrogen), Waltham, USA
Stellar Competent Cells	Clontech, Gothenburg, Sweden

3.1.6 Markers

Table 6: Markers

Name	Manufacturer
Gene Ruler 100 bp Plus DNA Ladder	Thermo Fisher Scientific, Waltham, USA
Gene Ruler 1kb Plus DNA Ladder	Thermo Fisher Scientific, Waltham, USA
ProSieve QuadColor Protein Marker	Lonza, Basel, Switzerland

3.1.7 Polymerases

Table 7: Polymerases

Name	Manufacturer
PrimeSTAR HS DNA Polymerase	Takara, Gothenburg, Sweden
Phusion High-Fidelity DNA Polymerase	New England Biolabs (NEB), Frankfurt, Germany

3.1.8 Antibiotics

Table 8: Antibiotics

Name	Manufacturer
4-hydroxytamoxifen	Sigma Aldrich, Darmstadt, Germany
Antibiotic-Antimycotic (100x)	Thermo Fisher Scientific (Gibco), Waltham, USA
Doxycycline -hyclate > 98% HPLC	Sigma Aldrich, Darmstadt, Germany

Geneticin	Thermo Fisher Scientific (Gibco), Waltham, USA
Kanamycin	Sigma Aldrich, Darmstadt, Germany
Penicillin/Streptomycin	Anprotec, Bruckberg, Germany
Puromycin dihydrochloride	Santa Cruz, Heidelberg, Germany

3.1.9 Devices

Table 9: Devices

Name	Manufacturer
Autoclave	Syntec, New Castle, USA
BioDocAnalyze BDR 5	Biometra, Göttingen, Germany
Biometra PS 300TP	Analytik jena, Göttingen, Germany
BioPhotometer	Eppendorf, Hamburg, Germany
Centrifuge Rotina 420R	Hettich, Tuttlingen, Germany
Centrifuge Mikro 200R	Hettich, Tuttlingen, Germany
Centrifuge Mini star	VWR International, Darmstadt, Germany
CKX53 Microscope	Olympus, Hamburg, Germany
Electrophoresis chambers	Biometra, Göttingen, Germany
Electroporator	Eppendorf, Hamburg, Germany
Fluorescence Microscope BioZero	Keyence, Neu-Isenburg, Germany
Freezer(-20°C)	Liebherr, Kirchdorf an der Iller, Germany
Freezer(-80°C)	Thermo Fisher Scientific, Waltham, USA
GelDoc Go	Bio-Rad Laboratories, Hercules, USA
Gene Explorer Thermal Cycler	Bioer, Zhejiang, China
Ice machine	Scotsman, Vernon Hills, USA
Incubator	Binder, St. Georgen, Germany
Infinite M1000Pro	Tecan, Männedorf, Switzerland
Magnetic stirrer iStir HP320	Neuation, Gandhinagar, India
Micropipettes	Brand/ Eppendorf, Stuttgart, Germany /Hamburg, Germany
Microscope EP50	Olympus, Hamburg, Germany

Microwave	Siemens, Forchheim, Germany
Mini-Protean Tetra	BioRad, Hercules, USA
MSC-Advantage™	Thermo Fisher Scientific, Waltham, USA
PH meter	Mettler Toledo, Columbus, USA
Polymax 1040	Heidolph, Erlangen, Germany
Refrigerator(4°C)	Bosch, Reutlingen, Germany
Refrigerator(4°C)	Liebherr, Kirchdorf an der Iller, Germany
Scale	Ohaus, Pine Brook, USA
Shaker Certomat H	Sartorius, Göttingen, Germany
Sterilbank Laminar Flow	Thermo Fisher Scientific, Waltham, USA
Thermal Cycler GeneExplorer	Bioer, Zhejiang, China
Thermomixer comfort	Eppendorf, Hamburg, Germany
Trans-Blot Turbo (Transfer System)	BioRad, Hercules, USA
VWR lab dancer Vortex Mixer	VWR International, Darmstadt, Germany
Water bath	PolyScience, Skokie, USA

3.1.10 Kits

Table 10: Kits

Name	**Manufacturer**
DNA clean & concentrator-25	Zymo Research, Irvine, USA
ECL Western Detection Kit	Amersham Bioscience, Bannockburn, USA
Gel and PCR Clean-Up	Macherey-Nagel, Düren, Germany
In-Fusion HD Ecodry Cloning Kit	Takara, Gothenburg, Sweden
NucleoSpin Plasmid	Macherey-Nagel, Düren, Germany
Pierce BCA Protein Assay Kits	Thermo Fisher Scientific, Waltham, USA
Plasmid Maxi Kit	Qiagen, Hilden, Germany
Plasmid Midi Kit	Qiagen, Hilden, Germany
PureLink Genomic DNA Mini Kit	Thermo Fisher Scientific (Invitrogen), Waltham, USA

3.1.11 Oligonucleotides

The oligonucleotides were acquired from Metabion (Planegg-steinkirchen, Germany) at 100 µM.

Table 11: Oligonucleotides

Name	**Sequence 5´→3´**
M13 for	CAGGAAACAGCTATGAC
M13 rev	GTAAAACGACGGCCAG
BGHrev	TAGAAGGCACAGTCGAGG
eGFPr1	CAGCTCGATGCGGTTCACCAGGGTGTCGCC
MY10GFPTLR	CTCTGGCTAACTAGAGAACCCACTGC
Wolle610	GACTATCATATGCTTACCGT
MY-68 T7 F	GTTTTGGCAGTACATCAATGGGCG
gesamtTLRf	GTTGACATTGATTATTGACTAGT
gesamtTLRr	CAGCTGGTTCTTTCCGCCTCAGAAG
GFPseqf	CTCCGCCCCATTGACGCAAATGGG
255	CTAGCTTGGGCTGCTCCAACTCCTC
MY-360	CACCCAGAGTTTCGCTGAGTTGCT
MY-361	AAACAGCAACTCAGCGAAACTCTG
BFP f	ATGAAGCTGTACATGGAGGGCA
BFP r	CCCCAGTTTGCTAGGGAGGT
SeqKas	AGCCCGACGTCGTCCAGATTG
BFP f	TCCAACGGCCCTGTGATGCAGA
pig-AsisIr	CGCGCCCCATTCGCTAGCGTAA
pig-mluI-f	ATTACGCGTATGGTGAGCAAGGGC
piggy-seq	GGAGGACATCTGGAAGAAGTTTG
TIDEf1	ATTGTCCGCAACTACAACGCCTAC
TIDEr	TCGGGGCGGATGTACACGTTG
BRETproseq	GCTTGCAGCGAGCCCACCACTGA
BRET-EF1af	CTGGCCTTTTGCTCAGGCTCCGGTGCCCGTCAG
BRET-EF1ar	TGGCGTAATCGCTAGTCACGACACCTGAAATGGAAG
Cmv-seq-r	GTGGGCAGTTTACCGTAAAT

BFP-BGH-f	TGGGGCACAAGCTTAATTGA
iCas+ef1af	GGCCAGATATACGCGGGCTCCGGTGCCCGTCAG
iCas+ef1ar	CCCATGGTGGCGGCCTCACGACACCTGAAATGGAAG
iCasseq	TAGTTAAGCCAGTATCTGCTCCC
Rluc+ef1ar	AAGTTTAAACGCTAGTCACGACACCTGAAATGGAAG
Rluc8seq	ATCTGCTCCCTGCTTGTGTGTTG
Rluc+ef1nr	GCTCGGTACCAAGCTTCACGACACCTGAAATGGAAG
ORF15+EF1a rev	CCGTTTAAACGCTAGTCACGACACCTGAAATGGAAG
PARP1+EF1a for	ATGCATTAGTTATTAGGCTCCGGTGCCCGTCAG
PARP1+EF1a rev	GTCCGGTAGCGCTAGTCACGACACCTGAAATGGAAG
PARP1seq	CGCCAGCAACGCGGCCTTTTTAC
ORF15seq	TACAATCTGCTCTGATGCCGCAT

3.1.12 Plasmids

Table 12: Plasmids

Name	**Supplier**
BRET-Reporter (pRLuc8 AvrII/BsiWI-GFP2)	(Wimmer et al., 2021).
px459 (pSpCas9(BB)-2A Puro (PX459) V2.0)	a gift from Feng Zhang (Addgene plasmid # 62988; http://n2t.net/addgene:62988; RRID: Addgene_62988) (Ran et al., 2013)
p-CMV-RLuc8	a gift from Sanjiv Sam Gambhir (Addgene plasmid # 87121; http://n2t.net/addgene:87121 ; RRID:Addgene_87121) (Loening et al., 2006).
pCMV-PARP1-3xFlag WT	a gift from Thomas Muir (Addgene plasmid # 111575;

	http://n2t.net/addgene:111575; RRRID: Addgene111575) (Liszczak et al., 2018)
FH-TET3-pEF	a gift from Anjana Rao (Addgene plasmid #49446; http://n2t.net/addgene:49446;RRID: Addgene_49446) (Ko et al., 2013)
iCas	a gift from Meng How Tan (Addgene plasmid#84232; http://n2t.net/addgene:84232; RRID: Addgene_84232), (Liu et al., 2016)
peGFPN1	Clonetech / Takara Bio Europe SAS, Gothenburg, Sweden
pSIN4-EF2-O2S	a gift from James Thomson (Addgene plasmid # 21162; http://n2t.net/addgene:21162; RRRID: Addgene21162) (Junying et al., 2009)
PARP1 KO-gRNA/Cas9 (PARP1 Knockout) (2,4)	The guide oligonucleotides were cloned into the px459 vector (Addgene #62988). Introducing PARP1 knockout by disrupting the reading frame within the human *PARP1* gene

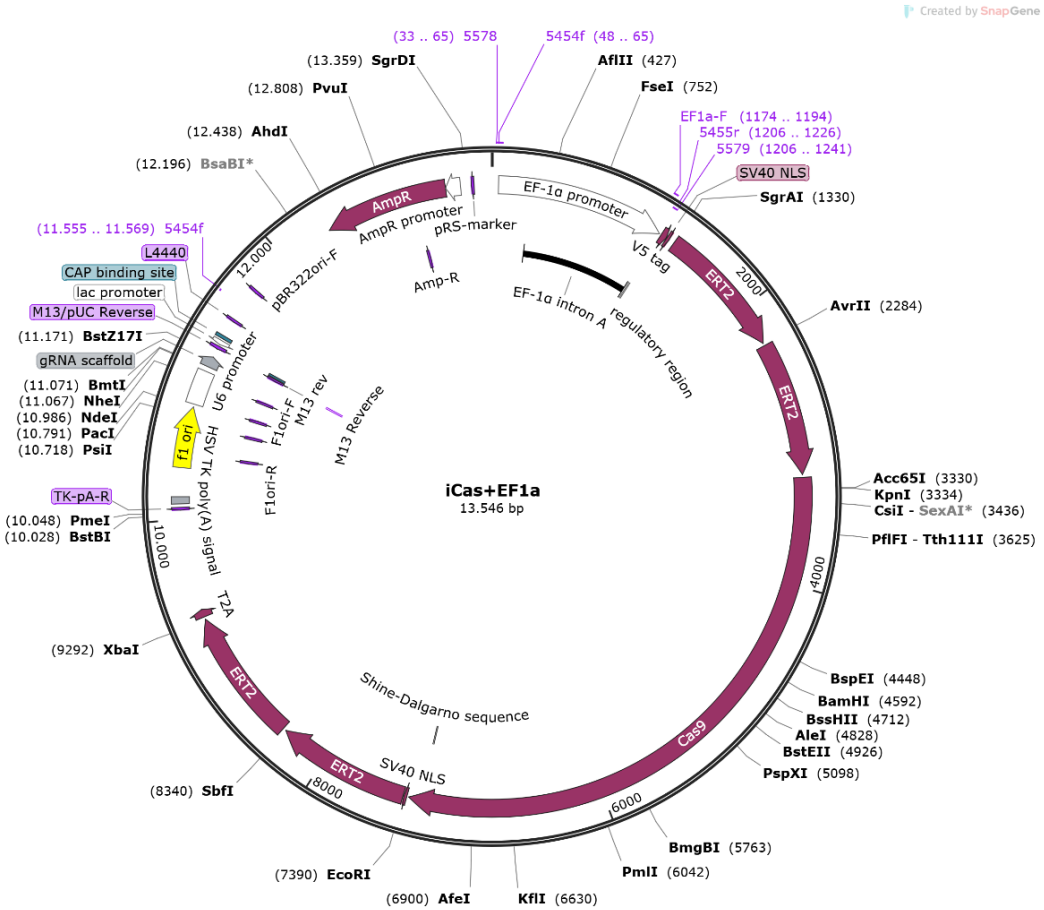

Figure 8: iCas vector map with EF1α promoter containing ERT2 domains attached to SpCas9, which 4-OHT controls.

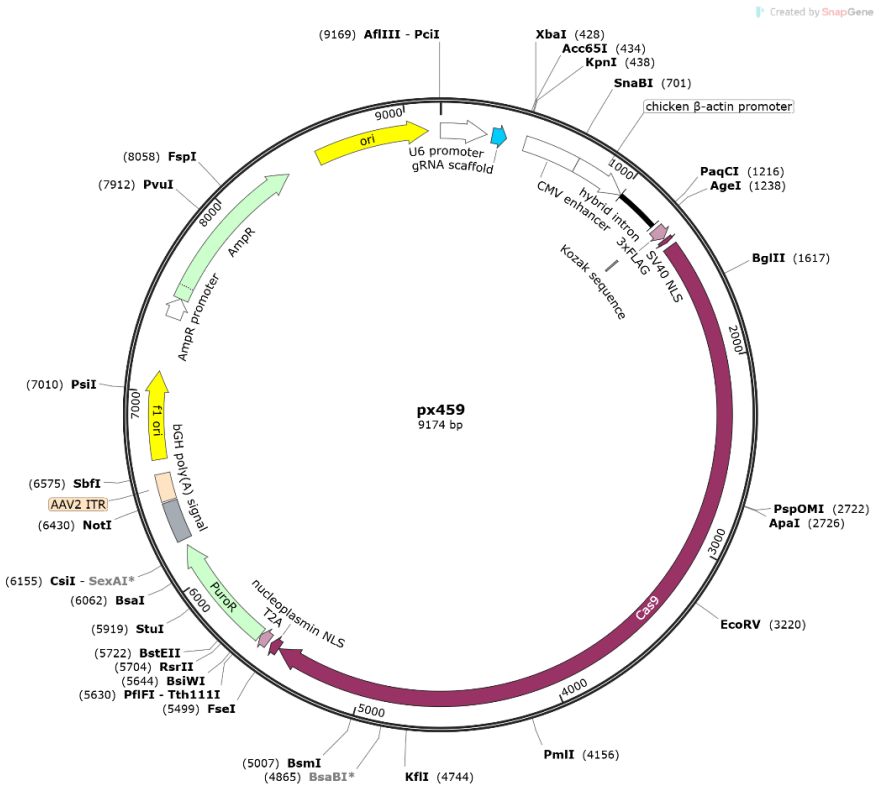

Figure 9: CRISPR Cas9 gRNA expression plasmid.

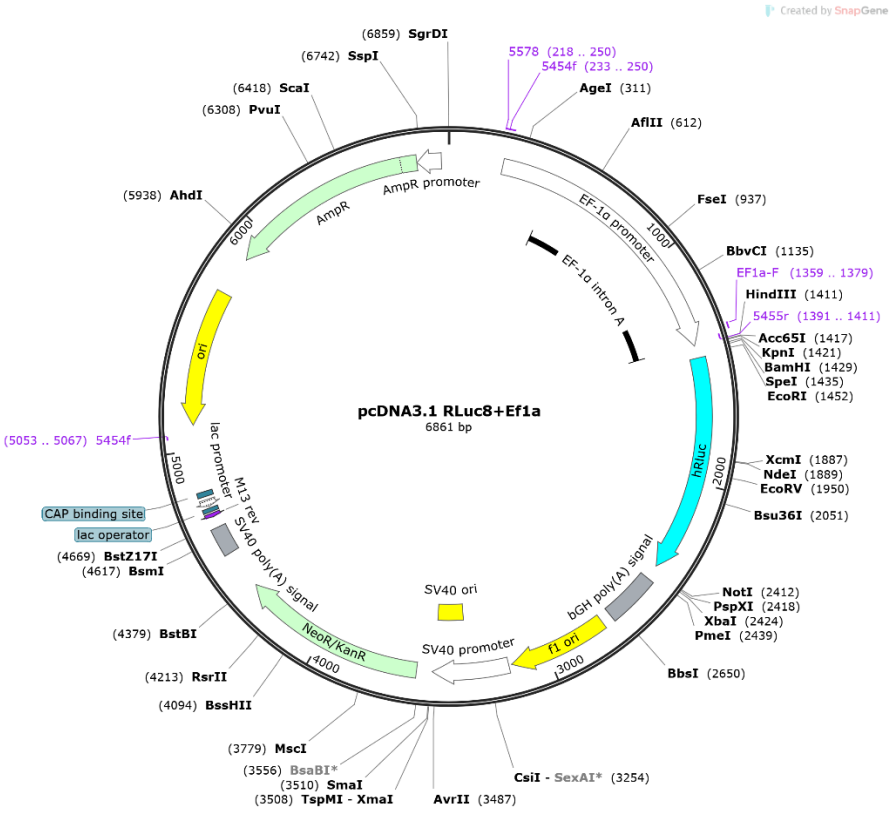

Figure 10: Rluc8 vector map with EF1α promoter.

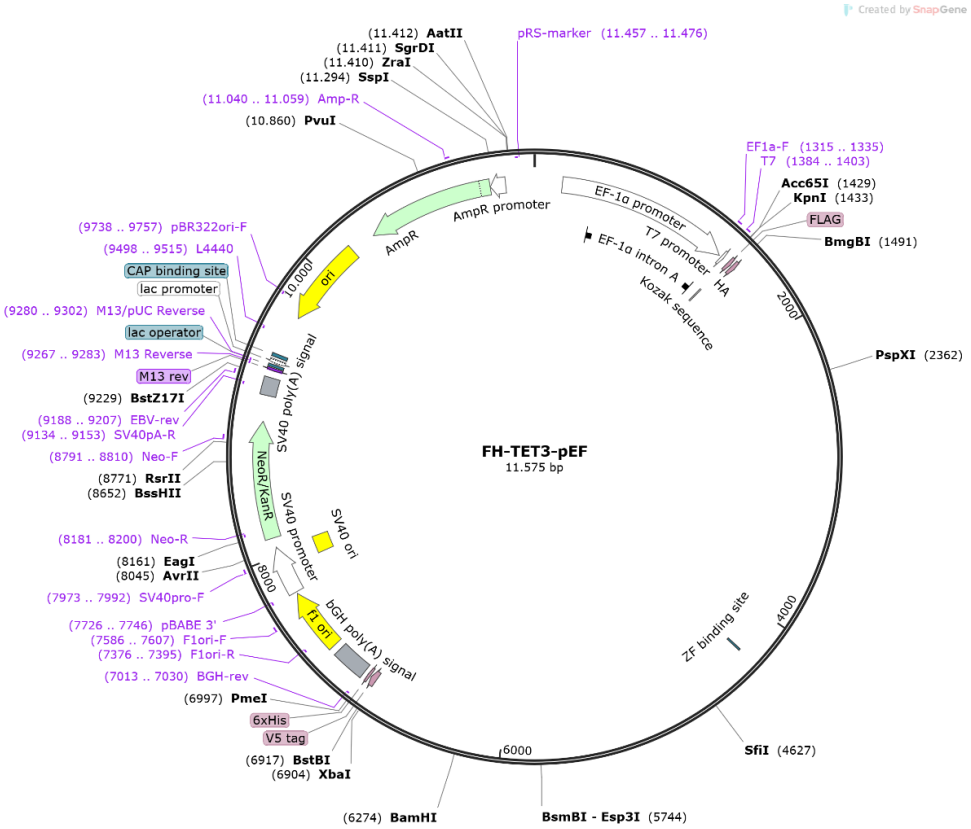

Figure 11: TET3 overexpression plasmid map.

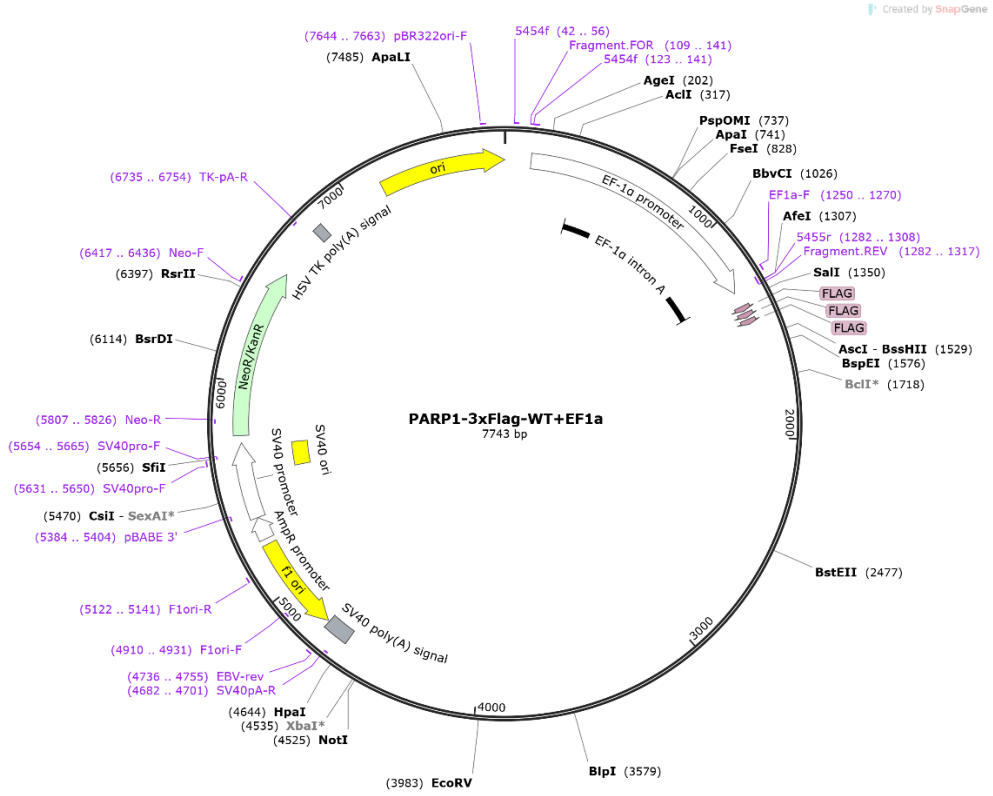

Figure 12:PARP1 overexpression plasmid map with EF1α promoter.

3.1.13 Cell lines

Table 13: Cell lines

Name	Supplier
HEK293T Cells #ATCC-CRL-3216	LGC, Middlesex, United Kingdom
iNGN WT	Dr. Stylianos Michalakis (Institute of Pharmacology, Ludwig-Maximilians-University Munich)
iNGN TET3KO	Dr. Stylianos Michalakis (Institute of Pharmacology, Ludwig-Maximilians-University Munich)

3.1.14 Software

Table 14: Software

Name	Manufacturer
BZ-8100 Observation Application v.1.10	Keyence, Neu-Isenburg, Germany
EPview	Olympus, Hamburg, Germany
Fusion-capt advance fx7 software	Vilber, Maurepas, France
i-control v.1.11	Tecan, Männedorf, Switzerland
Mendeley Reference Manager	Elsevier, Oxford, United Kingdom
Microsoft Excel	Microsoft Corporation, Redmond, USA
Microsoft PowerPoint	Microsoft Corporation, Redmond, USA
Microsoft Word	Microsoft Corporation, Redmond, USA
SigmaPlot Version 12	Systat, Schaumburg, USA
Snapgene viewer	GSL Biotech, USA

3.1.15 Consumables

Table 15: Consumables

Name	Manufacturer
Cell culture plate Cellstar 100 x 20 mm	Greiner, Kremsmünster, Austria
Cell culture plates (6-well/ 24-well/96-well)	Greiner/ Sarstedt, Kremsmünster, Austria/Nümbrecht, Germany
Cell scrapers	Sarstedt, Nümbrecht, Germany
Coverslips (20x26mm)	Thermo Fisher Scientific, Waltham, USA
Falcon tubes (15 mL/50 mL)	Greiner, Kremsmünster, Austria
Hemocytometer chamber	Neubauer, Waltham, USA
Immobilon-P Membrane, PVDF	Millipore, Darmstadt, Germany
Microtiter plate Costar 96 well white	Corning, Wiesbaden, Germany
Mini-PROTEAN TGX™ Precast Gels	BioRad, Hercules, USA
Parafilm M	Bemis, Chicago, USA
PCR tube	Biozym,Sarstedt, Germany
Pipette tips	Brand/Sarstedt/Biozym, Marktheidenfeld, Germany /Nümbrecht, Germany /Sarstedt, Germany
Reaction tube 1.5 mL/2 mL	Sarstedt/Biozym, Nümbrecht, Germany /Sarstedt, Germany
Shaker Certomat H	Sartorius, Goettingen, Germany
Sterile Serological Pipets (25 mL/10 mL/5 mL)	Greiner, Kremsmünster, Austria
vacuum filtration „rapid “-Filtermax	TPP, Schopfheim, Germany

3.2 Methods

3.2.1 Working with cell lines

3.2.1.1 Maintenance of the cells

HEK293T cells were maintained and seeded on a culture plate with prewarmed DMEM high glucose (Anprotec) supplemented with 10% FBS (Anprotec), 4 mM L-glutamine (Anprotec), and 1% Penicillin-Streptomycin (Anprotec). They were incubated at 37°C with 5% CO_2. The cells were passaged every 4-5 days by dissociating the adherent cells with 2 mL Accutase (Anprotec) after washing with 5 mL PBS. The detached cells were resuspended in 8 mL supplemented DMEM, and 1 mL of the suspension was mixed with 9 ml medium and transferred to a new plate.

INGN cell lines (iNGN WT/iNGN TET3KO) were seeded on a Matrigel-coated plate. To prepare the plates, a 100 µg/mL Matrigel aliquot was diluted in 12 mL of chilled DMEM/F-12 (1:1) + L-Glutamine + 15 mM HEPES. The plates were covered and incubated for 24 hours at 37°C with 5% CO_2. Sealed plates with Parafilm were stored at 2 - 8˚C for up to 7 days.

The cells were maintained with sterile filtered StemFlex medium containing StemFlex basal medium (Gibco), StemFlex supplement (Gibco), and 1% Antibiotic-Antimycotic (Anti-Anti) (Gibco) at 37°C with 5% CO2. The medium was changed daily or every other day to keep the cells alive.

For subculturing every 4-5 days, the cells were washed with 3 mL DPBS (Gibco), dissociated with 1 mL TrypLE (Gibco), and incubated for 5 minutes at 37°C. 1 mL DPBS was added, and the mix was transferred to a 15 mL falcon tube with 4 mL DPBS and centrifuged at 300xg for 7 minutes. The supernatant was discarded, and the pellet was resuspended in 1mL Stemflex medium with 1% RevitaCells supplement (Gibco). The cells were counted, and 300,000 cells were transferred to a coated 6-well plate with 2 mL medium and incubated at 37°C with 5% CO_2.

3.2.1.2 Thawing the cells

To thaw the HEK-293T cells, the cryotube was removed from liquid nitrogen and placed under running water. The cells were seeded in supplemented DMEM, incubated overnight at 37°C with 5% CO_2, and passaged the next day.

To thaw iNGN cell lines, the cryotube was removed from liquid nitrogen and placed under running water. The cells were transferred to a 15 mL Falcon tube, and 2-3 mL DPBS was added dropwise until the total volume reached 6 mL. The cells were centrifuged at 300 x g for 7 minutes. The supernatant was discarded, and the pellet was resuspended in 1mL Stemflex medium with 1% RevitaCells supplement (Gibco). The cell suspension was transferred to a coated 6-well plate with another 1 mL medium and incubated at 37°C with 5% CO_2**.**

3.2.1.3 Counting the Cells

The estimated cell count was determined using a clean hemocytometer chamber with a coverslip, viewed under a 10x magnification, and counted with a hand tally counter. The diluted cell suspension was counted in all four sets of 16 squares, and the average was taken and calculated using this equation: average cell counts per square x dilution factor x 10^4,

3.2.1.4 iNGN cell lines differentiation

In order to differentiate the iNGN cell lines within 4 days, 0.5 µg/mL doxycycline (Sigma Aldrich) was added to the culture medium. The neurobasal medium containing Neurobasal-A medium (Gibco), 1% Anti-Anti (Gibco), 1% GlutaMAX (Gibco), and 2% B27 (Gibco) was prepared. On the first day, the cells were cultured in StemFlex medium with RevitaCells supplement (Gibco) and doxycycline. The medium was changed to 50% StemFlex medium, 50% Neurobasal medium, and doxycycline the next day. After 24h, the medium was changed to 100% neurobasal medium and doxycycline. The medium was changed daily or every other day to keep the cells in culture.

3.2.1.5 Transfection

The day before transfection, HEK293T cells were seeded in a 24-well plate and incubated for 24 h in a humidified incubator at 37°C and 5% CO2. The medium was replaced with a fresh prewarmed supplemented DMEM. In a 1.5 reaction tube, 30 µL NaCl (150 mM) and 0.5-1 µg DNA were added and vortexed, then 40 µL PEI (Polysciences) was added, vortexed thoroughly, and incubated for 10 minutes. The mix was added dropwise in each well and incubated at 37°C with 5% CO_2. After 4-6 h, the medium was changed with fresh DMEM. The transfection was monitored the next day with a fluorescence microscope.

INGN cell lines were transfected with Lipofectamine Stem transfection reagent after 24h of seeding 70,000-100,000 cells/well in a 24-well plate at 37°C with 5% CO_2. The media used in the transfection protocol was a fresh, prewarmed DMEM with RevitaCell supplement. The transfection mixtures were prepared as follows:

Table 16: Transfection components

Tube 1	25 µL DMEM + 2 µL Lipofectamine Stem transfection reagent
Tube 2	25 µL DMEM + 400-500 ng DNA

The solution from tube 2 was added to the solution in tube 1, thoroughly vortexed, and incubated for 10 minutes at room temperature. Meanwhile, the StemFlex Medium was replaced with 0.5 mL of DMEM medium containing RevitaCell Supplement, and 50 µL of the transfection mixture was added. The cells were then incubated for 4 to 6 hours at 37°C with 5% CO_2. After this incubation period, 500 µL of StemFlex medium supplemented with RevitaCell was added. When using the iCas system, 1000 nM of 4-hydroxytamoxifen was added 4 to 6 hours post-transfection to induce the system. The cells were further incubated for 24 hours at 37°C with 5% CO_2. The results were visualized the following day using fluorescence microscopy.

3.2.1.6 BRET Assay

To perform a BRET (bioluminescence resonance energy transfer) assay after 24 hours of transfection, the medium was discarded, and the wells were washed with 500 µL 1x PBS. Then, 100 µL 1x PBS was added. The cells were detached using a cell scraper and transferred to a 1.5 mL reaction tube. The cells were subjected to two freeze-thaw cycles using liquid nitrogen and centrifuged at 21,382 × g for five minutes at 4 °C. The luciferase substrate (1µg/µL), Coelenterazine 400a (Nanolight Inc), was diluted 1:100 in 1x PBS and incubated for 20 minutes. Each sample was measured in quadruples, requiring 100 µL of the diluted substrate per well. Equal volumes (10-20 µL) of cell lysate were added to each well of a Costar white 96-well plate and measured using the Infinite M1000Pro plate photometer (Tecan). Using Microsoft Excel (Microsoft Corporation), the BRET ratio I_{GFP2}/I_{Rluc8} (I: light intensity in photons/s) and frameshift rates were determined after calculating each sample's mean and standard deviation. The values were normalized using the RLuc8 BRET ratio, 100% frameshift rate, and the uncleaved BRET reporter BRET ratio considered a 0% frameshift rate.

3.2.2 Working with DNA

3.2.2.1 PCR

PCR was performed in a Gene Explorer Thermal Cycler (Bioer) under the PCR protocol and cycling conditions listed in Tables 17 and 18 for Phusion DNA Polymerase (NEB) and in Tables 19 and 20 for PrimeSTAR HS DNA Polymerase (Takara). The Annealing temperature varies according to the primers, and a gradient PCR was performed to determine the exact temperature required.

Table 17: PCR using Phusion DNA Polymerase (NEB)

Component	**20 µL Reaction**
DNA	5 ng
$MgCl_2$ (50mM)	0.3 µL
5X Phusion HF Buffer	4 µL

10 mM dNTPs	0.4 µL
10 µM Forward Primer	1 µL
10 µM Reverse Primer	1 µL
DNA Polymerase Phusion	0.2 µL
ddH_2O	to 20 µL

Table 18: Thermocycling conditions for Phusion PCR

Step	**Number of cycles**	**Temperature**	**Time**
Initial denaturation	1X	98 °C	30 s
Denaturation	35 Cycles	98 °C	10 s
Annealing		X	20 s
Elongation		72 °C	30 s
Final Elongation	1X	72 °C	10 min
Hold	1X	10 °C	10 min

Table 19: PCR using PrimeSTAR HS DNA Polymerase (Takara)

Component	**25 µL Reaction**
DNA	(10-100 ng)
DMSO	1 µL
5X PrimeSTAR Buffer	5 µL
10 mM dNTPs	2 µL
10 µM Forward Primer	1 µL
10 µM Reverse Primer	1 µL

PrimeSTAR HS DNA Polymerase	0.25 µL
ddH_2O	to 25 µL

Table 20: Thermocycling conditions for PrimeSTAR PCR

Step	**Number of cycles**	**Temperature**	**Time**
Initial denaturation	1X	98 °C	5 s
Denaturation	40 Cycles	98 °C	10 s
Annealing		X	5 s
Elongation		72 °C	2 min
Final Elongation	1X	72 °C	10 min
Hold	1X	10 °C	10 min

3.2.2.2 Gel electrophoresis

To perform gel electrophoresis, a 1% gel with DNA Stain Clear G (SERVA) was prepared. 1 g of agarose was added to 100 mL of 1x TBE buffer and was microwaved for 1-3 min until the agarose was completely dissolved. The agarose solution was cooled to 50 °C and then poured into a gel tray with a comb in place. After 20 min, the marker and samples were loaded after adding 6X Purple loading dye (NEB) to each sample. Electrophoresis was performed at 120 V in 1% TBE buffer for 45-60 minutes. The gel was visualized using GelDoc Go (Bio-Rad Laboratories).

3.2.2.3 DNA extraction of agarose gel

After performing gel electrophoresis, the bands were cut out of the gel under UV light using proper UV protection. The gel slice was weighed and then purified with a Gel and PCR Clean-Up kit (Macherey-Nagel). For each 100 mg of agarose gel, 200 µL of provided buffer was added. The sample was incubated for 10 min at 50 °C and vortexed every 2 min until dissolved. The mixture was transferred to a column placed in a

collection tube and centrifuged at 11,000 x g for 30 sec, followed by two washing steps and a drying step. The DNA was eluted using ddH_2O.

3.2.2.4 Cloning

The instructions for In-Fusion cloning were followed to insert the desired fragment. The vector was linearized through restriction digestion. PCR primers were designed using the In-Fusion Cloning Primer Design Tool, and the insert was amplified by PCR. The amplified insert was then analyzed by agarose gel electrophoresis, isolated from the gel, and quantified. Utilizing an In-Fusion molar ratio calculator and a 2:1 insert-to-vector molar ratio, 10 µL of a mixture containing the linearized vector, the insert, and ddH_2O were added to the In-Fusion HD EcoDry pellet (Takara), incubated for 15 minutes at 37 °C, then for an additional 15 minutes at 50 °C, and finally placed on ice before proceeding with chemical transformation.

3.2.2.5 Isolation of genomic DNA

The genomic DNA of the cells was isolated using the PureLink Genomic DNA Mini Kit (Invitrogen). The cells were dissociated, transferred to a 15 mL Falcon tube containing 4 mL of DPBS, and centrifuged at 300 x g for 7 minutes. The supernatant was discarded, and the pellet was resuspended in 200 µL of 1x PBS and transferred to a tube with 20 µL of Proteinase K. Next, 20 µL of RNase A and lysis buffer were added, and the mixture was vortexed and incubated at 55°C for 10 minutes. Subsequently, 200 µL of 96-100% ethanol was added to the lysate, followed by purification steps using a column placed in a collection tube.

3.2.2.6 PCR clean up

The DNA was extracted from agarose gels using the Gel and PCR Clean-Up kit (Macherey-Nagel) as mentioned in Section (3.2.2.3). To purify DNA from reaction mixtures, the DNA Clean & Concentrator-25 (Zymo Research) was used with a column placed in a collection tube.

3.2.2.7 Restriction digestion of DNA

DNA digestion was performed using restriction enzymes obtained mainly from New England Biolabs' single and double digestion reactions. The reactions were then incubated at 37°C overnight, followed by heat inactivation if applicable. The digested DNA was analyzed using gel electrophoresis.

Table 21: Restriction digestion reaction setup

Component	**Single Digestion**	**Double Digestion**
DNA	1000 ng	1000 ng
10X Buffer	2 µL	2 µL
Restriction Enzyme	1 µL	1 µL
Restriction Enzyme	-	1 µL
ddH_2O	to 20 µL	to 20 µL

3.2.2.8 Ligation of DNA

Table 22: Ligation of DNA

Component	**Volume**
Plasmid DNA	2 µL
Insert DNA	5 µL
10 x T4 DNA ligase reaction buffer	2 µL
T4 DNA ligase (NEB)	1 µL
ddH_2O	10 µL
Total	20 µL

The samples were incubated overnight at 4 °C.

3.2.2.9 Sanger sequencing

12 µL (40 - 100 ng/µL) of plasmid DNA, 3 µL of a diluted sequencing primer (1:10), and ddH_2O were used to prepare 15 µL samples, which were sent to Microsynth Seqlab for sequencing using the Economy Run service and analyzed with SnapGene Viewer.

Table 23: Sanger sequencing samples setup

Component	Volume
Plasmid DNA (40 - 100 ng/µL) or PCR products (200 ng)	to 12 µL
Sequencing primer (1:10)	3 µL
ddH_2O	to 15 µL

3.2.3 Working with bacteria

3.2.3.1 Bacterial Culture in LB Medium

LB liquid cultures were prepared using an autoclaved LB medium and the appropriate antibiotic. The *E. coli* culture was incubated for 16-18h at 37°C and 180 rpm in 5 mL or 100 mL medium. For solid culture, LB agar plates were supplemented with the proper antibiotic. After plating *E. coli*, the plates were incubated at 37°C in an incubator.

Table 24: LB medium

Component	Volume
Luria-Broth Base	25 g
ddH_2O	to 1000 mL and autoclaved

Table 25: LB agar

Component	Volume
Luria-Broth Base	25 g
Luria-Broth Agar	7.5 g
ddH_2O	To 500 mL and autoclaved

3.2.3.2 Transformations

Electroporation was performed using a mixture of One Shot TOP10 Electrocomp *E. coli* (Invitrogen), thawed on ice, and 2.5 µL ligated plasmid DNA. The tube was incubated on ice for 5 minutes, and then 50 µL was transferred to a pre-chilled electroporation cuvette. The transformation was applied using an electroporator (Eppendorf) at 2,000 V and 5 ms. 1 mL SOC medium was immediately added to the cells, transferred into a 1.5 mL reaction tube, and incubated at 37 °C and 180 rpm for 60 min. After 1 h, the cells were centrifuged at 21,382 × g for 2 minutes. 800 µL was discarded, and the rest was used to resuspend the pellet. The cells were spread on an LB agar plate containing the appropriate antibiotic and incubated overnight at 37 °C.

For chemical transformation, Stellar Competent *E. coli* cells (Clontech) were thawed on ice. A mixture of 50 µL of competent cells and 2.5 µL ligated plasmid DNA was incubated on ice for 30 min, followed by heat shock at a 42°C water bath for 45 sec and back on ice for 1 min. Prewarmed 450 µL SOC medium was added and incubated at 37 °C 180 rpm for 60 min. The cells were centrifuged at 21,382 × g for 2 minutes, and then the supernatant was discarded. The pellet was resuspended in 100 µL SOC, spread on an LB agar plate containing the appropriate antibiotic, and incubated overnight at 37 °C.

Table 26 : SOC

Component	Volume
Tryptone	2 %
Yeast extract	0.5%
NaCl	10 mM
KCl	2.5 mM
$MgCl_2$	10 mM
$MgSO_4$	10 mM
Glucose	20 mM
ddH_2O	to 1000 mL and autoclaved

3.2.3.3 Plasmid DNA isolation

To isolate or purify plasmid DNA, the NucleoSpin Plasmid QuickPure (Macherey-Nagel) kit was used with a 5 mL overnight bacterial culture for small-scale isolation, and the final DNA pellets were resuspended in 27 µL of ddH_2O. The Qiagen Plasmid Midi or Maxi (Qiagen) kits were utilized for medium- or large-scale preparation. A 100 mL overnight bacterial culture was required, and the final DNA pellets were resuspended in 300-500 µL of ddH_2O.

3.2.3.4 Glycerol stock preparation

500 µL of the overnight culture was mixed with 500 µL of glycerol in a 2 mL cryotube and stored at -80°C.

3.2.4 Statistics

SigmaPlot Version 12 (Systat) Software was used to analyze scientific data statistically. The applied statistical tests are shown in figure legends. Statistical significance was labeled as $p < 0,05$ (*), $p < 0,01$ (**), $p \leq 0,001$ (***).

4 Results

In this study, the BRET reporter system was primarily used to evaluate DNA double-strand break repair mechanisms in iNGN cell lines, with HEK293T cells as a control. To determine the impact of TET3, the iNGN TET3KO cell line was examined, along with the overexpression of TET3 in iNGN TET3KO cells. Starting with the comparison of the Cas9 and iCas systems across all cell lines at the undifferentiated state (D0). Subsequently, iNGNs were evaluated throughout the differentiation process (D0-D4) using the CRISPR-Cas9 system. In addition, to assess the influence of PARP1 on DNA repair, PARP1 protein level modulation was investigated at D0 as well as during neuronal differentiation.

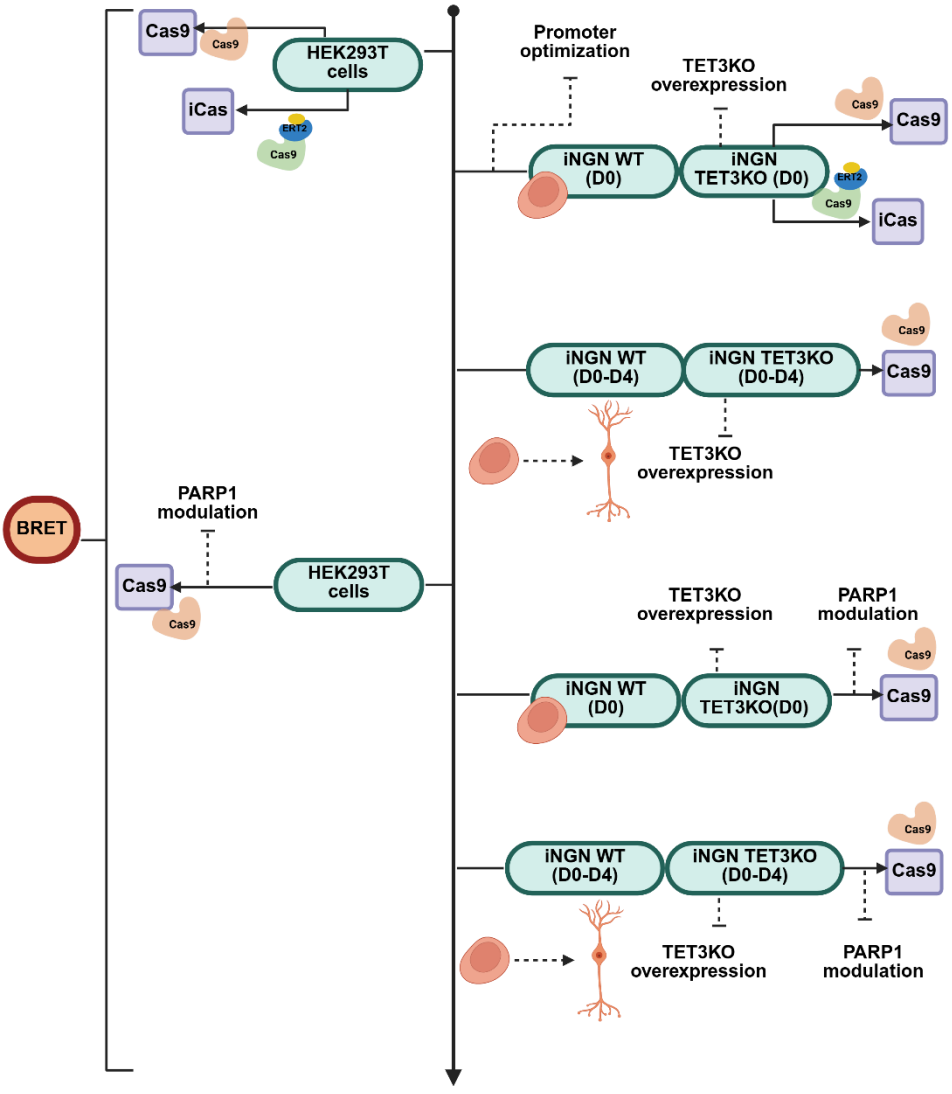

Figure 13:Graphical overview of the study

4.1 Promoter optimization

In this work, iNGN cell lines were used as *in-vitro* model systems to evaluate and study DNA repair mechanisms and genome editing in undifferentiated iPSCs, mature bipolar neurons, and throughout the differentiation process. The first essential step was ensuring proper transgene expression, which required promoter engineering. This involved replacing the CMV promoter, which can be suppressed in certain cell types, with the EF1α promoter. The process included linearizing the plasmids and removing the CMV promoter region using restriction enzymes (Figure 14A).

The EF1α promoter sequences from the pSIN4-EF2-O2S vector were amplified using PCR with the designed primers, followed by gel electrophoresis analysis and purification of the PCR products. The inserts were then added to the linearized plasmids in an in-fusion cloning reaction, followed by transformation and DNA isolation of several clones. The procedure was verified by Sanger sequencing, and the transfection results showed a significant improvement in reporter GFP expression (Figure 14B).

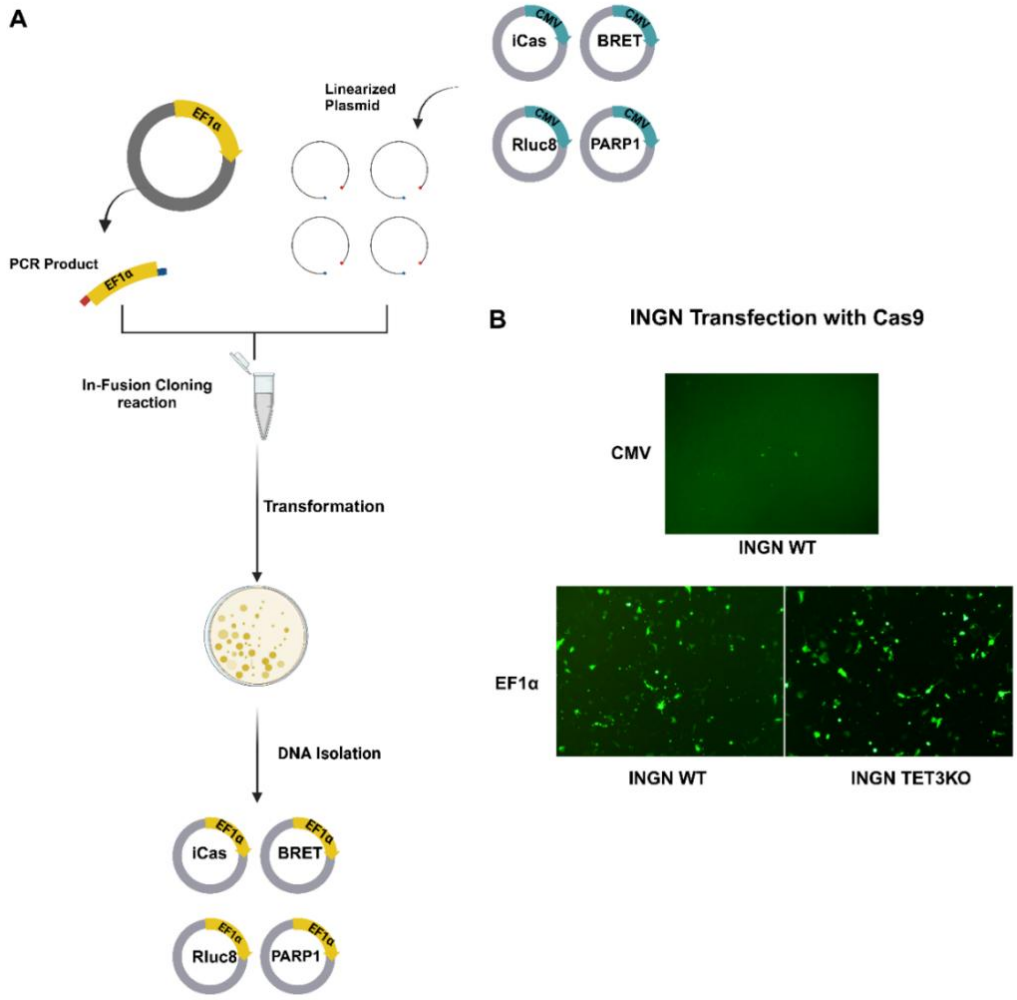

Figure 14: Promoter optimization process. (A) Generation of linearized vectors and elimination of the CMV promoter region using restriction enzymes. Design of primers, amplification of the EF1α promoter, and use of the purified PCR products in the In-Fusion cloning procedure, followed by transformation and DNA isolation. (B) Comparison of the fluorescence microscopy images after iNGN WT and TET3KO transfections with BRET reporter and Cas9 using CMV and EF1α promoters.

4.2 Comparison of Cas9 and the inducible Cas systems (iCas)

4.2.1 HEK293T cells

HEK293T cells were initially used to compare the inducible Cas system with the traditional Cas9 expression system, allowing sustained Cas9 expression. Cells were co-transfected with a BRET reporter assay plasmid containing different target sequences T1-

T3 ± Cas9 expression plasmid comprising the corresponding sgRNA/Cas9. The cells were also transfected with the peGFPN1 plasmid as a transfection control and the Rluc8 plasmid, which serves as a control for the BRET assay. The cells were visualized 24 hours after the transfection with fluorescence microscopy and showed a reduction in fluorescence after the induction of Cas9 expression due to frameshifting, mutagenic NHEJ DNA repair (Figure 15).

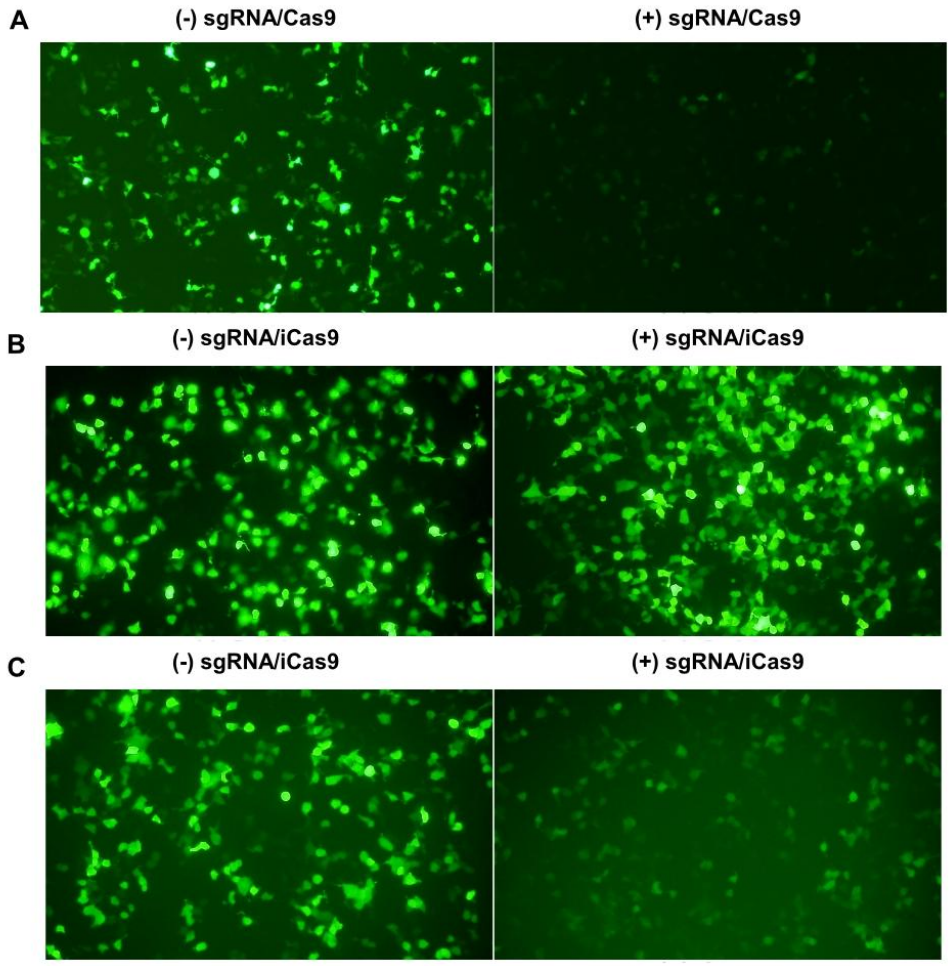

Figure 15: Fluorescence microscopy images of transfected HEK293T cells to show the cleavage activity of Cas9 and iCas9 after induction compared to the non-cleaved BRET reporter. (A) Transfected cells with BRET reporter ± sgRNA/Cas9. (B) Transfected cells with BRET reporter ± sgRNA/iCas9 in the absence of 4-OHT. (C) Transfected cells with BRET reporter and ± sgRNA/iCas9 after adding 4-OHT.

Next, a BRET assay was performed, with quadruple measurements recorded for each sample's acceptor and donor emissions. The differences between the mean BRET ratios were observed for T1 ± sgRNA/Cas9 (27.9 ± 1.6 cBU to 11.5 ± 0.7 cBU), T2 ± sgRNA/Cas9 (21.6 ± 0.6 cBU to 14.2 ± 1 cBU), and T3 ± sgRNA/Cas9 (21.6 ± 1 cBU to 11.6 ± 0.7 cBU) (Figure 16A). With the absence of DSBs, energy transfer from RLuc8 to GFP is high. In contrast, after mutagenic, frameshifting DSB repair, the energy transfer decreases due to frameshifts causing disturbed GFP2 expression (Wimmer et al., 2021). The frameshift rates [%] were calculated after normalizing the results with Rluc8 (2.8 ± 0.17 cBU) set as 100% and DSB as 0%, showing the best outcome in target T1 with (65.2 ± 6.9%) followed by T2 with (39.2 ± 6.5%), and T3 with (53.2 ± 6.7%), respectively (Figure 16B).

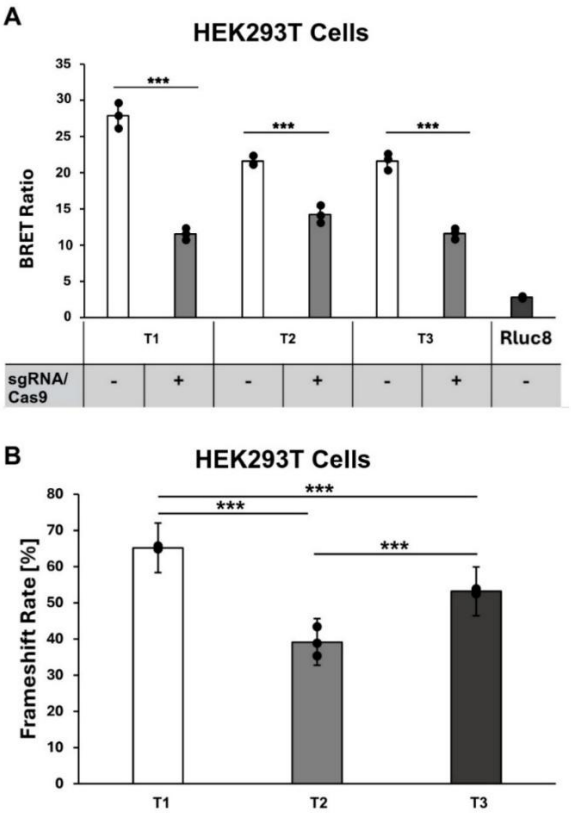

Figure 16: The evaluation of the frameshift rates and the cleavage activity of Cas9 in HEK293T cells. (A) The BRET ratios (cBU) of three target sequences, T1-T3 ± sgRNA/Cas9, with Rluc8 as a control. ***p ≤ 0.001 (t-test). (B) The calculated frameshift rates [%] of the different target sequences. ***p ≤ 0.001 (One-Way ANOVA with the Holm-Sidak method). Data points represent three individual replicates with quadruple measurements, n = 3.

To compare the Cas9 with the inducible Cas9 system, the system was tested in HEK293T cells by co-transfecting BRET reporter assay plasmid containing different target sequences (T1-T3) ± iCas plasmid comprising the corresponding sgRNA/iCas9, with and without 4-hydroxytamoxifen (4-OHT) 4 hours after transfection. After 24 hours, a BRET assay was performed. The BRET ratios of T1 decreased from 27.3 ± 0.8 cBU to 8.8 ± 0.4 cBU in the presence of 4-OHT but remained almost unchanged in its absence (24.9 ± 1.9 cBU to 24.98 ± 1.2 cBU). For T2, the BRET ratio decreased from 19.99 ± 0.65 cBU to 14.12 ± 0.9 cBU with 4-OHT. However, it showed almost no difference without 4-OHT (24.1 ± 1.6 cBU to 24.5 ± 1.8 cBU). For T3, the BRET ratio decreased from 20.59 ± 0.4 cBU to 11.55 ± 1 cBU with 4-OHT, but again showed no apparent change without 4-OHT (25.3 ± 2.38 cBU to 25.4 ± 1.97 cBU) (Figure 17A). The frameshift rates [%] calculated for both systems showed a higher rate for target T1 (74.7 ± 3.8%), with no significant differences observed in the other two target sequences T2 and T3 (Figure 17B).

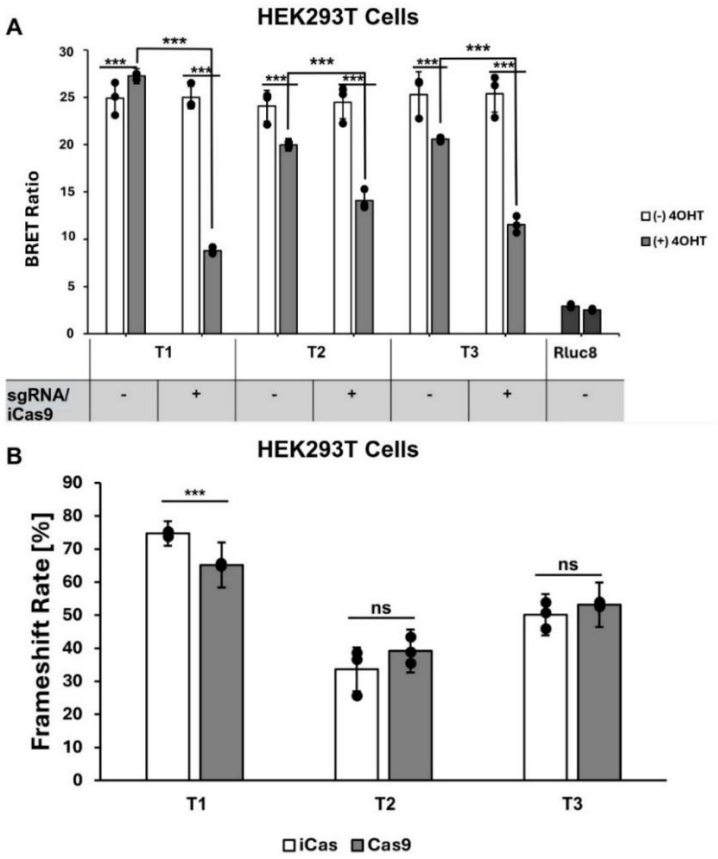

Figure 17: Assessment of the cleavage activity of iCas9 upon induction and the frameshift rates of Cas systems in HEK293T cells. (A) The BRET ratios (cBU) of 3 target sequences, T1-T3 ± sgRNA/iCas9 ± 4-OHT, with Rluc8 as a control. ***p ≤ 0.001 (t-test). (B)

Comparison between Cas9 and iCas frameshift rates [%] for 3 target sequences, T1-T3. ***$p \leq 0.001$, ns $p > 0.05$ (not significant) (t-test). Data points represent three individual replicates with quadruple measurements, n = 3.

4.2.2 Quantification of the frameshift rate in undifferentiated iNGN cell lines

To investigate the role of TET3 in undifferentiated iNGN cells as well as to compare the inducible Cas system with the traditional Cas9 expression system. First, iNGN WT and iNGN TET3KO cells were co-transfected with the promoter-optimized BRET reporter assay plasmid containing different target sequences (T1-T3) ± the px459 plasmid comprising the corresponding sgRNA/Cas9. The cells were also transfected with the peGFPN1 plasmid as a transfection control and a Rluc8 expressing plasmid as the BRET assay control. After 24h, a BRET assay was performed. All samples tested showed a significant ($p \leq 0.001$) reduction in the BRET ratio compared to their controls. For iNGN WT cells, the ratios decreased from 36.3 ± 2.6 cBU to 25.7 ± 1.6 cBU for target T1, and from 26 ± 0.87 cBU to 23.5 ± 1.6 cBU for target T3. In iNGN TET3KO cells, the BRET ratios for T1 decreased from 41.3 ± 1.49 cBU to 15.3 ± 1.55 cBU, followed by a reduction for T2 from 27 ± 1.1 cBU to 18.6 ± 1.4 cBU (Figure 18).

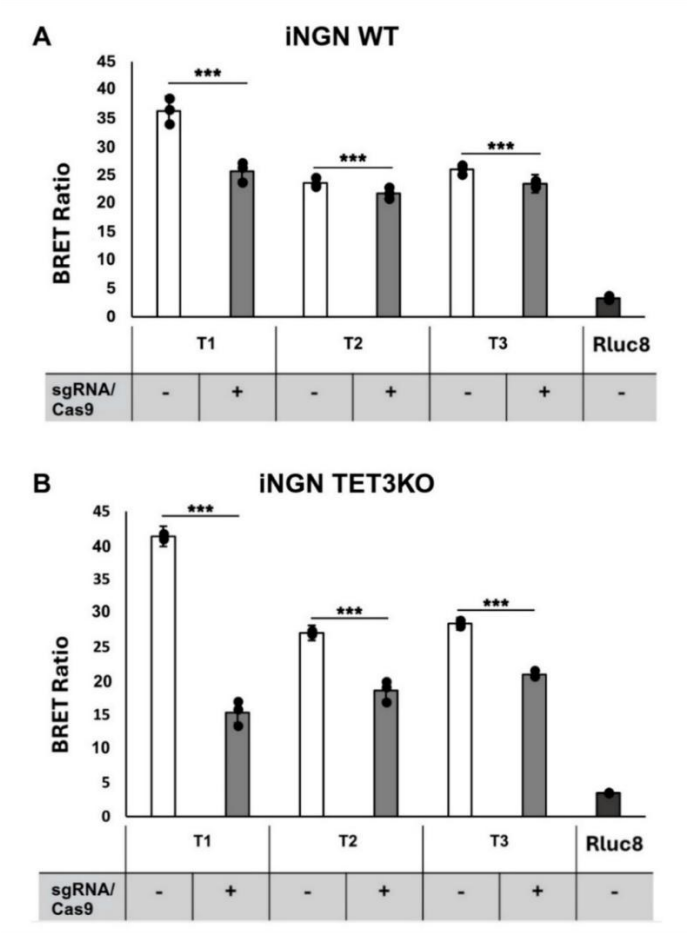

Figure 18 : The cleavage activity of Cas9 in undifferentiated iNGN cell lines. (A) iNGN WT BRET ratios (cBU) of target sequences T1-T3, ± sgRNA/Cas9, with Rluc8 as a control. (B) iNGN TET3KO BRET ratios (cBU). ***$p \leq 0.001$ (t-test). Data points represent three individual replicates with quadruple measurements, n = 3.

Further, the inducible iCas system was analyzed in undifferentiated iNGN WT and iNGN TET3KO cells by co-transfecting them with the BRET reporter assay plasmid containing target sequences (T1-T3) ± the iCas plasmid comprising the corresponding sgRNA/iCas9 and inducing Cas9 activation with 4-OHT added 4 hours after transfection. After 24 hours, a BRET assay was performed. The BRET ratios for iNGN WT cells were 36 ± 3.1 cBU to 29.3 ± 3.3 cBU for target sequence T1, and 26.5 ± 1.1 cBU to 24.7 ± 1.6 cBU for target sequence T3. In iNGN TET3KO cells, the BRET ratios for T1 were 30.4 ± 1.9 cBU to 15.4 ± 0.4 cBU, and for T3, 23.5 ± 0.4 cBU to 15.21 ± 0.35 cBU (Figure 19).

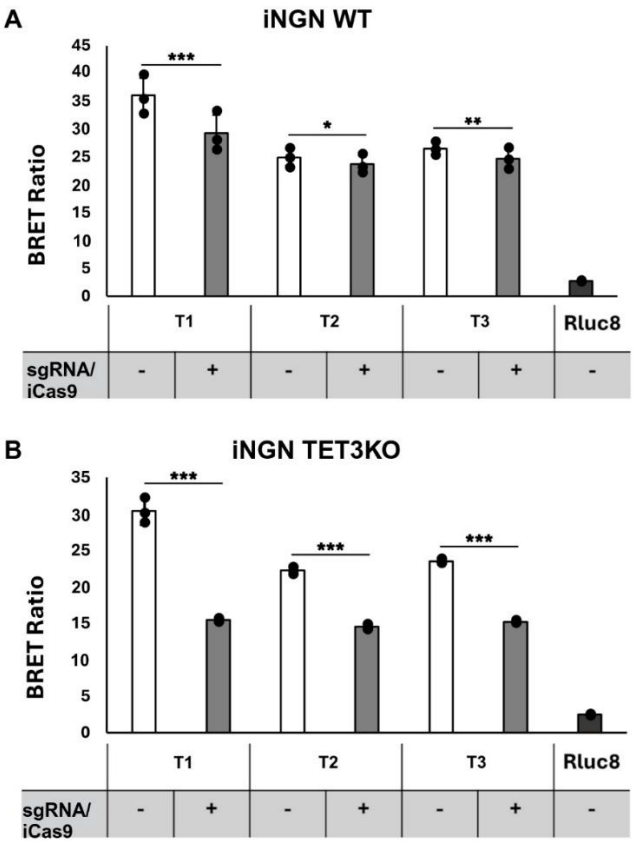

Figure 19: The reduction of the BRET ratio due to mutagenic, frameshifting DSB repair on three different target sequences using iCas in undifferentiated iNGN cell lines. (A) iNGN WT BRET ratios (cBU) of target sequences T1-T3, ± sgRNA/iCas9, with Rluc8 as a control. (B) iNGN TET3KO BRET ratios (cBU). ***$p \leq 0.001$, *$p < 0.05$ (t-test). Data points represent three individual replicates with quadruple measurements, n = 3.

To verify the effect of TET3 on these initial results, a TET3-containing plasmid (FH-TET3-pEF) was additionally transfected into iNGN TET3KO cells with Cas9 systems as an additional control. The frameshift rates were calculated for iNGN WT: for target sequence T1 with Cas9, the rate was 32.13 ± 9.3%, and for T3, it was 10.96 ± 8.4%. In iNGN TET3KO cells, T1 showed the highest value, 68.6 ± 5.7%, followed by T2, with 36 ± 7.7%. For TET3KO overexpression, the frameshift rates for T1 were 29.8 ± 7.5%, and for T3, 13.3 ± 7.9%, showing no significant difference compared to iNGN WT values. However, the iCas system's frameshift rates for iNGN WT were 20.4 ± 13.6% for T1 and 7.7 ± 8.4% for T3. In iNGN TET3KO cells, T1 was 53.7 ± 7% and T3 was 39.6 ± 2.7%. For TET3KO overexpression, T1 was 19 ± 8.6%, and T2 was 5.5 ± 6.7%, showing no significant difference compared to iNGN WT values. Overall, the results show higher

frameshift rates in iNGNs using the Cas9 system compared to the iCas system. The Restoration of the TET3 expression led to adjusting the frameshift rates to the WT state again, with no significant difference for all three target sequences tested. Target sequence T1 frameshift rates were the highest among the results of the target sequences used in both systems. T1 was chosen to proceed with the remaining experiments (Figure 20).

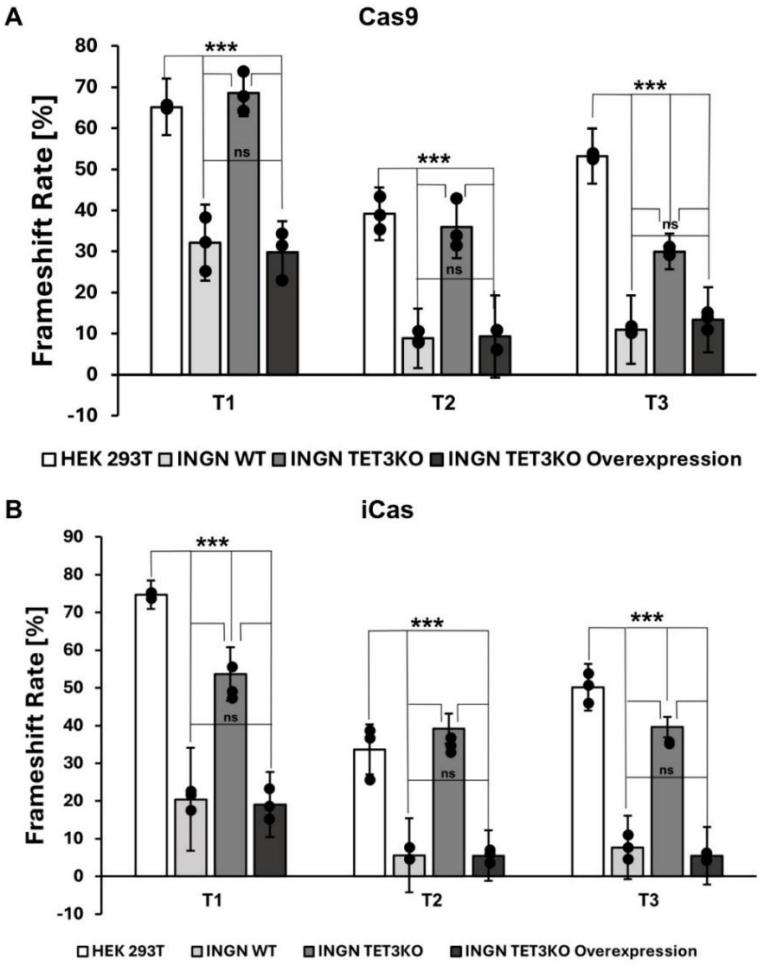

Figure 20: Comparison of the frameshift rates in iNGN cell lines. (A) The frameshift rates [%] of Cas9 for 3 target sequences T1-T3 show the differences between undifferentiated iNGN WT cells, iNGN TET3KO cells, and TET3KO overexpression. (B) The frameshift rates [%] of iCas. ***p ≤ 0.001, *p < 0.05, ns p > 0.05 (not significant) (One-Way ANOVA with the Holm-Sidak method). Data points represent three individual replicates with quadruple measurements, n = 3.

4.2.3 Evaluation of iCas at different induction times

To evaluate whether the inducible Cas system is functional by testing its ability to initiate cleavage activity at any time, the iNGN TET3KO cells were transfected with T1 in the undifferentiated state, and differentiation was induced after 4 hours by adding doxycycline to the culture medium. 4-OHT was added after 24, 48, 72, and 96 hours, and a BRET assay was performed the following day. Compared to the previous results, the BRET ratios show a decrease in cleavage activity in the first two time slots: after 24 hours (29.3 ± 0.5 cBU to 25.3 ± 0.2 cBU) and after 48 hours (33.6 ± 0.1 cBU to 32.1 ± 0.3 cBU). The last two samples have no significant difference, indicating that the inducible Cas loses its advantages, at least when applied to the iNGN cells (Figure 21). Due to the decrease in cleavage activity and the failure to use the inducible system's timing control advantage, the Cas9 system was used primarily in the rest of this work.

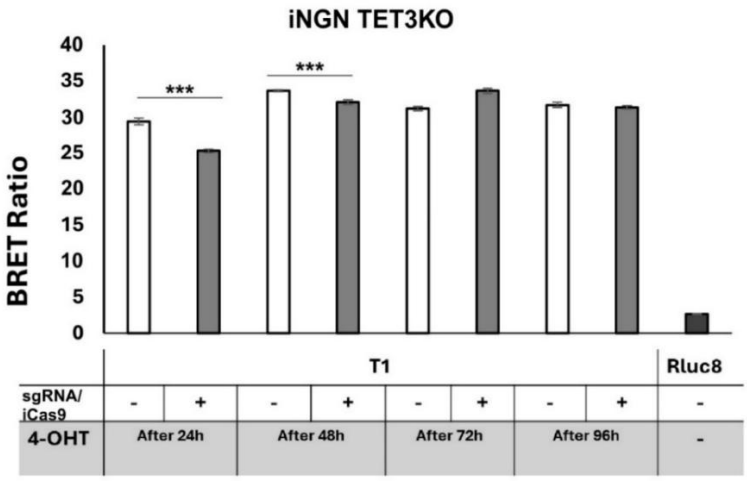

Figure 21: Evaluation of the cleavage activity of the iCas system in iNGN TET3KO cells at different induction times. The undifferentiated cells were transfected, and after 4h, doxycycline was added to initiate differentiation. 4-OHT was administered at different times, and BRET ratios were measured after 24h with quadruple measurements. ***p ≤ 0.001 (t-test), n = 1.

4.3 Evaluation of DNA repair during neuronal differentiation

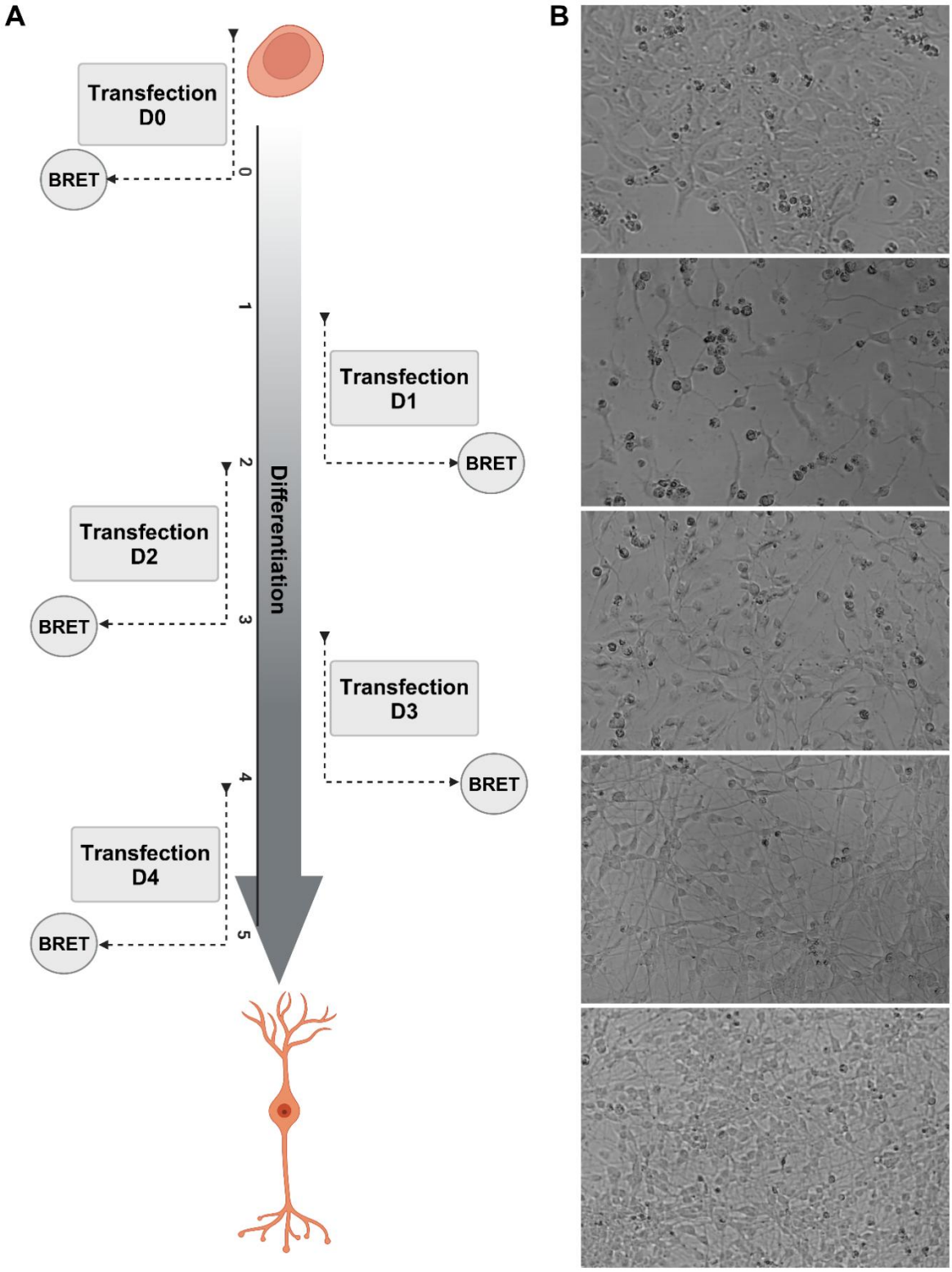

Figure 22: Schematic representation of the experimental setup. (A) Transfection of iNGN cell lines at different time points during differentiation (D0-D4), followed by BRET measurements after 24h. (B) Phase contrast images showing the morphological changes during the differentiation process of the iNGN WT cells from D0-D4.

To gain insight into DNA repair along iNGN differentiation and the impact of TET3, iNGN WT, and TET3KO cells were transfected with a BRET reporter assay plasmid containing T1 target sequences ± Cas9 expression plasmid comprising the corresponding sgRNA/Cas9. Transfections were performed at the undifferentiated state (D0) and from D1 to D4 after differentiation using doxycycline. BRET assays were performed 24h after each transfection (Figure 22). The BRET ratios for iNGN WT at D1 for target sequence T1 significantly decreased (***$p \leq 0.001$) from 30 ± 2.5 cBU to 23.4 ± 3 cBU, and at D4 (**$p < 0.01$), from 31.3 ± 1.9 cBU to 26.3 ± 2.9 cBU., the ratios for iNGN TET3KO at D1 showed a significant reduction (***$p \leq 0.001$) from 28.3 ± 3.7 cBU to 17.95 ± 3.7 cBU, and at D4 (*$p < 0.05$), the ratios decreased from 27.1 ± 3.7 cBU to 24.2 ± 2.9 cBU (Figure 23).

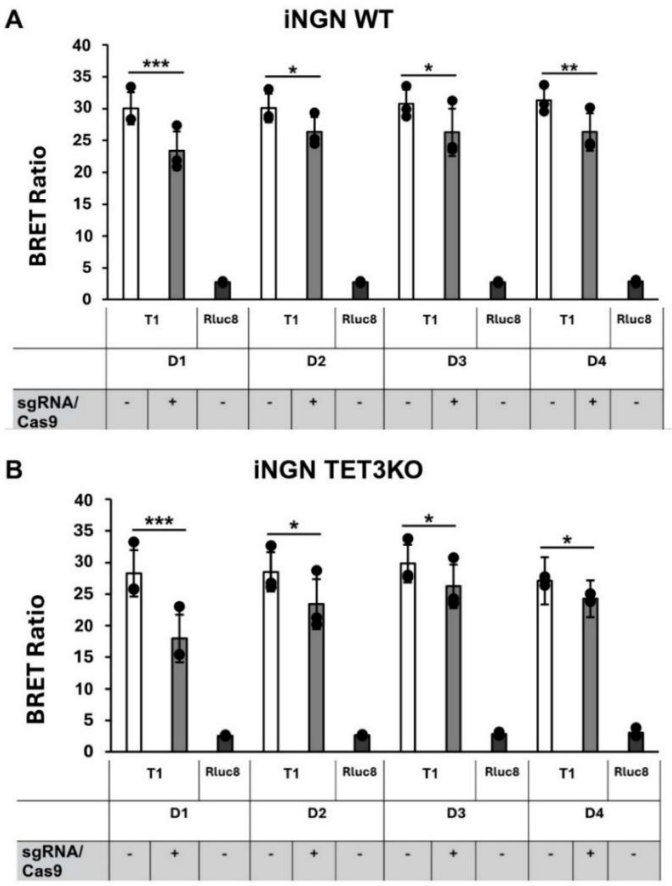

Figure 23: Assessment of the cleavage activity during iNGN cell lines differentiation. (A) BRET ratios (cBU) of iNGN WT for target T1, ± sgRNA/Cas9 at different differentiation times D1-D4, with Rluc8 as a control. (B) BRET ratios (cBU) of iNGN TET3KO. ***$p \leq 0.001$, **$p < 0.01$, *$p < 0.05$ (t-test). Data points represent three individual replicates with quadruple measurements, n = 3.

TET3 was overexpressed in iNGN TET3KO cells by transfecting with the TET3 (FH-TET3-pEF) plasmid. The frameshift rates were highest in iNGN TET3KO at D0, recording 68.6 ± 5.7%. A significant reduction occurred at D1, where the rate dropped to 40.2 ± 20.4% and further decreased to 11.9 ± 19.9% at D4. At D1, iNGN TET3KO showed a significant difference compared to iNGN WT. The frameshift rate for iNGN WT at D1 was 24.4 ± 14.4%, while TET3KO overexpression was 27.96 ± 9.4%, displaying no significant differences between the two. However, no significant differences were noted among the three variants on the remaining differentiation days (Figure 24).

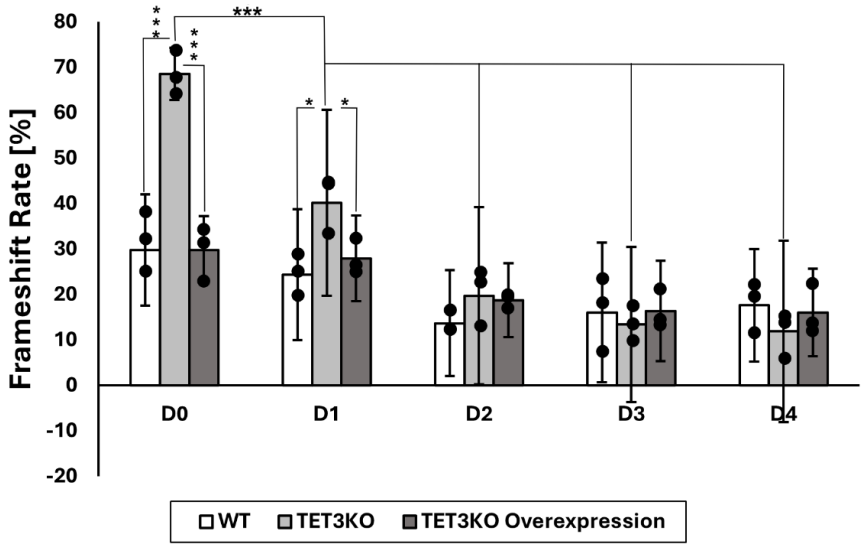

Figure 24: Comparison of iNGN cell lines at different differentiation states. The frameshift rates [%] of Cas9 for target sequence T1 show differences between iNGN WT cells, iNGN TET3KO cells, and TET3KO overexpression. ***$p \leq 0.001$, *$p < 0.05$ (One-Way ANOVA with the Holm-Sidak method). Data points represent three individual replicates with quadruple measurements, n = 3.

4.4 PARP1 level modulation

4.4.1 DNA Repair Modulation in HEK293 and iNGN cells

To test the influence of PARP1 on DNA repair in HEK293 and undifferentiated iNGNs, interventions in PARP1 expression were used. HEK293T cells were co-transfected with

the BRET reporter plasmid and its corresponding sgRNA/Cas9 plasmid for the target sequence 1, along with either a PARP1 overexpression plasmid (PARP1 high) or a PARP1 KO-gRNA/Cas9 complex (PARP1 low). Additionally, a 700 bp HDR-template was transfected to encourage HDR events. The HDR template harbors a target sequence that is not addressed by the complex used in this study. With normal PARP1 levels and without an HDR template, the BRET ratio decreased from 26.05 ± 1.7 cBU to 13.1 ± 0.8 cBU. Adding the HDR template increased the BRET ratio again to 19.3 ± 1.5 cBU, indicating HDR repair. Compared to the normal PARP level without the HDR template, PARP1 overexpression had an increased BRET ratio with 18.7 ± 1.4 cBU. A reduction of PARP1 (PARP1 low) further decreased the BRET ratio to 6.3 ± 0.3 cBU. The addition of the HDR template at PARP1 low again increased the BRET ratio due to HDR repair to 12 ± 1.6 cBU, and only a minor increase was observed in PARP1 high conditions (20.4 ± 1.3 cBU) (Figure 25).

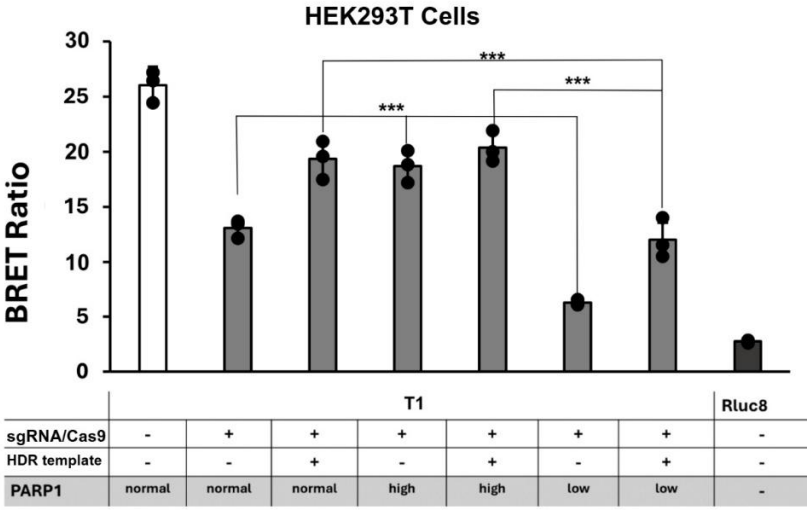

Figure 25: Assessment of the cleavage activity after PARP1 modulation in HEK293T cells. BRET ratios (cBU) of target T1, ± sgRNA, ± HDR template, with PARP1 overexpression (PARP1 high) or PARP1 knockout (PARP1 low), and Rluc8 as a control. ***p ≤ 0.001 (One-Way ANOVA with the Holm-Sidak method). Data points represent three individual replicates with quadruple measurements, n = 3.

The iNGN cells were initially transfected at D0, and the BRET reporter assay was performed 24 hours post-transfection. For iNGN WT cells without HDR template addition, the BRET ratio decreased from 37.7 ± 2.8 cBU to 26.9 ± 2.4 cBU due to mutagenic NHEJ DNA repair. In PARP1 high, the BRET ratio significantly increased to

32.3 ± 2 cBU, while in PARP1 low, it significantly decreased to 15.3 ± 1.5 cBU. The BRET ratio measurements after HDR template addition were increased again to 30.4 ± 2.7 cBU. In comparison, PARP1 high conditions show no significant difference with 33.2 ± 2.6 cBU and a significant decrease in PARP1 low with 18.3 ± 4.9 cBU (Figure 26A). For iNGN TET3KO cells, without HDR template addition, the BRET ratio decreased from 38.6 ± 5 cBU to 21.6 ± 2.5 cBU. In PARP1 high, the BRET ratio significantly increased to 28.5 ± 3 cBU, while in PARP1 low, it significantly decreased to 8.5 ± 1.1 cBU. With HDR template addition, the BRET ratio was 23.8 ± 2.7 cBU, showing a significant increase in PARP1 high (26.7 ± 3.3 cBU) and a significant decrease in PARP1 low (11.2 ± 2.1 cBU) (Figure 26B).

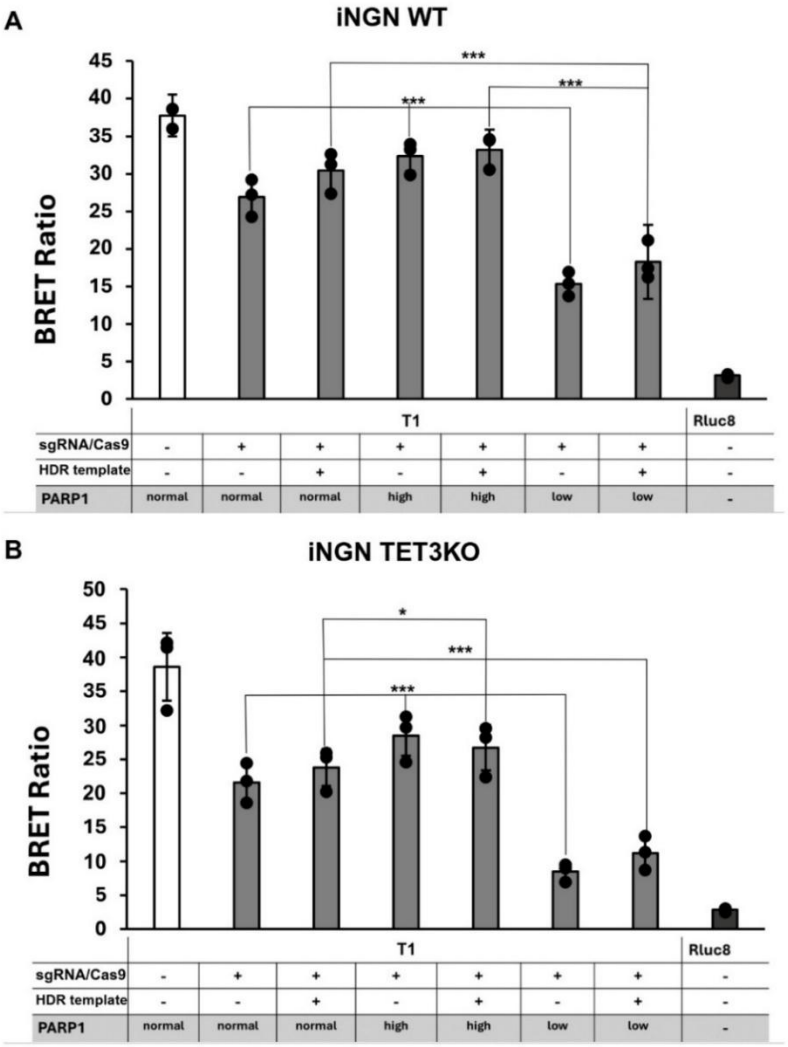

Figure 26: Evaluation of the cleavage activity of Undifferentiated iNGN cell lines after PARP1 modulation. (A) BRET ratios (cBU) of iNGN WT for target sequence T1, ±

sgRNA/Cas9, ± HDR template, with PARP1 overexpression (PARP1 high) or PARP1 knockout (PARP1 low), and Rluc8 as a control. (B) BRET ratios (cBU) of iNGN TET3KO. ***p ≤ 0.001, *p < 0.05 (One-Way ANOVA with the Holm-Sidak method). Data points represent three individual replicates with quadruple measurements, n = 3.

TET3 was overexpressed in TET3KO cells to analyze its effect and its interaction with PARP1 modulation. After BRET ratio measurements, the calculated frameshift rates of the different cell lines in HEK293T cells were (31.6 ± 9.4%) for PARP1 high and (84.9 ± 7.4%) for PARP1 low, showing no significant differences compared to iNGN TET3KO cells, which had (28.2 ± 16.4%) in PARP1 high and (84.3 ± 14.4%) in PARP1 low. The frameshift rates of the iNGN WT and TET3KO overexpressed cells showed significant differences compared to HEK293T cells, as well as among iNGN TET3KO cells with (15.6 ± 9.8%) (20.2 ± 16.4%) in PARP1 high and (64.8 ± 9%) (64.6 ± 7.4%) in PARP1 low for both samples, respectively (Figure 27A). By adding a template, HEK293T cell rates were (28.9 ± 9.8%), with (24.4 ± 9.2%) for PARP1 high and (60.4 ± 9.9%) for PARP1 low. There are significant differences between iNGN WT and TET3KO cells results, with (21.2 ± 11%) (41.4 ± 15.9%) in normal, (13 ± 11%) (33.3 ± 16.8%) in PARP1 high, and (56.3 ± 16.3%) (76.6 ± 15.2%) in PARP1 low, respectively (Figure 27B).

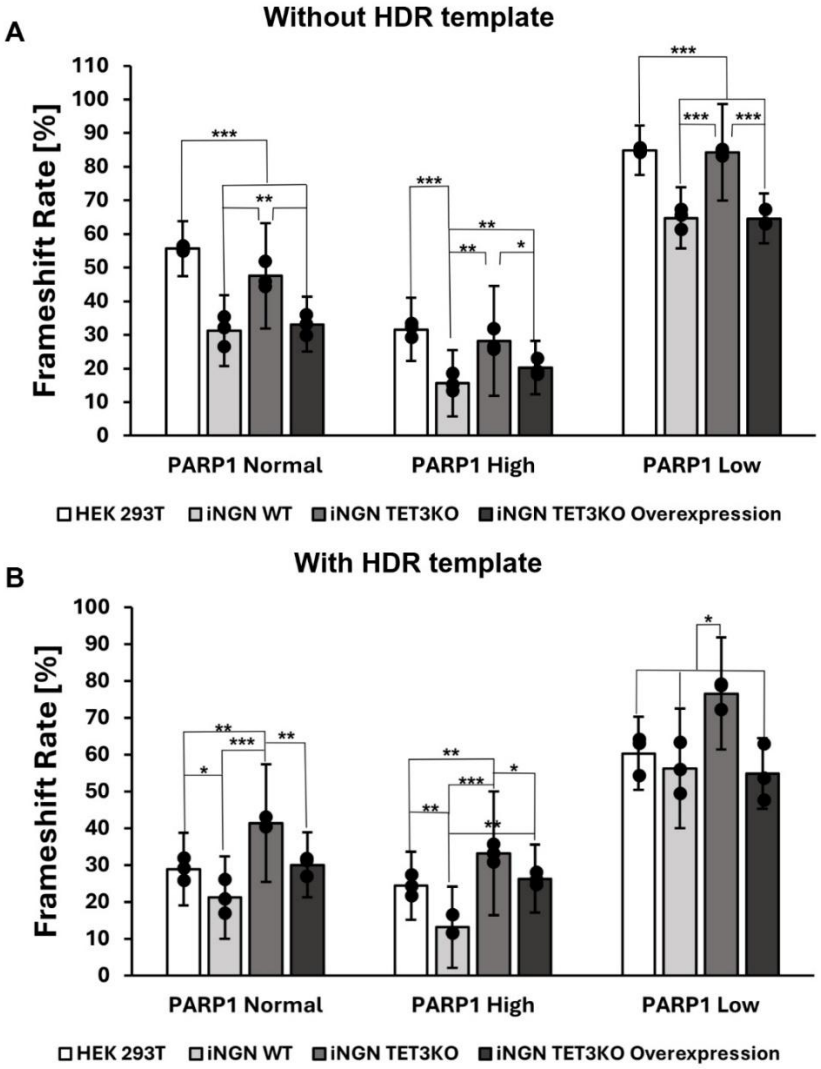

Figure 27: Comparison of the frameshift rates of different cell lines with PARP1 modulation and without including HDR templates. (A) The frameshift rates [%] of Cas9 without HDR templates for the T1 target sequence under different PARP1 conditions illustrate the differences between HEK293T cells, undifferentiated iNGN WT cells, and iNGN TET3KO cells, as well as TET3KO overexpression. (B) The frameshift rates [%] of Cas9 with HDR templates. ***$p \leq 0.001$, **$p < 0.01$, *$p < 0.05$, ns $p > 0.05$ (not significant) (One-Way ANOVA with the Holm-Sidak method). Data points represent three individual replicates with quadruple measurements, n = 3.

4.4.2 PARP1 modulation during neuronal differentiation

Following the experimental steps shown in Figure 22A, iNGN WT cells were transfected with a BRET reporter assay for T1 and a corresponding sgRNA/Cas9 plasmid, along with either PARP1 high or PARP1 low plasmids. The BRET assay was performed, and the frameshift rates were calculated. The results showed that the PARP1 low values throughout the differentiation stages (D0-D4) were significantly higher than PARP1 high and normal values, with the highest value at D1 (78.7 ± 8.4%) and the lowest value at D4 (47.9 ± 14%). The only significant difference between PARP1 normal and PARP1 high was observed at D0 (Figure 28A). In a similar experiment using iNGN TET3KO cells, the frameshift rates for PARP1 low remained stable throughout the differentiation stages (D0-D4) and were significantly higher than PARP1 high and normal values. Significant differences between PARP1 normal and PARP1 high were observed at both D0 and D1 (Figure 28B).

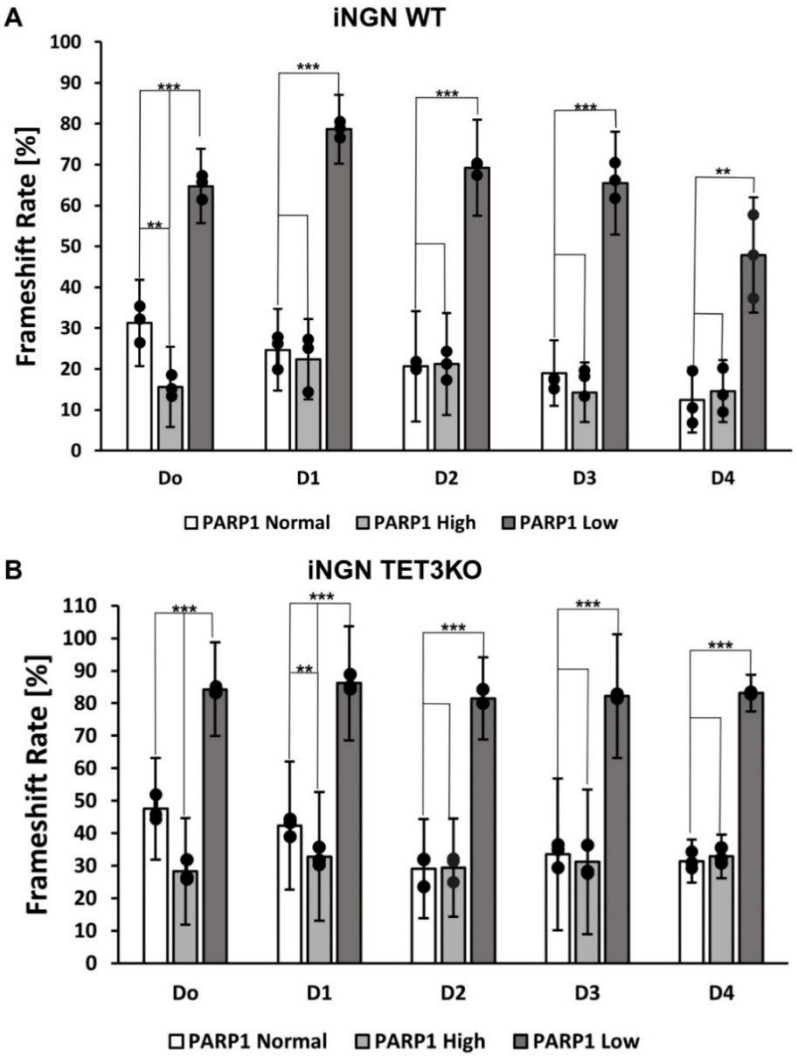

Figure 28: The calculated frameshift rates [%] of iNGN cell lines after PARP1 modulation at different differentiation states. (A) The frameshift rate [%] of iNGN WT for the T1 target sequence, without HDR templates and under different PARP1 conditions. (B) The frameshift rate of iNGN TET3KO without HDR templates. ***$p \leq 0.001$, **$p < 0.01$ (One-Way ANOVA with the Holm-Sidak method). Data points represent three individual replicates with quadruple measurements, n = 3.

The frameshift rate results of iNGN WT cells transfected with HDR templates showed that the PARP1 low values throughout the differentiation stages D0-D4 were significantly higher than the PARP1 high and normal values, with the highest value at D1(73.4 ± 8.7%) and the lowest value at D4 (29.4 ± 10.4%) (Figure 29A). As for the frameshift rate results

of iNGN TET3KO cells with HDR template transfection, the PARP1 low values throughout the differentiation stages (D0-D4) were significantly higher than the PARP1 high and unmodified values, with the highest value at D1 (82.4 ± 17.6%) and the lowest value at D4 (61.9 ± 6.5%) (Figure 29B).

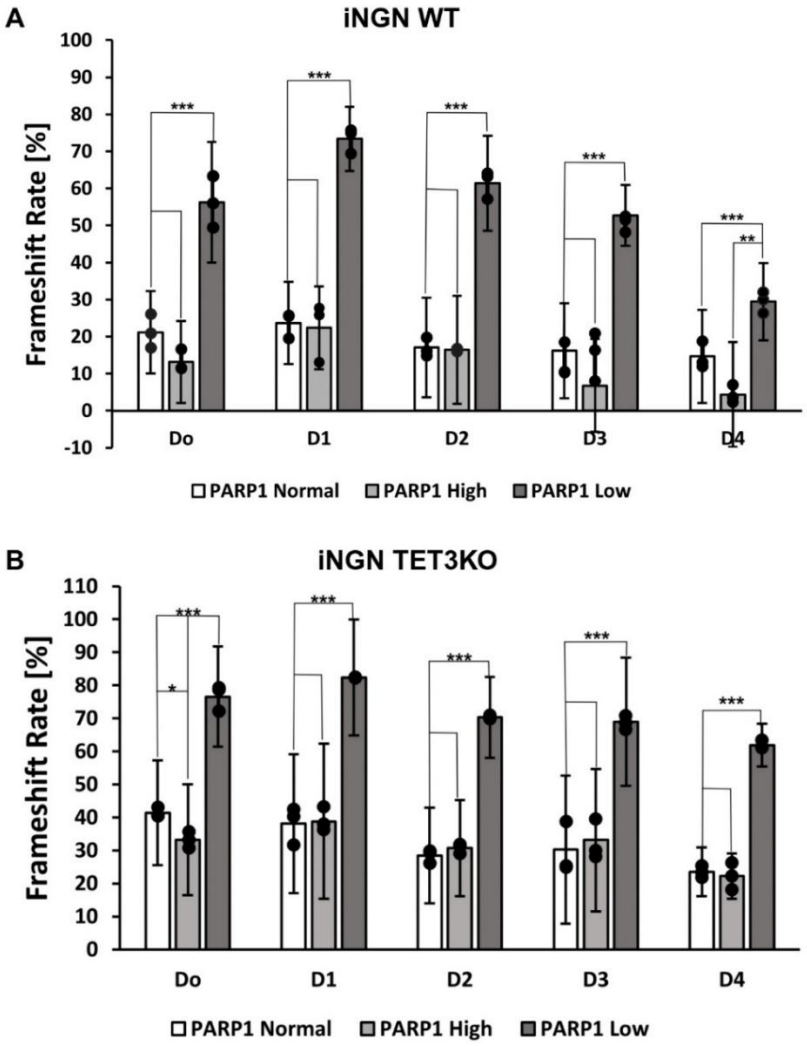

Figure 29: The calculated frameshift rates [%] of iNGN cell lines after PARP1 modulation and with HDR templates at different differentiation states. (A) The frameshift rate [%] of iNGN WT for the T1 target sequence, with HDR templates and under different PARP1 conditions. (B) The frameshift rate of iNGN TET3KO with HDR templates. ***$p \leq 0.001$, **$p < 0.01$, *$p < 0.05$ (One-Way ANOVA with the Holm-Sidak method). Data points represent three individual replicates with quadruple measurements, n = 3.

4.4.3 Comparison of INGNs upon PARP1 modulation

The differences between iNGN WT and iNGN TET3KO cells with PARP1 modulation were analyzed during the differentiation process from D0 to D4. To estimate the effect of TET3, TET3 was overexpressed in iNGN TET3KO cells. The frameshift rates of the PARP1 high values without the HDR template showed significantly higher values in iNGN TET3KO cells at D0, D3, and D4 compared to iNGN WT and TET3KO overexpression results. At D4, TET3KO cells showed (32.9 ± 6.7%) compared to iNGN WT (14.6 ± 7.6%) (Figure 30A). Furthermore, the frameshift rates of iNGN TET3KO cells with PARP1 low values without the HDR template were significantly higher than those of iNGN WT cells and after TET3 overexpression (Figure 30B).

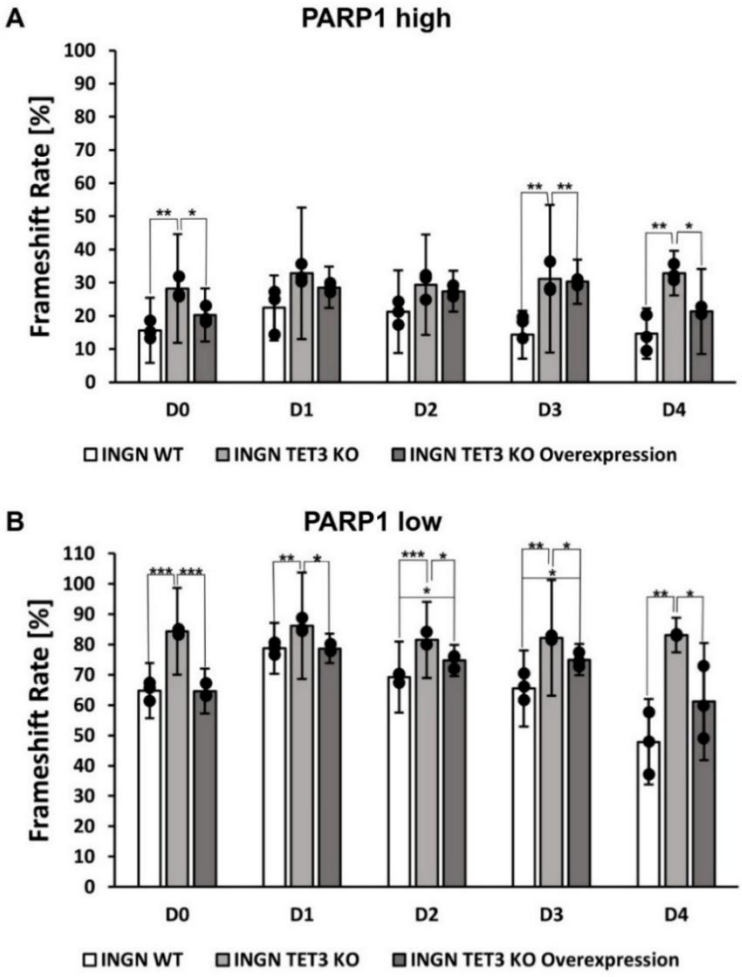

Figure 30: Comparison of the frameshift rates [%] of iNGN Cell lines after PARP1 modulation at different differentiation states. (A) The frameshift rates of Cas9 without HDR templates for the T1 target, with PARP1 overexpression (PARP1 high), illustrate the differences between iNGN WT cells, iNGN TET3KO cells, and TET3KO

overexpression at D0-D4 differentiation stages. (B) The frameshift rates of Cas9 without HDR templates for the T1 target, with PARP1 knockouts (PARP1 low). ***p ≤ 0.001, **p < 0.01, *p < 0.05 (One-Way ANOVA with the Holm-Sidak method). Data points represent three individual replicates with quadruple measurements, n = 3.

The frameshift rates of the PARP1 high values with the addition of the HDR template were significantly higher in iNGN TET3KO cells in D0-D3 compared to iNGN WT cells (Figure 31A). Throughout the differentiation process and with the addition of a template, the frameshift rates of iNGN TET3KO cells for PARP1 low values were significantly higher than those of iNGN WT cells (Figure 31B).

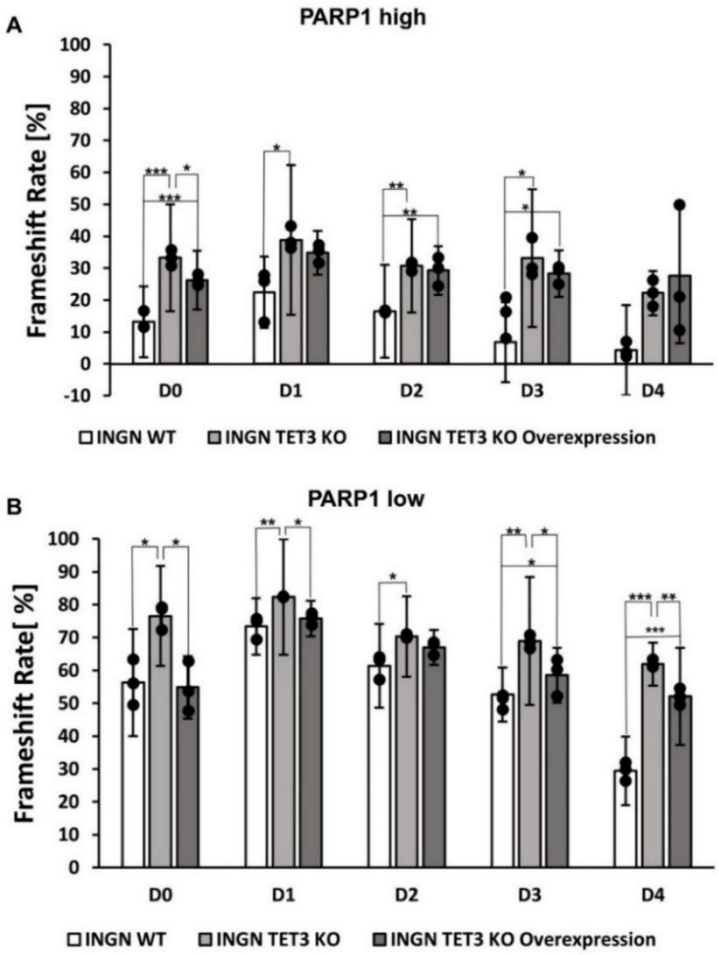

Figure 31: Comparison of the frameshift rates [%] of iNGN Cell lines after PARP1 modulation and HDR templates addition at different differentiation states. (A) The

frameshift rates of Cas9 with HDR templates for the T1 target, with PARP1 overexpression (PARP1 high), illustrate the differences between iNGN WT cells, iNGN TET3KO cells, and TET3KO overexpression at D0-D4 differentiation stages. (B) The frameshift rates of Cas9 with HDR templates for the T1 target, with PARP1 knockouts (PARP1 low). ***$p \leq 0.001$, **$p < 0.01$, *$p < 0.05$ (One-Way ANOVA with the Holm-Sidak method). Data points represent three individual replicates with quadruple measurements, $n = 3$.

5. Discussion

In this study, the human inducible Neurogenin iPS, known as iNGN cell lines, were used to establish a valid *in-vitro* model system to systemically analyze DNA repair in mature neurons and during differentiation after a Cas9-induced DSB. Using two Cas9 systems, the iNGN WT, and iNGN TET3KO cells were compared in the pluripotent state. Additionally, PARP1 modulation was examined in different differentiation stages. Notably, the PARP1 modulation demonstrated that DNA repair pathway engineering influences genome editing outcomes.

5.1 Cas9 and the inducible Cas systems

To improve CRISPR/Cas9 and enhance its outcomes, such as reducing off-targets, together with the timing control and the ability to switch Cas9 on and off, are substantial benefits (Liu et al., 2016). A 4-hydroxytamoxifen-inducible Cas9 system, known as iCas, was examined. This research demonstrates the differences between Cas9 and iCas systems using three different target sequences (T1-T3). First, the 4-OHT effect on the iCas system was validated by comparing the BRET measurements of the induced samples with those of the uninduced ones. The ratio results showed the endonuclease activity only after 4-OHT addition 4h post-transfection, which also confirmed the reduction in fluorescence (4.2.1). HEK293T cells, a human embryonic kidney HEK293 derivative cell line, were used as a control cell line due to its high transfection efficiency (Tan et al., 2021) and easy handling of the immortalized cell line. The frameshift rates of the two systems in HEK293T cells were target dependent. T1 was higher in iCas than Cas9, but T2 and T3 results were similar. In iNGN WT and iNGN TET3KO, the frameshift rate results of sgRNA/Cas9 for all target sequences were higher than those of the inducible Cas9. Zhao et al. stated that the inducible Cas9 systems usually have lower activity than the basic Cas9 (Zhao et al., 2018). That is anticipated because the non-inducible Cas has no external interferences influencing its activity. Yet, using the inducible system and benefiting from its advantages when applicable is a good compromise. Dependence on iCas9 induction at different time points was assessed. The BRET measurement findings revealed a decrease at 24h and 48h, with no effect observed at 72h and 96h (4.2.3). This experiment was conducted to evaluate the timing control specificity of the inducible system. These data hinder the application of the iCas system for studying DNA repair

across different differentiation stages, contradicting Liu et al., who reported that 4-OHT induction time can be controlled (Liu et al., 2016). In this system, the inducible Cas is transferred to the nucleus of the transfected cells upon 4-OHT induction, where the editing events are expected to occur. Conditional genome editing and testing specific stages of embryonic development or stem cell differentiation were noted as positive aspects of this system, along with the reduction of the off targets events.

5.2 DNA repair during neuronal differentiation

In order to overcome the limitations of directly transdifferentiating fibroblasts into neurons, which bypasses the progenitor stage, or using other methods that require a prolonged and unstable stem cell differentiation process resulting in a mixture of cells and insufficient neuron production, Busskamp et al. developed the iNGNs. Unlike previous approaches, this cell line offers several advantages, such as fast differentiation, easy culture, and the ability to study cells not only as bipolar neurons but also at different stages of differentiation (Busskamp et al., 2014). In this study, the DNA repair mechanism was evaluated through the quantification of the frameshift rates for the undifferentiated iNGNs (D0) as well as in various differentiation stages from D1 to D4 until cells reached the bipolar neurons state. Followed by quantifying the genome editing events using BRET assay 24h post-transfection. The transfection efficacy of the differentiated cells was lower than that of their pluripotent state, which is expected due to the obstacles of transfecting and expressing an exogenous construct in postmitotic neurons (Karra & Dahm, 2010). The iNGN WT frameshift rate results were consistent throughout the differentiation process, with a slight decrease following the onset of differentiation (4.3), aligning with the transcriptomic data reported by Pasquini et al., which is also similar to the results of the human retina (Pasquini et al., 2020). This proves that iNGNs mimic retinal neurons and can be used as an *in-vitro* model for DNA repair in retinal cells. Conversely, the frameshift rates of iNGN TET3KO cells demonstrate a significant decrease from the D0 results compared with the remaining differentiation stages.

5.3 The impact of TET3 on DNA repair

In this study, to further assess the function of TET3, it was overexpressed in the knockout cells, and the results were compared with those of the different cell lines. The cells were co-transfected with the BRET reporters of three targets, T1-T3, and the corresponding sgRNA in an undifferentiated state using both Cas9 as well as the inducible Cas9 systems. The frameshift rate results of the overexpressed cells resembled those of iNGN WT cells in both systems, suggesting that TET3 overexpression in TET3 knockout cells produces an analog to iNGN WT cells. Interestingly, in the iNGN TET3KO cells, the frameshift rate values were significantly higher and, in some instances, similar to HEK293T cell frameshift rates (4.2.2). The differences in genome editing events between the iNGNs suggest that the functional TET3 knockout has a positive influence on the editing results. In agreement with that, regardless of the Cas system and the used target, the iNGN TET3KO cell rates were greater. To determine how the TET3 protein impacts genome editing throughout differentiation, comparisons were made among the different iNGN cell lines and during the differentiation process from D0 to D4. As expected, the TET3 overexpression in the knockout cells illustrated similar frameshift rates to the iNGN WT cells throughout all stages of differentiation. Surprisingly, the results of iNGN TET3KO cells suggest that TET3 knockout influences are more prominent in the pluripotent and early stages of differentiation and diminish with further cell maturation (4.3). It was shown that TET3 is an important element in the neuronal differentiation process, and its knockout can negatively influence the differentiation and can increase DNA methylation (Santiago et al., 2014; Scott-Browne et al., 2017). Since TET3 protein increases in differentiation parallel to the elevation of 5hmC levels, this suggests the level of TET3 in the iNGN WT cells is lower in the undifferentiated state than after maturation. In accordance with this notion, the differences between WT and TET3KO cells were expected to be higher after differentiation and not in the pluripotent state. However, the results suggested that TET3 influences genome editing in the undifferentiated state and has minimal effects on mature neurons. This could be due to the relation between TET3 and CRISPR Cas9 genome editing, not to mention its function during differentiation, which promotes active demethylation, plus its interactions with different proteins impacting DNA repair pathways such as PARP1, which will be discussed in (5.4). Moreover, the 5mC level was discovered to be significantly higher in the iNGN TET3KO cells than in WT cells (Splith, 2019), proving that TET3 knockout increases DNA

methylation. This might also affect CRISPR Cas9 editing results in undifferentiated cells. After TET3 is knocked out, potential compensatory roles of the other TETs can rescue the differentiation process. It is tempting to speculate that the iNGN WT cells could mature at a faster rate than TET3KO cells. However, observing both cell lines using a microscope during differentiation showed no apparent difference. To determine whether the results may differ after a more extended differentiation period, further studying the cells in D8 or D10 post-differentiation can be helpful. The TET1/TET2/TET3 or TET2/TET3 knockout combination can have a more destructive effect on neuronal differentiation than TET3 alone. Further experiments are needed to verify whether studying these knockout combinations in relation to DNA repair may give different results. Moreover, TET3 overexpression in iNGN WT cells might help to understand its role in genome editing outcomes better.

5.4 Effect of PARP1 on DNA repair in undifferentiated iNGNs

PARP1 recognizes DSB and is involved in NHEJ, and HDR (Ray Chaudhuri & Nussenzweig, 2017). Here, the influence of PARP1 was investigated in undifferentiated neurons using BRET reporter system. The iNGNs and HEK293T cells, a standard cell line, were analyzed. All cell lines were co-transfected with a BRET reporter assay, the corresponding guide, with either PARP1 overexpression (PARP1 high) or Knockout (PARP1 low) plasmids. In HEK293T cells, PARP1 overexpression showed a significant decrease in the frameshift rate. In contrast, a considerable increase was noted in PARP1low frameshift rate values, which were significantly higher than PARP1 high. These data support the study by Du et al., which showed that PARP1 knockout in Mouse embryonic fibroblasts (MEFs) results in increased NHEJ activity compared to WT cells (Du et al., 2016). Moreover, they suggested that Fanconi anemia (FA) core complex and PARP1 influence DSB repair balance in hematopoietic stem and progenitor cells (HSPCs), where their knockouts lead to hyperactive NHEJ, which is restored after PARP1 re-expression (Du et al., 2016). The HEK293T data were consistent with those in undifferentiated iNGN WT and iNGN TET3KO cells, where the PARP1 high values are significantly lower than those of PARP1 low and the unmodified PARP1. Comparing the different cell lines, the frameshift rates of HEK293T resemble the values of the iNGN TET3KO cells, which both have significantly higher values than those of iNGN WT and TET3KO overexpressed cells, regardless of the PARP1 level (4.4.1). Lowering PARP1 in

all cell lines gave higher DNA repair outcomes than the rest, possibly due to the PARP1 interaction with the proteins regulating the NHEJ pathway. NHEJ is activated by binding Ku70/80 heterodimer to the DSB ends, and then the DNA-Ku scaffold stimulates the DNA-PKcs, creating the DNA-PKcs-Ku synaptic complex (Davis & Chen, 2013; Weterings & Chen, 2008; Yang et al., 2020). PARP1 PARylate DNA-PKcs, activating its kinase activity without Ku70/Ku80 complex assistance, and does not directly impact the repair pathway (Ray Chaudhuri & Nussenzweig, 2017). A study by Farmer et al. showed that BRCA1 and BRCA2-deficient cells, which are defective in HR repair, upon PARP1 inhibitor administration demonstrated loss of viability and instability in several models due to increased NHEJ repair mechanisms (Farmer et al., 2005). A possible interpretation is that PARP1 might have an inhibitory function toward NHEJ-mediated DNA repair, which may explain why the frameshift rates increased after downregulating PARP1 in all cell lines.

5.5 Effect of PARP1 on NHEJ during differentiation

It is important to know whether the results are also valid during differentiation and the mature non-replicative state, and not only in dividing cells. Moreover, a study has shown that neuronal differentiation was reduced in the PARP1 knockout neural stem cells (NSCs), which can also influence the outcomes (Hong et al., 2019). During the differentiation process from D0 to D4, the frameshift rates of the iNGN WT after PARP1 modulation indicated that the PARP1 low frameshift rate values were significantly higher throughout differentiation, and the PARP1 normal and high values were similar except for a slight decrease in PARP1 high at the undifferentiated stage. In harmony with these findings, the iNGN TET3KO cells' results followed similar trends to those of the WT cells regarding PARP1 modulation, except that the decreased PARP1 high rates were observed in both D0 and D1. However, after comparing the iNGNs, the iNGN TET3KO cells illustrated higher rates than those of iNGN WT and TET3KO overexpressed cells throughout differentiation, especially in PARP1 low values (4.4.3), and not only in the undifferentiated state or early stages of differentiation, like the previous results discussed. One might infer that this could be due to the interaction between TET3 and PARP1. PARP1 interacts with all TET members, but the relationship between PARP-mediated PARylation and TETs is not entirely clear. PARP inhibition enhances TET function. Niraparib-treated NIH3T3 cells and PARP1 knockout cells, as shown in Tolić et al.

exhibited decreased 5mC and increased 5hmC levels, indicating PARP1's inhibitory effect on TET hydroxylase activity. The PARP and TET families regulate DNA methylation and demethylation and may play a role in DNA damage repair (Tolić et al., 2022).

5.6 The impact of PARP1 on HDR

The results discussed so far are based on the error-prone NHEJ repair pathway, which is activated in both mitotic and post-mitotic neurons throughout the cell cycle. To gain insight into the HDR pathway, which is active in the S and G2 stages of the cell cycle in the dividing cells and hardly in post-mitotic neurons (Nishiyama et al., 2017), HDR template was additionally transfected. Pasquini et al. studied DSB repair pathways in several *in-vivo* and *in-vitro* models. The data showed similar results in adult human retinas, macaque, and mouse retinas. Moreover, in postmitotic neurons as well as retinal organoids, NHEJ is constant during differentiation. In contrast, HDR is downregulated but still present. These results resemble the *in-vivo* retinal activity (Pasquini et al., 2020). Due to the easier handling of the *in-vitro* models, this makes iNGNs a valuable candidate for studying DNA repair pathway engineering and achieving precise genome editing. In this study, after adding HDR template, HEK293T cell frameshift rates exhibited comparable behavior to those without HDR template, by which PARP1 low rate was higher than both PARP1 high and normal. Yet, all the frameshift rates were lower than those without HDR template addition except for PARP1 high values, which showed no significant difference. The frameshift rates are expected to be lower after adding the HDR template due to HDR repair of DSB after CRISPR Cas9 genome editing. One might reasonably hypothesize that the insignificant difference between the PARP1 overexpression frameshift rates with and without the HDR template is due to increased HDR suppression. PARP1 is important in HDR through its engagement of different proteins and their influences on the repair pathway (Ray Chaudhuri & Nussenzweig, 2017). However, unlike HEK293T cells, and supporting the study showing that HDR activity was not affected in PARP1 knockout cells, it seems that PARP1 has little direct effect on HDR (Schultz et al., 2003). There are no significant differences between the frameshift rates compared to those without HDR template in the undifferentiated state, just a minimum difference in PARP1 low in TET3KO cells. Moreover, acting in a consistent manner regardless of the HDR template, both iNGN WT and iNGN TET3KO cells' frameshift rates of PARP1 low were higher than those of PARP1 high and normal.

Assessing the various cell lines, the frameshift rates of undifferentiated iNGN TET3KO cells have significantly higher values than those of HEK293T cells, iNGN WT, and TET3KO overexpressed cells, regardless of the PARP1 modification. On the other hand, during differentiation, the PARP1 Low values were higher than the rest of the values throughout the process in all the iNGNs, with the TET3KO cells being higher. The results in Du et al. showed a decrease in HDR activity in MEFs PARP1 knockout cells compared to WT cells, especially under Paraquat-mediated oxidative stress. (Du et al., 2016). In addition, Hochegger et al. showed that PARP1 inhibits Ku activity, which results in HDR upregulation. Therefore, in PARP1 knockout cells, Ku increases NHEJ, and by knocking out both, HDR can operate better (Hochegger et al., 2006). As previously mentioned in Hong et al. PARP1 regulates neuronal differentiation of NSCs, and reductions in the expression of neurogenic factors of neuronal differentiation in the PARP1 knockout NSCs were noticed. Moreover, PARP1 controls neurogenesis during development as well as in adult mice. In PARP1 knockout mice, it may cause schizophrenia-like behavioral abnormalities (Hong et al., 2019). Here, in the present data, knowing that HDR is only active in dividing cells, and the NHEJ repair mechanism is expected to be the main repair pathway in post-mitotic neurons, with HDR activity declining during differentiation. However, a limitation of the BRET reporter quantification method is that HDR and NHEJ can occur simultaneously and cannot be distinguished with certainty. Despite the major advantages of this system, such as evaluating DNA repair independently of transfected cell concentration and number, which is beneficial in evaluating transfected neurons (Wimmer et al., 2021), Further assessment would ultimately clarify the results. Using another quantification method could be helpful. The Traffic Light Reporter 3 (TLR3) system could be used in the future as a reliable method for HDR quantification. In this system, HDR causes a green, fluorescent signal after repairing the GFP sequence utilizing a donor template, while one-third of NHEJ activates a blue, fluorescent signal (Song & Stieger, 2017).

Table 27: Comparison between quantification methods of genome editing

Quantification method	NHEJ	HDR	comments	References
Sequencing-based techniques				
Sanger sequencing	+	+	• Time-consuming • TIDE analysis	(Brinkman et al., 2014; Sanger et al., 1977)
Next-generation sequencing (NGS)	+	+	• Costly • Precise information	(Güell et al., 2014)
DNA denaturation-based techniques				
Single-stranded conformational polymorphism (SSCP)	+	-	• Only measure short fragments	(Inazuka et al., 1997)
Denat. high-performance liquid chromatography (DHPLC)	+	-	• Only measure short fragments	(Qiu et al., 2004)
Mismatch-sensitive endonucleases				
Surveyor nucleases	+	-	• Time-consuming • Give false positive outcomes	(K. Wang et al., 2015)
Fluorescent reporters				
TLR3 Reporter system	+	+	• 1/3 ratio of NHEJ events	(Song & Stieger, 2017).
BRET reporter system	+	+	• Cannot distinguish HDR from NHEJ	(Wimmer et al., 2021)

5.7 Outlook

DNA repair pathway engineering through the modulation of PARP1 has been investigated using iNGN cell lines and HEK293T cells. A significant change was noticed after the PARP1 level was downregulated. Additionally, the impact of TET3 on the genome editing outcomes throughout the differentiation process was analyzed. To verify the results obtained using the BRET reporter system at the genomic level, as well as to study the impacts of PARP1 and TET3 on the HDR repair pathway, applying the TLR3 system can be used as an alternative approach. Starting with generating the iNGN WT TLR3 and iNGN TET3KO TLR3 stable cell lines by integrating TLR3 into iNGN genomes. Then the same transfection protocol will be followed, and the results will be assessed using FACS. Moreover, for future research, it could focus on the TET1/TET2/TET3 or TET2/TET3 knockout combinations, which can affect neuronal differentiation and CRISPR Cas9 genome editing differently than TET3. Furthermore, TET3 overexpression in iNGN WT cells can also be tested to investigate and compare the results with those of TET3 knockout, along with evaluating the cells after an extended differentiation period. In adult photoreceptors, PARP1 is highly expressed, which makes MMEJ active in these cells. Therefore, in genome editing, MMEJ is of major importance to correct IRD mutations in the retina (Pasquini et al., 2020). Thus, evaluating MMEJ in iNGNs could be highly beneficial and should be further explored. This study focused on iNGNs as an *in-vitro* model. The results generated can be investigated using an *in-vivo* model and, eventually, disease models to validate potential therapeutic strategies using CRISPR Cas9.

6 Summary

Inherited retinal dystrophies are a group of genetically and clinically heterogeneous disorders that vary in their clinical presentation and progression, possibly leading to blindness. So far, about 332 genes, most expressed in photoreceptors, have been identified to be associated with these diseases. The relatively new genome editing field, particularly CRISPR-Cas9-mediated genome editing technology, which introduces DNA double-strand breaks (DSBs) that are subsequently repaired by the cells' repair systems, has recently drawn much attention. The major repair pathways are non-homologous end-joining (NHEJ) and homology-directed repair (HDR). One of the main obstacles to its application in the retina is the limited knowledge of DNA repair in photoreceptors.

This work aims to analyze the DNA repair mechanisms, improve CRISPR Cas9 genome editing efficacy by modulating and engineering the DNA repair pathways in mature neurons using the human inducible Neurogenin iPS (iNGN) cell line, and validate it as an *in vitro* model system. These cells are human-induced pluripotent stem cells that differentiate into mature neurons within 4 days. In addition, the iNGN TET3KO cell line was also investigated to determine the impact of the TET3 protein at various differentiation stages.

To achieve this, the iNGN cell lines and a control cell line, HEK293T cells, were transfected with BRET reporter assay plasmid using Cas9 and the inducible Cas systems (iCas). Promoter optimizations were done by replacing the CMV promoter, which can be silenced and suppressed in certain cell types, with a sustained EF1α promoter. Applying the Cas9 system, iNGN WT and iNGN TET3KO cells were tested throughout the differentiation process. Moreover, the modifications of PARP1 protein levels using PARP1 overexpression or knockout plasmids were necessary to study its influence on the DNA repair pathways of different cell lines. The BRET reporter assay was the primary quantitative technique used.

The results showed decreased frameshift rates for the undifferentiated iNGN using the iCas system compared to the Cas9 system, and along with failure to use its timing control advantage, the Cas9 system was mainly used for the remaining experiments. The undifferentiated iNGN TET3KO cells' frameshift rates, as well as at the beginning of differentiation, were significantly higher than iNGN WT ones. Furthermore, the frameshift rate results of the TET3KO overexpressed cells resembled those of iNGN WT

cells. After PARP1 modulation, the frameshift rates of PARP1 downregulation were greater throughout the differentiation process of the iNGNs, regardless of the HDR template addition. Interestingly, the results of the iNGN TET3KO cells were higher than those of the WT cells. For future assessment, the generation and application of iNGNs TLR3 cell lines is essential to verify the results obtained using the BRET reporter assay at the genomic level.

7 Zusammenfassung

Erbliche Retinadystrophien sind eine Gruppe genetisch und klinisch heterogener Erkrankungen, die in ihrer klinischen Präsentation und ihrem Verlauf variieren und möglicherweise zur Erblindung führen können. Bisher wurden etwa 332 Gene identifiziert, die größtenteils in Photorezeptoren exprimiert werden und mit diesen Erkrankungen in Zusammenhang stehen. Das relativ neue Gebiet der Genomeditierung, insbesondere die CRISPR-Cas9-vermittelte Genomeditierungstechnologie, die DNA-Doppelstrangbrüche (DSBs) einführt, die anschließend von den Reparatursystemen der Zellen repariert werden, hat in letzter Zeit viel Aufmerksamkeit auf sich gezogen. Die wichtigsten Reparaturwege sind die nicht-homologe Endverbindung (NHEJ) und die homologiegerichtete Reparatur (HDR). Eines der Haupthindernisse für die Anwendung in der Netzhaut ist das begrenzte Wissen über die DNA-Reparatur in Photorezeptoren.

Ziel dieser Arbeit ist es, die DNA-Reparaturmechanismen zu analysieren, die Wirksamkeit der CRISPR-Cas9-Genombearbeitung durch Modulation und Manipulation der DNA-Reparaturwege in reifen Neuronen zu verbessern und die menschliche induzierbare Neurogenin iPS (iNGN)-Zelllinie als In-vitro-Modellsystem zu validieren. Diese Zellen sind human-induzierte pluripotente Stammzellen, die sich innerhalb von 4 Tagen in reife Neuronen differenzieren. Darüber hinaus wurde auch die iNGN TET3KO-Zelllinie untersucht, um die Auswirkungen des TET3-Proteins in verschiedenen Differenzierungsstadien zu bestimmen.

Um dies zu erreichen, wurden die iNGN-Zelllinien und eine Kontrollzelllinie HEK293T-Zellen mit einem BRET-Reporter Assay-Plasmid unter Verwendung des Cas9- und der induzierbaren Cas-Systeme (iCas) transfiziert.Die Promotoroptimierungen wurden durch den Austausch des CMV-Promotors, der in bestimmten Zelltypen stummgeschaltet und unterdrückt werden kann, durch einen dauerhaften EF1α-Promotor durchgeführt.Unter Anwendung des Cas9-Systems wurden iNGN WT und iNGN TET3KO-Zellen während des gesamten Differenzierungsprozesses getestet. Darüber hinaus waren die Modifikationen der PARP1-Proteinspiegel mithilfe von PARP1-Überexpression oder Knockout-Plasmiden notwendig, um den Einfluss auf die DNA-Reparaturwege verschiedener Zelllinien zu untersuchen. Der BRET-Reporter-Assay war die primäre verwendete quantitative Technik.

Die Ergebnisse zeigten verringerte Frameshift-Raten für die undifferenzierten iNGN unter Verwendung des iCas-Systems im Vergleich zum Cas9-System.Da der Vorteil der Zeitsteuerung des iCas-Systems jedoch nicht genutzt wurde, wurde das Cas9-System für die verbleibenden Experimente hauptsächlich verwendet. Die Frameshift-Raten der undifferenzierten iNGN TET3KO-Zellen sowie zu Beginn der Differenzierung waren signifikant höher als die der iNGN WT. Darüber hinaus ähnelten die Frameshift-Ratenergebnisse der TET3KO-überexprimierten Zellen denen der iNGN WT-Zellen. Nach der PARP1-Modulation waren die Frameshift-Raten bei der PARP1-Herunterregulierung während des gesamten Differenzierungsprozesses der iNGNs höher, unabhängig von der Hinzufügung der HDR-Vorlage. Interessanterweise waren die Ergebnisse der iNGN TET3KO-Zellen höher als die der WT-Zellen. Für zukünftige Bewertungen ist die Erzeugung und Anwendung von iNGNs TLR3-Zelllinien entscheidend, um die mit dem BRET-Reporter-Assay auf genomischer Ebene erzielten Ergebnisse zu bestätigen.

I Abbreviations

%	percent
°C	celsius
µL	microlitre
3′	three prime
4-OHT	4-hydroxytamixofen
5′	five prime
5caC	5-carboxylcytosine
5fC	5-formylcytosine
5hmC	5-Hydroxymethylcytosine
5mC	5-methylcytosine
AF	autofluorescence imaging
alt-EJ	alternative end joining
AMD	auto-modification domain
ARTD1	diphtheria toxin-like ADP-ribosyltransferase
ATM	ataxia-telangiectasia mutated
ATR	Ataxia telangiectasia and Rad3 related
BFP	blue fluorescent protein
BFP	blue fluorescent protein
BIR	break-induced replication
BLM	bloom syndrome protein
bp	base pair
BRCA1/2	breast cancer type 1/2 susceptibility protein
BRET	bioluminescence resonance energy transfer
Cas9	CRISPR-associated protein 9
cBU	Centi BRET unit
CD	C-terminal catalytic domain
CDKs	cyclin-dependent kinases
CIP	chemically induced proximity systems
CMV	Cytomegalovirus
c-NHEJ	classical nonhomologous end joining
CRISPR	clustered regularly interspaced short palindromic repeats
crRNA	CRISPR RNAs
CtIP	C-terminal-binding protein-interacting protein
DBD	DNA binding domain
ddH2O	double-distilled water
DDR	DNA damage response
DHPLC	denaturing high-performance liquid chromatography
D-loop	displacement loop
DNA	deoxyribonucleic acid
Dna2	DNA Replication Helicase/Nuclease 2
DNA-PKcs	DNA-dependent protein kinase catalytic subunit
Dox	doxycycline
DSBR	double-strand break repair
DSBs	double-strand breaks
dsDNA	Double strand DNA
dsODN	single-stranded oligodeoxyribonucleotide

DSβH	double-stranded β-helix
EF1α	Human elongation factor-1 alpha
ERG	electroretinography
Exo1	exonuclease 1
FACS	fluorescence-activated cell sorting
Fe(II)/α-KG	iron(II)/α-ketoglutarate
FRET	fluorescence resonance energy transfer
GFP	green fluorescent protein
HDR	homology-directed repair
HEK293T	Human embryonic kidney 293 cells
HIT	Hybrid drug Inducible CRISPR
HNF 1α	hepatocyte nuclear factor-1
HNH	His-Asn-His
HR	homologous recombination
I_{em}	intensity of emissions
indel	insertion and deletion
iNGN	human inducible Neurogenin iPS
iPSCs	induced pluripotent stem cells
IRDs	Inherited retinal dystrophies
LB	Lysogeny broth
Lig3/Lig1	ligase III/I
MegNs	Meganucleases
MH	microhomologous sequences
min	minute
MITI	microhomology-dependent targeted integration
mL	milliliter
MMEJ	microhomology-mediated end-joining
MRN	MRE11-RAD50-NBS1
NAD+	nicotinamide adenine dinucleotide
NFκB	p65 of human nuclear factor
NGS	Next-generation sequencing
NHEJ	non-homologous end joining
nM	Nanomolar
OCT	optical coherence tomography
PALB2	partner and localizer of BRCA2
PAM	protospacer adjacent motif
PARP1	poly ADP-ribose polymerase-1
PARPi	PARP inhibitors
PBS	phosphate-buffered saline
PBS	phosphate-buffered saline
Pcmv	promoter sequence of the human cytomegalovirus promoter
PCR	polymerase chain reaction
PI3K	phosphoinositide 3-kinase
PR	photoreceptor cells
pre-crRNA	precursor CRISPR RNA
RAP80	receptor-associated protein 80
REST	RE1-silencing transcription factor
RLuc8	Renilla reniformis luciferase

RNA	ribonucleic acid
ROS	reactive oxygen species
RPA	replication protein A
RPE	retinal pigment epithelium
rtTA	reverse tetracycline-controlled transcriptional activator system
SATI	single homology arm donor-mediated intron-targeting integration
SCD	sickle cell disease
SDSA	synthesis-dependent strand-annealing
sgRNA	single guide RNA
SSA	single-strand annealing
SSCP	single-stranded conformational polymorphism
TALENs	transcription activator-like effector nucleases
TAM	Tamoxifen
TET	Ten-Eleven translocation
TET3FL	TET3 full-length
TET3o	TET3 oocytes
TET3s	TET3 short
tetO	tet operator sequences
TetR	Tetracycline repressor
TIDE	tracking of indels by decomposition
TLR	Traffic Light Reporter system
tracrRNA	Trans-activating crRNA
tTA	tetracycline-controlled transactivator system
tTS	tetracycline-controlled transcriptional silencer
UV	ultraviolet light
WES	whole exome sequencing
WGS	whole genome sequencing
WT	Wildtype
XLF	XRCC4-like factor
XRCC1	X-ray repair cross-complementing protein 1
XRCC4	X-ray repair cross-complementing protein 4
ZFNs	zinc finger nucleases
β	beta

II List of figures

III List of tables

References

Adli, M. (2018). The CRISPR tool kit for genome editing and beyond. *Nature Communications*, *9*(1). https://doi.org/10.1038/s41467-018-04252-2

Amé, J. C., Rolli, V., Schreiber, V., Niedergang, C., Apiou, F., Decker, P., Muller, S., Höger, T., Ménissier-de Murcia, J., & De Murcia, G. (1999). PARP-2, a novel mammalian DNA damage-dependent poly(ADP-ribose) polymerase. *Journal of Biological Chemistry*, *274*(25), 17860–17868. https://doi.org/10.1074/jbc.274.25.17860

Anzalone, A. V., Randolph, P. B., Davis, J. R., Sousa, A. A., Koblan, L. W., Levy, J. M., Chen, P. J., Wilson, C., Newby, G. A., Raguram, A., & Liu, D. R. (2019). Search-and-replace genome editing without double-strand breaks or donor DNA. *Nature*, *576*(7785), 149–157. https://doi.org/10.1038/s41586-019-1711-4

Bacaj, T., & Shaham, S. (2007). Temporal control of cell-specific transgene expression in Caenorhabditis elegans. *Genetics*, *176*(4), 2651–2655. https://doi.org/10.1534/genetics.107.074369

Barzilai, A., & Yamamoto, K. I. (2004). DNA damage responses to oxidative stress. *DNA Repair*, *3*(8–9), 1109–1115. https://doi.org/10.1016/j.dnarep.2004.03.002

BESTOR T.H., B. D. (2004). Transposon Silencing and Imprint Establishment in Mammalian Germ Cells. *Cold Spring Harbor Laboratory Press*, *69*(Cold Spring Harbor symposia on quantitative biology), 381–388.

Bétermier, M., Bertrand, P., & Lopez, B. S. (2014). Is Non-Homologous End-Joining Really an Inherently Error-Prone Process? *PLoS Genetics*, *10*(1). https://doi.org/10.1371/journal.pgen.1004086

Bouchard, V. J., Rouleau, M., & Poirier, G. G. (2003). PARP-1, a determinant of cell survival in response to DNA damage. *Experimental Hematology*, *31*(6), 446–454. https://doi.org/10.1016/S0301-472X(03)00083-3

Brinkman, E. K., Chen, T., Amendola, M., & Van Steensel, B. (2014). Easy quantitative assessment of genome editing by sequence trace decomposition. *Nucleic Acids Research*, *42*(22). https://doi.org/10.1093/nar/gku936

Burma, S., Chen, B. P. C., & Chen, D. J. (2006). Role of non-homologous end joining (NHEJ) in maintaining genomic integrity. *DNA Repair*, *5*(9–10), 1042–1048. https://doi.org/10.1016/j.dnarep.2006.05.026

Busskamp, V., Lewis, N. E., Guye, P., Ng, A. H., Shipman, S. L., Byrne, S. M., Sanjana, N. E., Murn, J., Li, Y., Li, S., Stadler, M., Weiss, R., & Church, G. M. (2014). Rapid neurogenesis through transcriptional activation in human

stem cells. *Molecular Systems Biology*, *10*(11), 1–21. https://doi.org/10.15252/msb.20145508

Certo, M. T., Ryu, B. Y., Annis, J. E., Garibov, M., Jarjour, J., Rawlings, D. J., & Scharenberg, A. M. (2011). Tracking genome engineering outcome at individual DNA breakpoints. *Nature Methods*, *8*(8), 671–676. https://doi.org/10.1038/nmeth.1648

Chapman, J. R., Taylor, M. R. G., & Boulton, S. J. (2012). Playing the End Game: DNA Double-Strand Break Repair Pathway Choice. *Molecular Cell*, *47*(4), 497–510. https://doi.org/10.1016/j.molcel.2012.07.029

Ciccarone, F., Valentini, E., Bacalini, M. G., Zampieri, M., Calabrese, R., Guastafierro, T., Mariano, G., Reale, A., Franceschi, C., & Caiafa, P. (2014). Poly(ADP-ribosyl)ation is involved in the epigenetic control of TET1 gene transcription. *Oncotarget*, *5*(21), 10356–10367. https://doi.org/10.18632/oncotarget.1905

Cox, D. B. T., Platt, R. J., & Zhang, F. (2015). Therapeutic genome editing: Prospects and challenges. *Nature Medicine*, *21*(2), 121–131. https://doi.org/10.1038/nm.3793

D'amours, D., Desnoyers, S., Silva, D. ', & Poirier, G. G. (1999). Poly(ADP-ribosyl)ation reactions in the regulation of nuclear functions. In *Biochem. J* (Vol. 342).

Das, A. T., Zhou, X., Vink, M., Klaver, B., Verhoef, K., Marzio, G., & Berkhout, B. (2004). Viral Evolution as a Tool to Improve the Tetracycline-regulated Gene Expression System. *Journal of Biological Chemistry*, *279*(18), 18776–18782. https://doi.org/10.1074/jbc.M313895200

Davis, A. J., & Chen, D. J. (2013). DNA double strand break repair via non-homologous end-joining. *Translational Cancer Research*, *2*(3), 130–143. https://doi.org/10.3978/j.issn.2218-676X.2013.04.02

Delatte, B., Deplus, R., & Fuks, F. (2014). Playing TET ris with DNA modifications . *The EMBO Journal*, *33*(11), 1198–1211. https://doi.org/10.15252/embj.201488290

Doudna, J. A., & Charpentier, E. (2014). The new frontier of genome engineering with CRISPR-Cas9. *Science*, *346*(6213). https://doi.org/10.1126/science.1258096

Du, W., Amarachintha, S., Wilson, A. F., & Pang, Q. (2016). Hyper-active non-homologous end joining selects for synthetic lethality resistant and pathological Fanconi anemia hematopoietic stem and progenitor cells. *Scientific Reports*, *6*. https://doi.org/10.1038/srep22167

European Medicines Agency. (2018). *Luxturna (voretigene neparvovec) receives marketing authorisation valid throughout the EU. https://www.ema.europa.eu/en/medicines/human/EPAR/Luxturna*

European Medicines Agency. (2024). *First gene editing therapy to treat beta thalassemia and severe sickle cell disease. https://www.ema.europa.eu/en/medicines/human/EPAR/casgevy*

Farmer, H., McCabe, H., Lord, C. J., Tutt, A. H. J., Johnson, D. A., Richardson, T. B., Santarosa, M., Dillon, K. J., Hickson, I., Knights, C., Martin, N. M. B., Jackson, S. P., Smith, G. C. M., & Ashworth, A. (2005). Targeting the DNA repair defect in BRCA mutant cells as a therapeutic strategy. *Nature*, *434*(7035), 917–921. https://doi.org/10.1038/nature03445

Feng, Y., Li, X., Cassady, K., Zou, Z., & Zhang, X. (2019). TET2 function in hematopoietic malignancies, immune regulation, and DNA repair. *Frontiers in Oncology*, *9*(APR), 1–9. https://doi.org/10.3389/fonc.2019.00210

Förster, T. (1948). Zwischenmolekulare Energiewanderung und Fluoreszenz. *Annalen Der Physik*, *437*(1–2), 55–75. https://doi.org/10.1002/andp.19484370105

Freundlieb, S., Schirra-Müller, C., & Bujard, H. (1999). A Tetracycline Controlled Activation/Repression System with Increased Potential for Gene Transfer into Mammalian Cells. *Journal of Gene Medicine*, *1*(1), 4–12. https://doi.org/10.1002/(SICI)1521-2254(199901/02)1:1<4::AID-JGM4>3.0.CO;2-Y

Fussenegger, M. (2001). The impact of mammalian gene regulation concepts on functional genomic research, metabolic engineering, and advanced gene therapies. *Biotechnology Progress*, *17*(1), 1–51. https://doi.org/10.1021/bp000129c

Gao, F., Kwon, S. W., Zhao, Y., & Jin, Y. (2009). PARP1 poly(ADP-ribosyl)ates Sox2 to control Sox2 protein levels and FGF4 expression during embryonic stem cell differentiation. *Journal of Biological Chemistry*, *284*(33), 22263–22273. https://doi.org/10.1074/jbc.M109.033118

Gasiunas, G., Barrangou, R., Horvath, P., & Siksnys, V. (2012). Cas9-crRNA ribonucleoprotein complex mediates specific DNA cleavage for adaptive immunity in bacteria. *Proceedings of the National Academy of Sciences of the United States of America*, *109*(39). https://doi.org/10.1073/pnas.1208507109

Gavande, N. S., Vandervere-Carozza, P. S., Pawelczak, K. S., Mendoza-Munoz, P., Vernon, T. L., Hanakahi, L. A., Summerlin, M., Dynlacht, J. R., Farmer, A. H., Sears, C. R., Nasrallah, N. Al, Garrett, J., & Turchi, J. J. (2020). Discovery and development of novel DNA-PK inhibitors by targeting the unique Ku-

DNA interaction. *Nucleic Acids Research*, *48*(20), 11536–11550. https://doi.org/10.1093/nar/gkaa934

Germini, D., Tsfasman, T., Zakharova, V. V., Sjakste, N., Lipinski, M., & Vassetzky, Y. (2018). A Comparison of Techniques to Evaluate the Effectiveness of Genome Editing. *Trends in Biotechnology*, *36*(2), 147–159. https://doi.org/10.1016/j.tibtech.2017.10.008

Giglia-Mari, G., Zotter, A., & Vermeulen, W. (2011). DNA damage response. *Cold Spring Harbor Perspectives in Biology*, *3*(1), 1–19. https://doi.org/10.1101/cshperspect.a000745

Gordon, K., Del Medico, A., Sander, I., Kumar, A., & Hamad, B. (2019). Gene therapies in ophthalmic disease. In *Nature Reviews Drug Discovery* (Vol. 18, Issue 6, pp. 415–416). Nature Publishing Group. https://doi.org/10.1038/d41573-018-00016-1

Gossen, M., Freundlieb, S., Bender, G., Müller, G., Hillen, W., & Bujard, H. (1995). Transcriptional Activation by Tetracyclines in Mammalian Cells. *Science*, *1766–1769*(268.5218).

Güell, M., Yang, L., & Church, G. M. (2014). Genome editing assessment using CRISPR Genome Analyzer (CRISPR-GA). *Bioinformatics (Oxford, England)*, *30*(20), 2968–2970. https://doi.org/10.1093/bioinformatics/btu427

Guiner, C., Stieger, K., Snyder, R., Rolling, F., & Moullier, P. (2007). Immune Responses to Gene Product of Inducible Promoters. *Current Gene Therapy*, *7*(5), 334–346. https://doi.org/10.2174/156652307782151461

Guo, J. U., Su, Y., Zhong, C., Ming, G. L., & Song, H. (2011). Emerging roles of TET proteins and 5-hydroxymethylcytosines in active DNA demethylation and beyond. *Cell Cycle*, *10*(16), 2662–2668. https://doi.org/10.4161/cc.10.16.17093

Gupta, R., Jha, A., Ambasta, R. K., & Kumar, P. (2021). Regulatory mechanism of cyclins and cyclin-dependent kinases in post-mitotic neuronal cell division. *Life Sciences*, *285*(July), 120006. https://doi.org/10.1016/j.lfs.2021.120006

Hartong, D., Berson, E., & Dryja, T. (2006). Retinitis pigmentosa Prevalence and inheritance patterns. *Lancet*, *368*, 1795–1809.

Hasan, M. N., Hyodo, T., Biswas, M., Rahman, M. L., Mihara, Y., Karnan, S., Ota, A., Tsuzuki, S., Hosokawa, Y., & Konishi, H. (2023). Flow cytometry-based quantification of genome editing efficiency in human cell lines using the L1CAM gene. *PLoS ONE*, *18*(11 NOVEMBER), 1–21. https://doi.org/10.1371/journal.pone.0294146

Helleday, T., Lo, J., van Gent, D. C., & Engelward, B. P. (2007). DNA double-strand break repair: From mechanistic understanding to cancer treatment. *DNA Repair*, *6*(7), 923–935. https://doi.org/10.1016/j.dnarep.2007.02.006

Helleday, T., Petermann, E., Lundin, C., Hodgson, B., & Sharma, R. A. (2008). DNA repair pathways as targets for cancer therapy. In *Nature Reviews Cancer* (Vol. 8, Issue 3, pp. 193–204). https://doi.org/10.1038/nrc2342

Herrup, K. (2013). Post-mitotic role of the cell cycle machinery. *Current Opinion in Cell Biology*, *25*(6), 711–716. https://doi.org/10.1016/j.ceb.2013.08.001

Hill, P. W. S., Amouroux, R., & Hajkova, P. (2014). DNA demethylation, Tet proteins and 5-hydroxymethylcytosine in epigenetic reprogramming: An emerging complex story. *Genomics*, *104*(5), 324–333. https://doi.org/10.1016/j.ygeno.2014.08.012

Hochegger, H., Dejsuphong, D., Fukushima, T., Morrison, C., Sonoda, E., Schreiber, V., Guang, Y. Z., Saberi, A., Masutani, M., Adachi, N., Koyama, H., De Murcia, G., & Takeda, S. (2006). Parp-1 protects homologous recombination from interference by Ku and Ligase IV in vertebrate cells. *EMBO Journal*, *25*(6), 1305–1314. https://doi.org/10.1038/sj.emboj.7601015

Hong, S., Yi, J. H., Lee, S., Park, C. H., Ryu, J. H., Shin, K. S., & Kang, S. J. (2019). Defective neurogenesis and schizophrenia-like behavior in PARP-1-deficient mice. *Cell Death and Disease*, *10*(12). https://doi.org/10.1038/s41419-019-2174-0

Hu, M. L., Edwards, T. L., O'Hare, F., Hickey, D. G., Wang, J. H., Liu, Z., & Ayton, L. N. (2021). Gene therapy for inherited retinal diseases: progress and possibilities. *Clinical and Experimental Optometry*, *104*(4), 444–454. https://doi.org/10.1080/08164622.2021.1880863

Hu, Z., Shi, Z., Guo, X., Jiang, B., Wang, G., Luo, D., Chen, Y., & Zhu, Y. S. (2018). Ligase IV inhibitor SCR7 enhances gene editing directed by CRISPR-Cas9 and ssODN in human cancer cells. *Cell and Bioscience*, *8*(1). https://doi.org/10.1186/s13578-018-0200-z

Huang, D., & Kraus, W. L. (2022). The expanding universe of PARP1-mediated molecular and therapeutic mechanisms. *Molecular Cell*, *82*(12), 2315–2334. https://doi.org/10.1016/j.molcel.2022.02.021

Huletsky, A., de Murcia, G., Muller, S., Hengartner, M., Ménard, L., Lamarre, D., & Poirier, G. G. (1989). The Effect of poly(ADP-ribosyl)ation on Native and H1-depleted Chromatin. *Journal of Biological Chemistry*, *264*(15), 8878–8886. https://doi.org/10.1016/s0021-9258(18)81875-0

Hwang, E., Song, J., & Zhang, J. (2019). Integration of nanomaterials and bioluminescence resonance energy transfer techniques for sensing biomolecules. *Biosensors*, *9*(1). https://doi.org/10.3390/bios9010042

Inazuka, M., Wenz, H.-M., Sakabe, M., Tahira, T., & Hayashi, K. (1997). *A Streamlined Mutation Detection System: Multicolor Post-PCR Fluorescence Labeling and Single-Strand Conformational Polymorphism Analysis by Capillary Electrophoresis*.

Ishino, Y., Krupovic, M., & Forterre, P. (2018). History of CRISPR-Cas from Encounter with a Mysterious Repeated Sequence to Genome Editing Technology. *Journal of Bacteriology*, *200*(7), e00580-17.

Jaenisch, R., & Bird, A. (2003). Epigenetic regulation of gene expression: How the genome integrates intrinsic and environmental signals. In *Nature Genetics* (Vol. 33, Issue 3S, pp. 245–254). https://doi.org/10.1038/ng1089

Jiang, D., Wei, S., Chen, F., Zhang, Y., & Li, J. (2017). TET3-mediated DNA oxidation promotes ATR-dependent DNA damage response. *EMBO Reports*, *18*(5), 781–796. https://doi.org/10.15252/embr.201643179

Jin, S. G., Zhang, Z. M., Dunwell, T. L., Harter, M. R., Wu, X., Johnson, J., Li, Z., Liu, J., Szabó, P. E., Lu, Q., Xu, G. liang, Song, J., & Pfeifer, G. P. (2016). Tet3 Reads 5-Carboxylcytosine through Its CXXC Domain and Is a Potential Guardian against Neurodegeneration. *Cell Reports*, *14*(3), 493–505. https://doi.org/10.1016/j.celrep.2015.12.044

Jinek, M., Chylinski, K., Fonfara, I., Hauer, M., Doudna, J. A., & Charpentier, E. (2012). *A Programmable Dual-RNA-Guided DNA Endonuclease in Adaptive Bacterial Immunity*. https://www.science.org

Junying, Y., Kejin, H., Kim, S. O., Shulan, T., Stewart, R., Slukvin, I. I., & Thomson, J. A. (2009). Human induced pluripotent stem cells free of vector and transgene sequences. *Science*, *324*(5928), 797–801. https://doi.org/10.1126/science.1172482

Kamaletdinova, T., Fanaei-Kahrani, Z., & Wang, Z. Q. (2019). The enigmatic function of parp1: From parylation activity to par readers. *Cells*, *8*(12), 1–20. https://doi.org/10.3390/cells8121625

Karakaidos, P., Karagiannis, D., & Rampias, T. (2020). Resolving DNA damage: Epigenetic regulation of DNA repair. In *Molecules* (Vol. 25, Issue 11). MDPI AG. https://doi.org/10.3390/molecules25112496

Karra, D., & Dahm, R. (2010). Transfection techniques for neuronal cells. In *Journal of Neuroscience* (Vol. 30, Issue 18, pp. 6171–6177). https://doi.org/10.1523/JNEUROSCI.0183-10.2010

Kass, E. M., & Jasin, M. (2010). Collaboration and competition between DNA double-strand break repair pathways. *FEBS Letters*, *584*(17), 3703–3708. https://doi.org/10.1016/j.febslet.2010.07.057

Khalil, A. M. (2020). The genome editing revolution: review. *Journal of Genetic Engineering and Biotechnology*, *18*(1), 68. https://doi.org/10.1186/s43141-020-00078-y

Ko, M., An, J., Bandukwala, H. S., Chavez, L., Äijö, T., Pastor, W. A., Segal, M. F., Li, H., Koh, K. P., Lähdesmäki, H., Hogan, P. G., Aravind, L., & Rao, A. (2013). Modulation of TET2 expression and 5-methylcytosine oxidation by the CXXC domain protein IDAX. *Nature*, *497*(7447), 122–126. https://doi.org/10.1038/nature12052

Kohli, R. M., & Zhang, Y. (2013). TET enzymes, TDG and the dynamics of DNA demethylation. *Nature*, *502*(7472), 472–479. https://doi.org/10.1038/nature12750

Kong, X., Gong, Z., Zhang, L., Sun, X., Ou, Z., Xu, B., Huang, J., Long, D., He, X., Lin, X., Li, Q., Xu, L., & Xuan, A. (2019). JAK2/STAT3 signaling mediates IL-6-inhibited neurogenesis of neural stem cells through DNA demethylation/methylation. *Brain, Behavior, and Immunity*, *79*(January), 159–173. https://doi.org/10.1016/j.bbi.2019.01.027

Lam, R. S., Töpfer, F. M., Wood, P. G., Busskamp, V., & Bamberg, E. (2017). Functional maturation of human stem cell-derived neurons in long-term cultures. *PLoS ONE*, *12*(1), 1–26. https://doi.org/10.1371/journal.pone.0169506

Langelier, M. F., Riccio, A. A., & Pascal, J. M. (2014). PARP-2 and PARP-3 are selectively activated by 5' phosphorylated DNA breaks through an allosteric regulatory mechanism shared with PARP-1. *Nucleic Acids Research*, *42*(12), 7762–7775. https://doi.org/10.1093/nar/gku474

Langelier, M. F., Servent, K. M., Rogers, E. E., & Pascal, J. M. (2008). A third zinc-binding domain of human poly(ADP-ribose) polymerase-1 coordinates DNA-dependent enzyme activation. *Journal of Biological Chemistry*, *283*(7), 4105–4114. https://doi.org/10.1074/jbc.M708558200

Li, C., Chu, W., Gill, R. A., Sang, S., Shi, Y., Hu, X., Yang, Y., Zaman, Q. U., & Zhang, B. (2023). Computational Tools and Resources for CRISPR/Cas Genome Editing. *Genomics, Proteomics and Bioinformatics*, *21*(1), 108–126. https://doi.org/10.1016/j.gpb.2022.02.006

Li, T., Yang, D., Li, J., Tang, Y., Yang, J., & Le, W. (2015). Critical Role of Tet3 in Neural Progenitor Cell Maintenance and Terminal Differentiation. *Molecular Neurobiology*, *51*(1), 142–154. https://doi.org/10.1007/s12035-014-8734-5

Li, X., & Heyer, W. D. (2008). Homologous recombination in DNA repair and DNA damage tolerance. *Cell Research*, *18*(1), 99–113. https://doi.org/10.1038/cr.2008.1

Lin, S., Staahl, B. T., Alla, R. K., & Doudna, J. A. (2014). Enhanced homology-directed human genome engineering by controlled timing of CRISPR/Cas9 delivery. *ELife*, *3*, e04766. https://doi.org/10.7554/eLife.04766

Liszczak, G., Diehl, K. L., Dann, G. P., & Muir, T. W. (2018). Acetylation blocks DNA damage–induced chromatin ADP-ribosylation. *Nature Chemical Biology*, *14*(9), 837–840. https://doi.org/10.1038/s41589-018-0097-1

Liu, K. I., Ramli, M. N. Bin, Woo, C. W. A., Wang, Y., Zhao, T., Zhang, X., Yim, G. R. D., Chong, B. Y., Gowher, A., Chua, M. Z. H., Jung, J., Lee, J. H. J., & Tan, M. H. (2016). A chemical-inducible CRISPR-Cas9 system for rapid control of genome editing. *Nature Chemical Biology*, *12*(11), 980–987. https://doi.org/10.1038/nchembio.2179

Loening, A. M., Fenn, T. D., Wu, A. M., & Gambhir, S. S. (2006). Consensus guided mutagenesis of Renilla luciferase yields enhanced stability and light output. *Protein engineering, design & selection : PEDS*, *19*(9), 391–400. https://doi.org/10.1093/protein/gzl023

Masutani, M., Suzuki, H., Kamada, N., Watanabe, M., Ueda, O., Nozaki, T., Jishage, K.-I., Watanabe, T., Sugimoto, T., Nakagama, H., Ochiya, T., & Sugimura, T. (1999). Poly(ADP-ribose) polymerase gene disruption conferred mice resistant to streptozotocin-induced diabetes (gene targetingislet cellNADinsulin-dependent diabetes mellitus). In *Medical Sciences* (Vol. 96). www.pnas.org.

Ménissier de Murcia, J., Ricoul, M., Tartier, L., Niedergang, C., Huber, A., Dantzer, F., Schreiber, V., Amé, J., Dierich, A., LeMeur, M., Sabatier, L., Chambon, P., & de Murcia, G. (2003). Functional interaction between PARP-1 and PARP-2 in chromosome stability and embryonic development in mouse. *The EMBO Journal*, *22*(9), 2255–2263. https://doi.org/https://doi.org/10.1093/emboj/cdg206

Ménissier, J., Murcia, D. E., Niedergang, C., Trucco, C., Ricoul, M., Dutrillaux, B., Mark, M., Oliver, F. J., Masson, M., Dierich, A., Lemeur, M., Walztinger, C., Chambon, P., & De Murcia, G. (1997). Requirement of poly(ADP-ribose) polymerase in recovery from DNA damage in mice and in cells (cellular response to DNA damage-raysalkylating agentsG2 arrestapoptosis). In *Cell Biology* (Vol. 94). www.pnas.org.

Milligan, G. (2004). Applications of bioluminescence- and fluorescence resonance energy transfer to drug discovery at G protein-coupled receptors. *European*

Journal of Pharmaceutical Sciences, *21*(4), 397–405. https://doi.org/10.1016/j.ejps.2003.11.010

Nash, B. M., Wright, D. C., Grigg, J. R., Bennetts, B., & Jamieson, R. V. (2015). Retinal dystrophies, genomic applications in diagnosis and prospects for therapy. *Translational Pediatrics*, *4*(2), 139–163. https://doi.org/10.3978/j.issn.2224-4336.2015.04.03

Nishiyama, J., Mikuni, T., & Yasuda, R. (2017). Virus-Mediated Genome Editing via Homology-Directed Repair in Mitotic and Postmitotic Cells in Mammalian Brain. *Neuron*, *96*(4), 755-768.e5. https://doi.org/10.1016/j.neuron.2017.10.004

Ogata, N., Ueda, K., Kawaichi, M., & Hayaishi, O. (1981). *THE JOURNAL OF BIOLOGICAL CHEMISTRY Poly(ADP-Ribose) Synthetase, a Main Acceptor of Poly(ADP-Ribose) in Isolated Nuclei** (Vol. 256, Issue 9).

Okano, S., Lan, L., Caldecott, K. W., Mori, T., & Yasui, A. (2003). Spatial and Temporal Cellular Responses to Single-Strand Breaks in Human Cells. *Molecular and Cellular Biology*, *23*(11), 3974–3981. https://doi.org/10.1128/mcb.23.11.3974-3981.2003

Ozawa, T., Yoshimura, H., & Kim, S. B. (2013). Advances in fluorescence and bioluminescence imaging. *Analytical Chemistry*, *85*(2), 590–609. https://doi.org/10.1021/ac3031724

Pardo, B., Gómez-González, B., & Aguilera, A. (2009). DNA double-strand break repair: How to fix a broken relationship. *Cellular and Molecular Life Sciences*, *66*(6), 1039–1056. https://doi.org/10.1007/s00018-009-8740-3

Pasquini, G., Cora, V., Swiersy, A., Achberger, K., Antkowiak, L., Müller, B., Wimmer, T., Fraschka, S. A. K., Casadei, N., Ueffing, M., Liebau, S., Stieger, K., & Busskamp, V. (2020). Using transcriptomic analysis to assess double-strand break repair activity: Towards precise in vivo genome editing. *International Journal of Molecular Sciences*, *21*(4). https://doi.org/10.3390/ijms21041380

Patterson-Fortin, J., & D'Andrea, A. D. (2020). Exploiting the Microhomology-Mediated End-Joining Pathway in Cancer Therapy. *Cancer Research*, *176*(1), 100–106. https://doi.org/10.1177/0022146515594631.Marriage

Pawelczak, K. S., Gavande, N. S., VanderVere-Carozza, P. S., & Turchi, J. J. (2018). Modulating DNA Repair Pathways to Improve Precision Genome Engineering. In *ACS Chemical Biology* (Vol. 13, Issue 2, pp. 389–396). American Chemical Society. https://doi.org/10.1021/acschembio.7b00777

Perera, A., Eisen, D., Wagner, M., Laube, S. K., Künzel, A. F., Koch, S., Steinbacher, J., Schulze, E., Splith, V., Mittermeier, N., Müller, M., Biel, M.,

Carell, T., & Michalakis, S. (2015). TET3 is recruited by REST for context-specific hydroxymethylation and induction of gene expression. *Cell Reports*, *11*(2), 283–294. https://doi.org/10.1016/j.celrep.2015.03.020

Perina, D., Mikoč, A., Ahel, J., Ćetković, H., Žaja, R., & Ahel, I. (2014). Distribution of protein poly(ADP-ribosyl)ation systems across all domains of life. *DNA Repair*, *23*, 4–16. https://doi.org/10.1016/j.dnarep.2014.05.003

Pfleger, K. D. G., & Eidne, K. A. (2006). Illuminating insights into protein-protein interactions using bioluminescence resonance energy transfer (BRET). *Nature Methods*, *3*(3), 165–174. https://doi.org/10.1038/nmeth841

Prado, D. A., Acosta-Acero, M., & Maldonado, R. S. (2020). Gene therapy beyond luxturna: A new horizon of the treatment for inherited retinal disease. *Current Opinion in Ophthalmology*, *31*(3), 147–154. https://doi.org/10.1097/ICU.0000000000000660

Qiu, P., Shandilya, H., D'Alessio, J. M., O'Connor, K., Durocher, J., & Gerard, G. F. (2004). Mutation detection using Surveyor™ nuclease. In *BioTechniques* (Vol. 36, Issue 4, pp. 702–707). Eaton Publishing Company. https://doi.org/10.2144/04364pf01

Ramsahoye, B. H., Biniszkiewicz, D., Lyko, F., Clark, V., Bird, A. P., & Jaenisch, R. (2000). *Non-CpG methylation is prevalent in embryonic stem cells and may be mediated by DNA methyltransferase 3a*. www.pnas.org

Ran, F. A., Hsu, P. D., Wright, J., Agarwala, V., Scott, D. A., & Zhang, F. (2013). Genome engineering using the CRISPR-Cas9 system. *Nature Protocols*, *8*(11), 2281–2308. https://doi.org/10.1038/nprot.2013.143

Ranjha, L., Howard, S. M., & Cejka, P. (2018). Main steps in DNA double-strand break repair: an introduction to homologous recombination and related processes. *Chromosoma*, *127*(2), 187–214. https://doi.org/10.1007/s00412-017-0658-1

Ray Chaudhuri, A., & Nussenzweig, A. (2017). The multifaceted roles of PARP1 in DNA repair and chromatin remodelling. *Nature Reviews Molecular Cell Biology*, *18*(10), 610–621. https://doi.org/10.1038/nrm.2017.53

RetNet 2025. The Retinal Information Network, https://RetNet.org

Robert, F., Barbeau, M., Éthier, S., Dostie, J., & Pelletier, J. (2015). Pharmacological inhibition of DNA-PK stimulates Cas9-mediated genome editing. *Genome Medicine*, *7*(1). https://doi.org/10.1186/s13073-015-0215-6

Ross, S. E., & Bogdanovic, O. (2019). TET enzymes, DNA demethylation and pluripotency. *Biochemical Society Transactions*, *47*(3), 875–885. https://doi.org/10.1042/BST20180606

Ruppel, W. G. (1899). Zur Chemie der Tuberkelbacillen.

Sanger, F., Air, G. M., Barrell, B. G., Brownt, N. L., Coulson, A. R., Fiddes, J. C., Hutchison, C. A., Slocombe~, P. M., & Smith·, M. (1977). Nucleotide sequence of bacteriophage <DX174 DNA. In *Nature* (Vol. 265). Nature Publishing Group.

Santiago, M., Antunes, C., Guedes, M., Sousa, N., & Marques, C. J. (2014). TET enzymes and DNA hydroxymethylation in neural development and function - How critical are they? *Genomics*, *104*(5), 334–340. https://doi.org/10.1016/j.ygeno.2014.08.018

Schultz, N., Lopez, E., Saleh-Gohari, N., & Helleday, T. (2003). Poly(ADP-ribose) polymerase (PARP-1) has a controlling role in homologous recombination. *Nucleic Acids Research*, *31*(17), 4959–4964. https://doi.org/10.1093/nar/gkg703

Scott-Browne, J. P., Lio, C. W. J., & Rao, A. (2017). TET proteins in natural and induced differentiation. In *Current Opinion in Genetics and Development* (Vol. 46, pp. 202–208). Elsevier Ltd. https://doi.org/10.1016/j.gde.2017.07.011

Seol, J. H., Shim, E. Y., & Lee, S. E. (2018). Microhomology-mediated end joining: Good, bad and ugly. *Mutation Research - Fundamental and Molecular Mechanisms of Mutagenesis*, *809*, 81–87. https://doi.org/10.1016/j.mrfmmm.2017.07.002

Sfeir, A., & Symington, L. S. (2015). Microhomology-mediated end joining: a back-up survival mechanism or dedicated pathway? *Trends in Biochemical Sciences*, *176*(10), 139–148. https://doi.org/10.1016/j.tibs.2015.08.006.Microhomology-mediated

Sfeir, A., Tijsterman, M., & McVey, M. (2024). Microhomology-Mediated End Joining Chronicles: Tracing the Evolutionary Footprints of Genome Protection. *Annual Review of Cell and Developmental Biology*, 1–24. https://doi.org/10.1146/annurev-cellbio-111822-014426

Shockett, P. E., & Schatz, D. G. (1996). Diverse strategies for tetracycline-regulated inducible gene expression. *Proceedings of the National Academy of Sciences*, *93*(11), 5173–5176. https://doi.org/10.1073/pnas.93.11.5173

Shrivastav, M., De Haro, L. P., & Nickoloff, J. A. (2008). Regulation of DNA double-strand break repair pathway choice. *Cell Research*, *18*(1), 134–147. https://doi.org/10.1038/cr.2007.111

Smirnikhina, S. A., Zaynitdinova, M. I., Sergeeva, V. A., & Lavrov, A. V. (2022). Improving Homology-Directed Repair in Genome Editing Experiments by

Influencing the Cell Cycle. *International Journal of Molecular Sciences*, *23*(11). https://doi.org/10.3390/ijms23115992

Song, F., & Stieger, K. (2017). Optimizing the DNA Donor Template for Homology-Directed Repair of Double-Strand Breaks. *Molecular Therapy Nucleic Acids*, *7*(June), 53–60. https://doi.org/10.1016/j.omtn.2017.02.006

Splith, V. (2019). *Genome Editing and Transcriptional Activation Using Crispr-Cas9 Technology*.

Stieger, K., Le Meur, G., Lasne, F., Weber, M., Deschamps, J. Y., Nivard, D., Mendes-Madeira, A., Provost, N., Martin, L., Moullier, P., & Rolling, F. (2006). Long-term doxycycline-regulated transgene expression in the retina of nonhuman primates following subretinal injection of recombinant AAV vectors. *Molecular Therapy*, *13*(5), 967–975. https://doi.org/10.1016/j.ymthe.2005.12.001

Sun, S., Yang, X., Wang, Y., & Shen, X. (2016). In vivo analysis of protein–protein interactions with bioluminescence resonance energy transfer (BRET): Progress and prospects. *International Journal of Molecular Sciences*, *17*(10). https://doi.org/10.3390/ijms17101704

Sun, W., Guan, M., & Li, X. (2014). 5-hydroxymethylcytosine-mediated DNA demethylation in stem cells and development. *Stem Cells and Development*, *02155*(781), 1–28.

Tan, E., Chin, C. S. H., Lim, Z. F. S., & Ng, S. K. (2021). HEK293 Cell Line as a Platform to Produce Recombinant Proteins and Viral Vectors. In *Frontiers in Bioengineering and Biotechnology* (Vol. 9). Frontiers Media S.A. https://doi.org/10.3389/fbioe.2021.796991

Tolić, A., Ravichandran, M., Rajić, J., Đorđević, M., Đorđević, M., Dinić, S., Grdović, N., Jovanović, J. A., Mihailović, M., Nestorović, N., Jurkowski, T. P., Uskoković, A. S., & Vidaković, M. S. (2022). TET-mediated DNA hydroxymethylation is negatively influenced by the PARP-dependent PARylation. *Epigenetics and Chromatin*, *15*(1), 1–12. https://doi.org/10.1186/s13072-022-00445-8

US. Food and Drug Administration. (2017). *Approval letter and summary basis for regulatory action: Voretigene neparvovec-rzyl (LUXTURNA).* https://www.fda.gov/vaccines-blood-biologics/cellular-gene-therapy-products/luxturna

US. Food and Drug Administration. (2023). *FDA approves first CRISPR/Cas9 genome-edited cell therapy (Casgevy) for treatment of sickle cell disease.* https://www.fda.gov/vaccines-blood-biologics/casgevy

Van Vu, T., Thi Hai Doan, D., Kim, J., Sung, Y. W., Thi Tran, M., Song, Y. J., Das, S., & Kim, J. Y. (2021). CRISPR/Cas-based precision genome editing via microhomology-mediated end joining. *Plant Biotechnology Journal*, *19*(2), 230–239. https://doi.org/10.1111/pbi.13490

Vilaboa, N., Boellmann, F., & Voellmy, R. (2011). Gene Switches for Deliberate Regulation of Transgene Expression: Recent Advances in System Development and Uses. *Journal of Genetic Syndromes & Gene Therapy*, *02*(03). https://doi.org/10.4172/2157-7412.1000107

Vítor, A. C., Huertas, P., Legube, G., & de Almeida, S. F. (2020). Studying DNA Double-Strand Break Repair: An Ever-Growing Toolbox. *Frontiers in Molecular Biosciences*, *7*(February), 1–16. https://doi.org/10.3389/fmolb.2020.00024

Wang, H., & Xu, X. (2017). Microhomology-mediated end joining: New players join the team. *Cell and Bioscience*, *7*(1), 4–9. https://doi.org/10.1186/s13578-017-0136-8

Wang, J. Y., & Doudna, J. A. (2023). CRISPR technology: A decade of genome editing is only the beginning. *Science*, *379*(6629). https://doi.org/10.1126/science.add8643

Wang, K., Mei, D. Y., Liu, Q. N., Qiao, X. H., Ruan, W. M., Huang, T., & Cao, G. S. (2015). Research of methods to detect genomic mutations induced by CRISPR/Cas systems. *Journal of Biotechnology*, *214*, 128–132. https://doi.org/10.1016/j.jbiotec.2015.09.029

Weng, Y. L., An, R., Shin, J., Song, H., & Ming, G. li. (2013). DNA Modifications and Neurological Disorders. *Neurotherapeutics*, *10*(4), 556–567. https://doi.org/10.1007/s13311-013-0223-4

Weterings, E., & Chen, D. J. (2008). The endless tale of non-homologous end-joining. *Cell Research*, *18*(1), 114–124. https://doi.org/10.1038/cr.2008.3

Wimmer, T., Bonthu, D., Moeschl, V., Kleekamp, P., Thiel, C., Lytvynchuk, L., Ellinwood, M., & Stieger, K. (2021). A Bioluminescence Resonance Energy Transfer-Based Reporter System: Characterization and Applications. *CRISPR Journal*, *4*(6), 884–895. https://doi.org/10.1089/crispr.2021.0023

Wu, X., & Zhang, Y. (2017). TET-mediated active DNA demethylation: Mechanism, function and beyond. *Nature Reviews Genetics*, *18*(9), 517–534. https://doi.org/10.1038/nrg.2017.33

Xu, Y., Xu, C., Kato, A., Tempel, W., Abreu, J. G., Bian, C., Hu, Y., Hu, D., Zhao, B., Cerovina, T., Diao, J., Wu, F., He, H. H., Cui, Q., Clark, E., Ma, C., Barbara, A., Veenstra, G. J. C., Xu, G., … Shi, Y. G. (2012). Tet3 CXXC domain and dioxygenase activity cooperatively regulate key genes for

xenopus eye and neural development. *Cell*, *151*(6), 1200–1213. https://doi.org/10.1016/j.cell.2012.11.014

Xue, C., & Greene, E. C. (2021). DNA repair pathway choices in CRISPR-Cas9 mediated genome editing. *Trends in Genetics*, *176*(1), 139–148. https://doi.org/10.1016/j.tig.2021.02.008.DNA

Yamakawa, Y., Ueda, H., Kitayama, A., & Nagamune, T. (2002). Rapid. Homogeneous Immunoassay of Peptides Based on Bioluminescence Resonance Energy Transfer from Firefly Luciferase. In *JOURNAL OF BIOSCIENCE AND BIOENGINEERING* (Vol. 93, Issue 6).

Yang, H., Ren, S., Yu, S., Pan, H., Li, T., Ge, S., Zhang, J., & Xia, N. (2020). Methods favoring homology-directed repair choice in response to crispr/cas9 induced-double strand breaks. *International Journal of Molecular Sciences*, *21*(18), 1–20. https://doi.org/10.3390/ijms21186461

Yang, Y., & Herrup, K. (2007). Cell division in the CNS: Protective response or lethal event in post-mitotic neurons? *Biochimica et Biophysica Acta - Molecular Basis of Disease*, *1772*(4), 457–466. https://doi.org/10.1016/j.bbadis.2006.10.002

Yanik, M., Müller, B., Song, F., Gall, J., Wagner, F., Wende, W., Lorenz, B., & Stieger, K. (2017). In vivo genome editing as a potential treatment strategy for inherited retinal dystrophies. *Progress in Retinal and Eye Research*, *56*, 1–18. https://doi.org/10.1016/j.preteyeres.2016.09.001

Yoshikawa, K. (2000). Cell cycle regulators in neural stem cells and postmitotic neurons. *Neuroscience Research*, *37*(1), 1–14. https://doi.org/10.1016/S0168-0102(00)00101-2

Yu, H., Su, Y., Shin, J., Zhong, C., Guo, J. U., Weng, Y. L., Gao, F., Geschwind, D. H., Coppola, G., Ming, G. L., & Song, H. (2015). Tet3 regulates synaptic transmission and homeostatic plasticity via DNA oxidation and repair. *Nature Neuroscience*, *18*(6), 836–843. https://doi.org/10.1038/nn.4008

Zhang, J., Chen, L., Zhang, J., & Wang, Y. (2019). Drug Inducible CRISPR/Cas Systems. *Computational and Structural Biotechnology Journal*, *17*, 1171–1177. https://doi.org/10.1016/j.csbj.2019.07.015

Zhao, C., Zhao, Y., Zhang, J., Lu, J., Chen, L., Zhang, Y., Ying, Y., Xu, J., Wei, S., & Wang, Y. (2018). HIT-Cas9: A CRISPR/Cas9 Genome-Editing Device under Tight and Effective Drug Control. *Molecular Therapy - Nucleic Acids*, *13*, 208–219. https://doi.org/10.1016/j.omtn.2018.08.022

Zhou, X., Vink, M., Klaver, B., Berkhout, B., & Das, A. T. (2006). Optimization of the Tet-On system for regulated gene expression through viral evolution. *Gene Therapy*, *13*(19), 1382–1390. https://doi.org/10.1038/sj.gt.3302780

Zhu, Z., Zheng, T., Lee, C. G., Homer, R. J., & Elias, J. A. (2002). Tetracycline-controlled transcriptional regulation systems: advances and application in transgenic animal modeling. *Seminars in Cell and Developmental Biology*, *13*(02), 243–249. https://doi.org/10.1016/S1084

Ziccardi, L., Cordeddu, V., Gaddini, L., Matteucci, A., Parravano, M., Malchiodi-Albedi, F., & Varano, M. (2019). Gene therapy in retinal dystrophies. *International Journal of Molecular Sciences*, *20*(22), 1–25. https://doi.org/10.3390/ijms20225722

List of figures permissions

Figure number	Citation	Permission
Figure 1	(Hartong et al., 2006)	With permission from Elsevier, License Number 5907230508337
Figure 2	(Janik et al., 2020).	Licensed under CC BY 4.0. https://creativecommons.org/licenses/by/4.0/
Figure 3	(Smirnikhina et al., 2022).	Licensed under CC BY 4.0. https://creativecommons.org/licenses/by/4.0
Figure 4	(Wu & Zhang, 2017).	With permission from Springer Nature, License Number 5911011011468
Figure 5	(Ray Chaudhuri & Nussenzweig, 2017).	With permission from Springer Nature, License Number 5907231325083
Figure 6	(Zhang et al., 2019).	Licensed under CC BY 4.0. https://creativecommons.org/licenses/by/4.0
Figure 7	(Wimmer et al., 2021).	With permission from Mary Ann Liebert, Inc., License Number 5907250237267
Figure 8	Adapted from Addgene plasmid # 84232; http://n2t.net/addgene:84232; RRID:	With permission from Nature Chemical Biology, License Number 6085360050582

	Addgene_84232 (Liu et al., 2016)	
Figure 9	Addgene plasmid # 62988; http://n2t.net/addgene:62988; RRID: Addgene_62988 (Ran et al., 2013)	With permission from Nature Protocols, License Number 6085521004787
Figure 10	Addgene plasmid # 87121; http://n2t.net/addgene:87121; R RID: Addgene_87121) (Loening et al., 2006).	With permission from Protein Engineering, Design and Selection, License Number 6085530127486
Figure 11	Addgene plasmid #49446; http://n2t.net/addgene:49446;RRID: Addgene_49446 (Ko et al., 2013)	With permission from Nature , License Number 6085530524573
Figure 12	Adapted from Addgene plasmid # 111575; http://n2t.net/addgene:111575; RRRID: Addgene111575 (Liszczak et al., 2018)	With permission from Nature Chemical Biology, License Number 6085530897168

Declaration

I declare that I have completed this dissertation single-handedly without the unauthorized help of a second party and only with the assistance acknowledged therein. I have appropriately acknowledged and referenced all text passages that are derived literally from or are based on the content of published or unpublished work of others, and all information that relates to verbal communications. I have abided by the principles of good scientific conduct laid down in the charter of the Justus Liebig University of Giessen in carrying out the investigations described in the dissertation.

Place and Date:	Signature:

Acknowledgments

First and foremost, I am grateful to Almighty God for His countless blessings and for giving me the strength to complete this journey. I would like to express my sincerest gratitude to Prof Dr. Dr. Knut Stieger for his guidance, encouragement, and insight throughout these years.

My deepest appreciation goes to Dr. Tobias Wimmer for his constructive feedback and kind support. My sincere thanks go to Prof. Dr. Birgit Lorenz and Prof. Dr. Lyubomyr Lytvynchuk for allowing us to use their lab facility and offices during the first half of my PhD. I am also thankful to the lab chief, PD Dr. Markus Preising.

Special thanks go to Annabella Janise-Libawski for her tremendous help, patience, and caring personality. Many thanks also go to all the experimental ophthalmology group, including Dr. Brigitte Müller, Bärbel Fühler, Bettina Gill, and Kerstin Walther. I am incredibly thankful to Dr. Maria Weller and Lasse Stöhr. Working beside each of you made this journey both enriching and fun.

I would like to thank my family and friends for their continuous support. I am grateful to my late father, whose memory will live forever in our hearts. He would definitely be proud. I am especially thankful to my loving mother. Your prayers have always been my ultimate source of power. To my encouraging brothers, their wonderful families, and my creative and amazing sister, thank you for all your love and motivation. I also want to thank my second family, my in-laws, who have supported me throughout this journey. Your love and kindness are beyond description. I want to thank my biggest supporter, my small family, my lover and husband, Akram, and my beloved son, Mohammed, for their patience and understanding throughout these years, especially during my countless weekend lab visits. Without you, this achievement would not have been possible. Lastly, to my unborn baby, thank you for being a source of hope and purpose.